LA-11498-HDR

C.3

CIC-14 REPORT COLLECTION
REPRODUCTION
COPY

ICFT: An Initial Closed-Loop Flow Test of the Fenton Hill Phase II HDR Reservoir

LOS ALAMOS NATIONAL LABORATORY
3 9338 00323 4191

Los Alamos

Los Alamos National Laboratory is operated by the University of California for the United States Department of Energy under contract W-7405-ENG-36.

This work was supported by the US Department of Energy, Division of Geothermal Technologies, and the New Energy Development Organization of Japan through an International Energy Agency agreement.

An Affirmative Action/Equal Opportunity Employer

This report was prepared as an account of work sponsored by an agency of the United States Government. Neither the United States Government nor any agency thereof, nor any of their employees, makes any warranty, express or implied, or assumes any legal liability or responsibility for the accuracy, completeness, or usefulness of any information, apparatus, product, or process disclosed, or represents that its use would not infringe privately owned rights. Reference herein to any specific commercial product, process, or service by trade name, trademark, manufacturer, or otherwise, does not necessarily constitute or imply its endorsement, recommendation, or favoring by the United States Government or any agency thereof. The views and opinions of authors expressed herein do not necessarily state or reflect those of the United States Government or any agency thereof.

LA-11498-HDR

UC-251
Issued: February 1989

ICFT: An Initial Closed-Loop Flow Test of the Fenton Hill Phase II HDR Reservoir

Zora V. Dash, Editor
Ronald G. Aguilar
Bert R. Dennis
Donald S. Dreesen
Michael C. Fehler
Robert H. Hendron
Leigh S. House
Hisao Ito*
Sharad M. Kelkar
Mark V. Malzahn**
James R. Miller
Hugh D. Murphy
W. Scott Phillips**
Sharon B. Restine†
Peter M. Roberts†
Bruce A. Robinson
Wilfred R. Romero, Jr.‡

*Geological Survey of Japan, 1-1-3 Higashi, Yatabe, Ibaraki, 305 JAPAN.
**Mechanical Design Services, 421 Camino Santa Cruz, Española, NM 87532.
†Graduate Research Assistant at Los Alamos.
‡Undergraduate Student at Los Alamos. Route 1, Box 167, Santa Fe, NM 87501.

LOS ALAMOS NATL. LAB. LIBS.
3 9338 00323 1191

Los Alamos
Los Alamos National Laboratory
Los Alamos, New Mexico 87545

TABLE OF CONTENTS

	Page
LIST OF ILLUSTRATIONS	vii
LIST OF TABLES	xi
LIST OF PLATES	xii
ABSTRACT	1
SUMMARY	1
I. INTRODUCTION	4
A. Background	6
B. Objectives	10
II. SYSTEM DESCRIPTION, OPERATIONS, AND PERFORMANCE	13
A. Wellbore Configurations	13
B. Surface System	18
C. Data Acquisition	21
D. Loop Operations	25
E. Borehole Performance	26
III. THERMAL BEHAVIOR	32
A. Temperature Measurements	32
B. Modeling Thermal Performance	38
C. Estimation of Thermal Power Production	44
IV. RESERVOIR HYDRAULICS	45
A. Pressure Rate Response	45
B. Impedance	60
C. Water Loss	61
V. GEOCHEMISTRY AND TRACERS	63
A. Geochemistry Data	63
B. Interpretation of Geochemistry	66
C. Chemical Effects on Operations	73
D. Tracer Experiments	77
VI. SEISMOLOGY	79
A. Data Collection and Processing	79
B. ICFT Seismicity	85
C. Seismic Attenuation	92
D. Environmental Monitoring	93
VII. CONCLUSIONS	94
A. Comparison of HDR Reservoirs	94
B. Conclusions from Thermal and Hydraulic Analysis	96
C. Conclusions from Geochemistry and Tracer Analysis	97
D. Conclusions from Microseismic Analysis	98
E. Conclusions about Loop Operations and Equipment	99
F. Conclusions about Instrumentation and Control	99

VII. RECOMMENDATIONS FOR THE LONG-TERM FLOW TEST 100
A. Loop Operations and Equipment 100
B. Instrumentation and Control 104

ACKNOWLEDGMENTS 106

REFERENCES 107

APPENDIX A. SURFACE SYSTEM 109

APPENDIX B. DATA CHANNELS AND TAPE SETUPS 112

APPENDIX C. CHRONOLOGICAL SUMMARY OF ICFT PUMPING AND OPERATIONS . 114

APPENDIX D. GEOCHEMISTRY NOMENCLATURE 126

APPENDIX E. ENVIRONMENTAL MONITORING: DISCRIMINATION CRITERIA . . 127

LIST OF ILLUSTRATIONS

Figure		Page
I-1.	Perspective view of Phase II boreholes and typical geophone tool emplaced for microearthquake monitoring during fracturing.	7
I-2.	Hypocentral locations of microearthquakes induced by massive hydraulic fracturing in injection well EE-2. Left-hand side presents elevation view, looking north, while right-hand side is plan view, looking down.	8
I-3.	Elevation view of reservoir, looking north. Packer shown allowed supplementary stimulation of EE-3A, which resulted in low flow resistance connection between EE-2 and EE-3A. The flow paths indicated are inferred from joint locations determined from a temperature survey in EE-3A..	9
II-1.	EE-2 well configuration during the ICFT..	14
II-2.	EE-3A well configuration before the ICFT well completion. .	16
II-3.	EE-3A well configuration after installation of a permanent packer at 3560 m (11 685 ft). The packer failed after 3 days and was removed.	16
II-4.	EE-3A well configuration after installation of the cemented-in liner. This was the configuration of the well for the ICFT..	17
II-5.	Schematic of the ICFT surface system.	19
II-6.	Schematic of the Hot Dry Rock seismic digital event detecting and recording system.	23
II-7.	EE-3A backside flow compared to EE-3A and EE-2 pressures: a) EE-3A frontside pressure, b) EE-3A backside pressure (there is some evidence of a 2-day response on the backside to pressure changes on the frontside), c) EE-3A backside flow data (negative flow occurred as the well was cooled and liquid was added to the backside to make up for fluid contraction), d) EE-2 frontside pressure, and e) EE-2 backside pressure..	30
II-8.	EE-2 backside pressure (a) compared to b) EE-2 annulus pressure, c) EE-2 frontside pressure (an intermittent connection from the frontside to the backside is indicated), d) EE-2 surface production temperature (backside pressure intermittently responded to temperature changes in the tubing, indicating the leak on the backside was occasionally sealing off), and e) EE-3A frontside pressure (the reservoir connection is evident but subtle).. .	31

III-1. Pre- and post-ICFT temperature surveys of EE-3A run by Los Alamos. 33

III-2. High-pressure temperature surveys of EE-3A run by OWP.. . . 33

III-3. Comparison of the pre-ICFT survey with post-ICFT surveys showing thermal recovery of EE-3A with time.. 34

III-4. Kuster temperature surveys of EE-2 during the ICFT compared to a post-ICFT temperature survey.. 35

III-5. A calculated boiling pressure curve (based on the EE-2 surface production temperatures) compared to the EE-2 annulus pressure data.. 36

III-6. EE-2 temperature logs with interpretation of the 1984 cement bond log amplitude shown. The bond log was run following the squeeze cement jobs conducted during the 1984 EE-2 repair. 37

III-7. EE-1 and GT-2B temperature surveys. 38

III-8. EE-3A injection flow rate versus time.. 39

III-9. WBHT projection of EE-3A bottom-hole temperature. 40

III-10. WBHT projection of EE-3A temperature surveys compared to OWP surveys: a) OWP survey 86/05/28; b) OWP survey 86/06/16; and c) OWP survey 86/06/23. 40

III-11. EE-2 production flow rate.. 41

III-12. EE-2 wellhead production temperature compared to WBHT projection of production temperature using wellhead measured flow rates and using heat exchanger rates. . . . 42

III-13. EE-2 Kuster temperature surveys compared to WBHT projections using wellhead flow rates.. 42

III-14. EE-2 production flow rate estimated from difference between makeup flow and injection flow measurements.. 43

III-15. Kuster measurements with WBHT projections of downhole temperature using heat exchanger flow rates.. 44

III-16. Thermal power production during the ICFT estimated using heat exchanger flow rates.. 45

IV-1. EE-3A pressure and flow rate. 46

IV-2. EE-3A pressure buildup during first step-rate test. 48

IV-3. EE-3A pressure buildup during second step-rate test.. . . . 48

IV-4. Bottom-hole fracture closure pressure for five experiments. 50

IV-5. Shut-in curve for the final shut-in.. 51

IV-6. Slope of shut-in curves versus volume injected for EE-3A falloffs. 52

IV-7. Six different shut-in curves during the ICFT. 53

IV-8. Horner curve for EE-3A wellhead pressure. 55

IV-9. Horner curve for EE-2 wellhead pressure.. 55

IV-10. Fracture closure pressure versus depth for several experiments.. 56

IV-11. EE-2 pressure and flow rate.. 57

IV-12. EE-2 and EE-3A pressure.. 57

IV-13. EE-2 and EE-3A flow rate. 58

IV-14. EE-2 pressure during the first 8 hours of the ICFT. 59

IV-15. EE-1 and GT-2B response to the ICFT pressurization. 59

IV-16. Overall reservoir impedance.. 60

IV-17. Wellbore impedance for EE-3A and EE-2. 61

IV-18. Percent water loss. 62

V-1. Schematic of the sampling apparatus for production fluid liquids and gases.. 63

V-2. Concentration-time behavior of the major dissolved species in the production fluid.. 64

V-3. Dissolved CO_2 concentration in the production fluid.. . . . 66

V-4. Dimensionless concentration versus produced fluid volume for inert species during initial reservoir operation. Concentrations start at high downhole values and decline to injection fluid concentration. 67

V-5. Different types of concentration-volume behavior observed during initial reservoir operation. 68

V-6. Boron versus chloride for fluid samples collected in the Fenton Hill HDR reservoir over the past 6 years.. 69

V-7. Silica and Na-K-Ca geothermometer temperatures. 72

V-8. Corrosion rates measured on the hot and cold sides of the heat exchanger. Each value is obtained from a determination of weight-loss for a coupon exposed to fluid during the times labeled. 74

V-9. Pressure required to keep CO_2 - H_2O solution single phase for different CO_2 concentrations and temperatures. Dotted line is a typical (P,T) curve for an element of fluid passing through the surface loop equipment. 76

V-10. Residence time distribution curves obtained from the two radioactive tracer experiments. 78

VI-1. Seismic stations used during the ICFT. 80

VI-2. Event location changes with addition of EE-1 data. Filled circles represent locations based on P- and S-wave data from PC-1 and GT-1 and P-wave data from PC-2. Line segments represent the location change when P- and S-waves data from EE-1 are added and S-wave data from PC-1 are removed. A cluster of locations on the map view were not given line segment extensions since their horizontal changes were small. 85

VI-3. ICFT seismicity histogram. Time is measured in days from May 19 00:00 MDT. The top bar under the histogram indicates the times that the MASSCOMP was operating. The lower bar indicates the times that the EE-1 geophone was downhole. Injection pressure curve for the ICFT is also included for comparison. 86

VI-4. Event locations for the ICFT. Only results that have been assigned qualities "A" or "B" are shown. 87

VI-5. Histograms of various seismic clusters that appear in the ICFT results (see Fig. VI-4). MASSCOMP and EE-1 operation times are as in Fig. VI-3; note the different scales on the "number of events" axes. 89

VI-6. Times of anomalous northerly events (solid circles) and production well pressures indicating initial and final shut-ins. All events in group 5 (see Fig. VI-4) fall within the time interval depicted. 90

VI-7. Event locations for the massive hydraulic fracture experiment; "A" and "B" qualities only. 91

VI-8. ICFT events that were strong enough to be recorded by surface network stations. A histogram is included, with MASSCOMP and EE-1 operation indicated as in Fig. VI-3. . . 92

LIST OF TABLES

Table		Page
I-I.	SUMMARY OF PERTINENT PHASE II RESERVOIR INJECTIONS	11
II-I.	RESULTS OF RA VELOCITY LOGS IN EE-3A	28
II-II.	EE-3A EXPANSION JOINT PERFORMANCE	29
IV-I.	EE-3A SHUT-INS	47
IV-II.	COMPARISON OF EXPERIMENT 2067 RESULTS WITH PREVIOUS TESTS	49
IV-III.	ESTIMATED EE-3A BOTTOM-HOLE PRESSURES AND TEMPERATURES	50
IV-IV.	EE-3A FRACTURING PRESSURE COMPARISON WITH 1985 DRILLING CAMPAIGN	56
V-I.	TYPICAL ION CONCENTRATIONS	65
VI-I.	FENTON HILL SEISMIC STATION LOCATIONS AND CORRECTIONS	81
VI-II.	EE-1 TRIAXIAL GEOPHONE DOWNHOLE (MDT)	81
VI-III.	SETUP PARAMETERS	83
VI-IV.	TRIGGER PARAMETERS	83
VI-V.	ICFT MAGNETIC TAPE BACKUP TO MASSCOMP (MDT)	84
VI-VI.	LOCATION QUALITIES	86
VI-VII.	RESULTS OF PLANE-WAVE PROGRAM	93
VII-I.	COMPARISON OF THREE HDR RESERVOIRS AFTER 30 DAYS OF OPERATION	95
B-I.	ICFT DATA CHANNELS	112
B-II.	EXPERIMENT 2067 (ICFT) TAPE SETUP NO. 1	113
B-III.	EXPERIMENT 2067 (ICFT) TAPE SETUP NO. 3	113

LIST OF PLATES

Plate I. Event Chronology with ICFT Performance Data.

Plate II. ICFT Performance Data.

ICFT: AN INITIAL CLOSED-LOOP FLOW TEST OF THE FENTON HILL PHASE II HDR RESERVOIR

by

Zora V. Dash (Ed.), Ronald G. Aguilar, Bert R. Dennis, Donald S. Dreesen, Michael C. Fehler, Robert H. Hendron, Leigh S. House, Hisao Ito, Sharad M. Kelkar, Mark V. Malzahn, James R. Miller, Hugh D. Murphy, W. Scott Phillips, Sharon B. Restine, Peter M. Roberts, Bruce A. Robinson, and Wilfred R. Romero, Jr.

ABSTRACT

A 30-day closed-loop circulation test of the Phase II Hot Dry Rock reservoir at Fenton Hill, New Mexico, was conducted to determine the thermal, hydraulic, chemical, and seismic characteristics of the reservoir in preparation for a long-term energy-extraction test. The Phase II heat-extraction loop was successfully tested with the injection of 37 000 m^3 of cold water and production of 23 300 m^3 of hot water. Up to 10 MW_t was extracted when the production flow rate reached 0.0139 m^3/s at 192°C. By the end of the test, the water-loss rate had decreased to 26% and a significant portion of the injected water was recovered; 66% during the test and an additional 20% during subsequent venting. Analysis of thermal, hydraulic, geochemical, tracer, and seismic data suggests the fractured volume of the reservoir was growing throughout the test.

SUMMARY

The Initial Closed-Loop Flow Test (ICFT), Experiment 2067, was designed as a precursor to a long-term energy-extraction experiment in the Phase II Hot Dry Rock (HDR) reservoir at Fenton Hill. The ICFT successfully evaluated the Phase II heat-extraction loop from May 19 through June 18, 1986. Cold water was injected under high pressures at EE-3A and hot water was produced at EE-2, cooled, and reinjected (Hendron, 1987).

Well EE-2 was completed with a packer and tubing set at 3170 m and well EE-3A with a cemented-in liner and tubing set at 3485 m. A temporary experimental surface system was constructed to meet the needs of the ICFT and was operated 24 hours per day using rotating shifts. Temperatures, pressures, and flow rates were recorded in the Data Acquisition Trailer (DAT) throughout the experiment and subsequent shut-in, as were seismic data collected by the MASSCOMP data acquisition system. A series of borehole temperature surveys were also made to monitor the condition of the wellbores during injection and production. A chronology of operations and various performance parameters (i.e., pressure, flow rate, temperature, etc.) are plotted versus time on Plates I and II.

A total of 37 000 m^3 (9.76 million gal.) of water was injected while 23 300 m^3 (6.15 million gal.) of hot water was produced. The injection rates at the surface ranged up to 0.0265 m^3/s (420 gpm), although most of the pumping was done at rates of 0.0106 m^3/s (168 gpm) and 0.0185 m^3/s (294 gpm), with surface pressures around 26.9 MPa (3900 psi) and 30.3 MPa (4400 psi), respectively. The production well surface pressure was controlled at around 3.5 MPa (500 psi), resulting in surface production flow rates from 0.0063 m^3/s (100 gpm) to 0.0139 m^3/s (220 gpm).

The EE-2 production temperature increased throughout the test, reaching a maximum of 192°C at the surface and 232°C at the bottom of the well near the end of the test. The production flow rate also increased throughout the test. This increase was related to the significant amount of time required to inflate the reservoir to a pseudo steady-state volume. A slight reduction in the production wellbore impedance was also observed. As a result of the temperature and production increases, there was a corresponding increase in power production, which reached a maximum of 10 MW_t after 28 days.

The bottom-hole pressure in EE-3A did not change much with injection rate or time, indicating fracture inflation and stimulation were occurring near the injection wellbore. The near-wellbore impedance at EE-3A decreased from 0.72 $GPa \cdot s/m^3$ (6.6 psi/gpm) to 0.002 $GPa \cdot s/m^3$ (0.02 psi/gpm) during the early part of the test because of cooling and pressurization near the well. The decline in the production well

impedance during the test was not as significant. The decrease in overall reservoir impedance, from 7 GPa·s/m^3 (64 psi/gpm) to 2 GPa·s/m^3 (18 psi/gpm), resulted primarily from stimulation of the reservoir, especially near the injection well. However, the injection well impedance was only a minor portion of the overall impedance, indicating that strategies for reducing the impedance of the reservoir should concentrate on the region surrounding the production well.

The rate of water loss decreased throughout the test, starting at 70% after 4 days of pumping and reducing to 26% after 30 days. The apparently high water-loss rate during the early portion of the test was due primarily to the water requirement of inflating or filling the fractures that make up the reservoir. Of the total injected water, 66% was recovered during the test and an additional 20% was recovered during a subsequent vent-down.

The geochemical behavior of the fluid produced at EE-2 was monitored continuously to determine the concentration of dissolved anions, cations, and gases. The concentration of most species was two to three times higher than encountered in the shallower Phase I reservoir, probably because of higher reservoir temperatures and a larger contribution from the in situ pore fluid. The Na-K-Ca and SiO_2 geothermometers yielded temperatures that agree well with the downhole temperature measured during fully equilibrated temperature surveys. Several periods of high dissolved CO_2 concentration in the production stream created a temporary two-phase flow condition at a shallow depth in the production wellbore and in the surface loop, indicating future operations will require gas separation.

Studies of corrosion coupons placed in the flow loop during the test indicated generalized, uniform corrosion at rates of 0.25 to 0.38 mm/yr (10 to 15 mpy). One case of pitting, attributed to increased concentration of dissolved O_2, was observed. To minimize pitting in future operations, an oxygen scavenger will be used. Scale deposition was minimal and did not affect operations.

Results of the two radioactive tracer experiments suggest flow was occurring through a large, highly fractured region of rock. Modal volumes were about twice as large as that of the previous shallower reservoir at Fenton Hill and tracer recoveries were lower, indicating

fluid was flowing through a large number of fractures. Calculations indicate this fractured rock volume is equivalent to a sphere with diameter approximately equal to the separation distance between the injection and production points in the two wells.

The new MASSCOMP seismic data acquisition system operated successfully during the 30-day ICFT experiment. Data from almost 700 microseismic events were collected. A number of the smallest events collected could not be located because of low signal-to-noise ratio, which indicates that the data set is complete in terms of locatable events.

The resulting seismicity fell into the now familiar, nearly vertical, northerly striking tabular region, yet occupied only half of the volume defined by the seismicity of Expt. 2032, the massive hydraulic fracture (MHF) in 1983. The active region was located entirely in the southern or injection end of the Expt. 2032 active volume. This pattern may have been caused by a pressure asymmetry set up by the source-sink "dipole" at the injection and production points. This implies that seismicity, reservoir extension, and possibly water loss could be controlled by introducing additional production wells surrounding the injection point.

The northern portion of the reservoir was only active following shut-in. The large size of many of these events was curious since shut-in pressures should not have been enough to exceed the fracture extension threshold. It is possible these events occurred in the lower-pressure, Phase I reservoir region.

The reservoir was continually enlarging during the ICFT. Microseismic locations generally fell to the east of previous seismic clouds (Expt. 2032). A significant breakthrough to previously inactive shallow depths in the southern portion of the active region occurred midway through the experiment. This activity was not associated with any major change in injection pressures.

I. INTRODUCTION

The primary objective of the U.S. Hot Dry Rock (HDR) Program is to develop an economical, commercially usable technology for recovering

thermal energy from hot rock at accessible depths in the earth's crust. The Program so far has concentrated on hot crystalline rock of low initial permeability, on the use of fluid pressure (hydraulic fracturing) to create flow passages and heat-transfer surface in that rock, and on the operation of a closed, recirculating, pressurized-water loop to extract heat from the rock and transport it to the earth's surface. Large-scale field experiments are conducted at Fenton Hill in the Jemez Mountains of northern New Mexico, and supporting activities are conducted primarily at Los Alamos National Laboratory, about 35 km east of the Fenton Hill site. The latter include development of new or improved downhole equipment and instruments, field and laboratory experimental techniques, and analytical and numerical data analyses and modeling procedures. Many of these developments have been found useful in other experimental programs and in a variety of industrial applications. Other HDR programs are underway in the Federal Republic of Germany, France, Japan, Sweden, the United Kindom, and the USSR.

The technical issues faced in HDR development are challenging. Wells must be drilled to depths where temperatures (200-300°C) are suitable for electricity generation. Even in regions with favorable geothermal gradients, such temperatures are found at great depths, 3 to 5 km, where the minimum component of the in situ earth stress is likely to be 35 to 100 MPa. One must then fracture the rock formation at this great stress and hold open the fractures so that the permeability remains high and the flow resistance is low. Large areas of hot rock must be adequately bathed by the injected water to result in high heat production. At the same time, since all water must be provided from an external source, one must avoid excessive water losses to the country rock surrounding the fractured reservoir. Furthermore, the potential for damaging earthquakes caused by downhole accumulation of this water loss must be considered. One must also avoid or counter potential geochemical problems, such as scaling of surface equipment with precipitated products of aqueous rock dissolution and corrosion of surface and downhole piping.

The incentive for meeting these challenges is the enormous resource base that HDR energy provides. Unlike hydrothermal reservoirs, which are rarely found, potential HDR reservoirs underlie much of the world.

Even if one considers just the high-grade resources, i.e., regions with geothermal gradients greater than 40°C/km, where high temperatures can be attained at relatively shallow depths, the HDR resource base in the U.S. alone represents a thermal energy equivalent to nearly 100 million megawatt centuries, about 10 times that of coal deposits.

A. Background

The world's first hot dry rock geothermal energy system was completed at Fenton Hill in 1977 and is referred to as the Phase I system. It was created by drilling a hole from the surface into granitic rock to a depth of approximately 3000 m, at about 195°C, producing hydraulic fractures centered at about 2600-m depth, and then directionally drilling a second hole to intersect those fractures. Water was produced from the man-made reservoir at temperatures and thermal power rates as high as 140°C and 5 MW_t. The system was enlarged in 1979 by additional hydraulic fracturing and then operated successfully for almost a year. Additional results of these early reservoir tests are provided by Dash et al. (1983).

To extend the technology to the temperatures and rates of heat production required to support a commercial power plant, construction of a larger, hotter, hot dry rock system was initiated at Fenton Hill in 1979. This is referred to as the Phase II system. Two new holes, about 50 m apart at the surface, were drilled directionally, the deeper one to a vertical depth of 4.39 km where the rock temperature was 327°C. Based upon experience in the shallower system described above, it was expected that hydraulic fractures produced from the new wells would be substantially vertical, with an approximately north-northwest strike. To provide the horizontal separation required to isolate a series of such fractures, the bottom 1000 m of each hole were drilled toward the east-northeast and inclined at 35° to the vertical. Figure I-1 shows a perspective view. The upper well, EE-3, lies 300 m above the lower well, EE-2, in the slanted interval. Also shown in Fig. I-1 is a Phase I reservoir well, which contains a geophone sonde. This sonde and similar seismic sensors emplaced in other boreholes detect microearthquakes triggered during hydraulic fracturing (House et al., 1985).

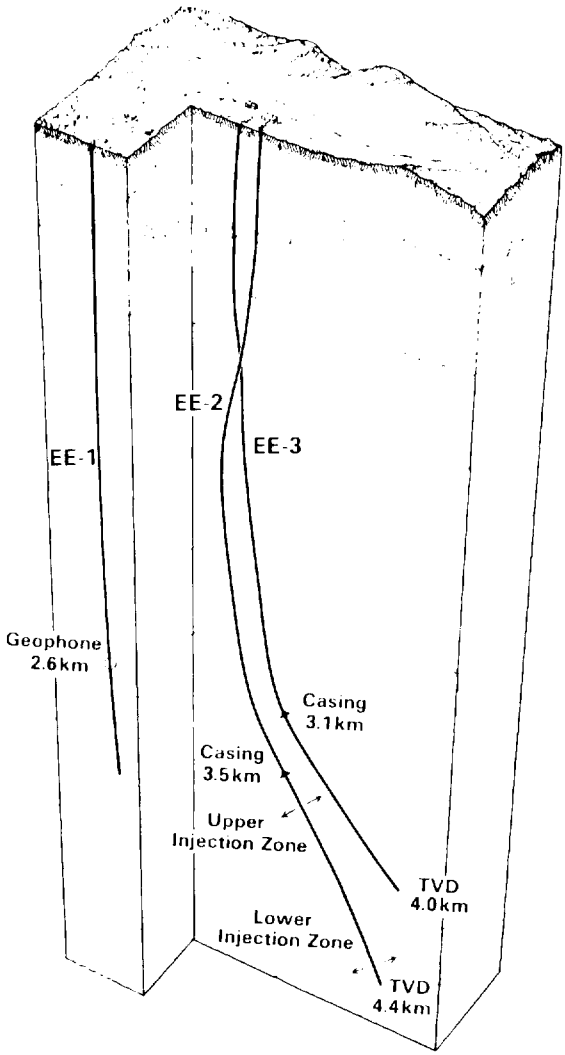

Figure I-1. Perspective view of Phase II boreholes and typical geophone tool emplaced for microearthquake monitoring during fracturing.

In 1982, hydraulic fracturing experiments were conducted at the greatest depths in the two new wells. Unexpectedly, the fracture zones produced were three-dimensional distributed networks of stimulated natural joints rather than single planar fractures. Furthermore, the fracture zones were inclined rather than vertical and did not connect the two wells hydraulically. The unexpected nonvertical inclination may be related to the presence of a cooling magma body beneath a volcanic caldera a few kilometers east of Fenton Hill, which altered the earth stresses.

In December 1983 a massive hydraulic fracturing operation was conducted in which 21 200 m^3 of water was injected at 3.5 km in the lower well at a downhole pressure of 83 MPa with an average flow rate

of 100 l/s. Details are provided by Dreesen and Nicholson (1985) and House et al. (1985). Figure I-2 shows the locations of the induced microearthquakes. Because of the extremely low background noise, the downhole seismic sensors detect events with extrapolated Richter body wave magnitudes as low as -5, however Fig. I-2 shows only the 850 high-quality events with magnitudes from -3 to 0. Note that seismicity is induced over an ellipsoidal rock volume that is about 0.8 km high, 0.8 km wide in the north-south direction, and about 0.15 km thick, or about 0.05 km^3 of fractured rock volume. This rock volume is about 2500 times greater than the water volume injected.

Despite the huge volume of water injected into the lower well during the massive hydraulic fracturing in 1983, the hydraulically fractured zone did not propagate into the vicinity of the upper well, as shown in Fig. I-2, and hydraulic communication between the two wells was

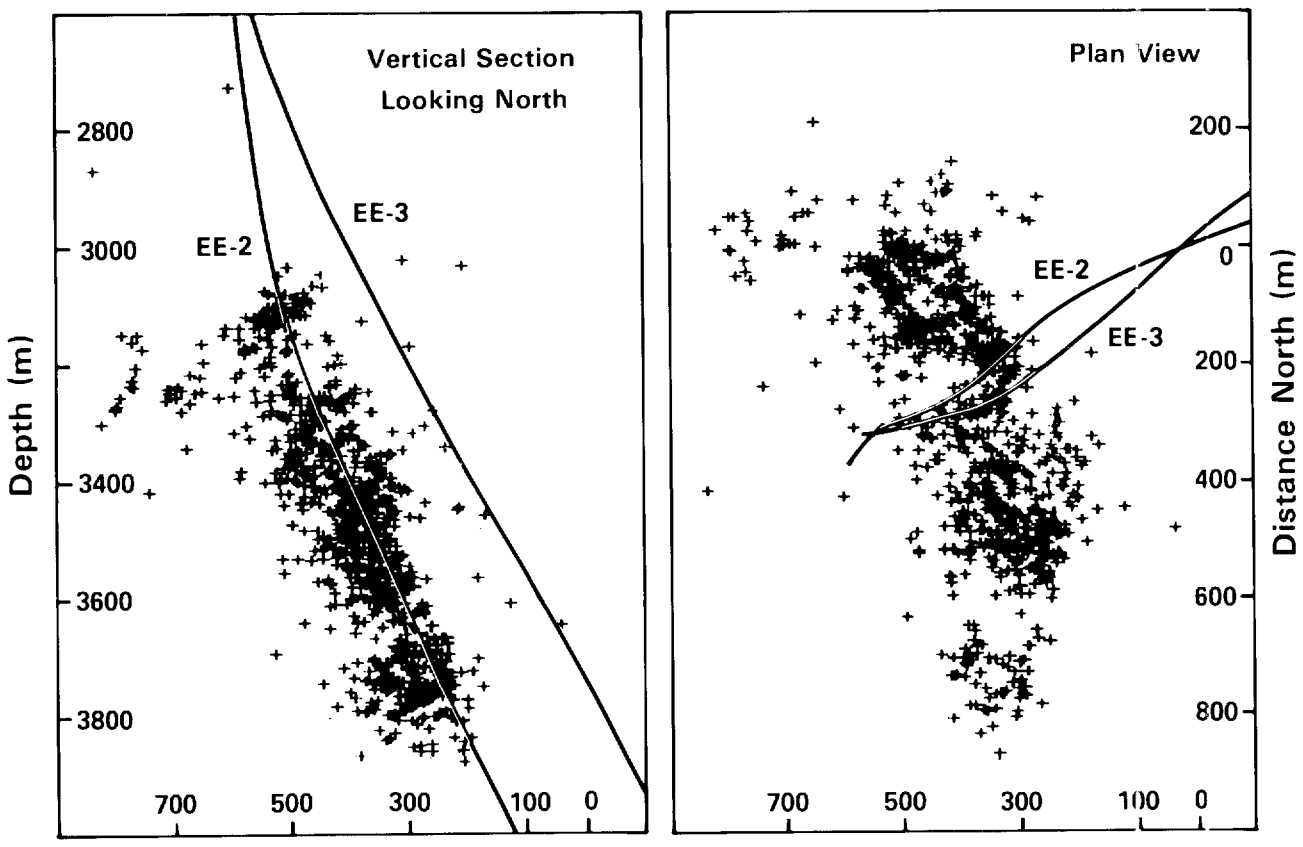

Figure I-2. Hypocentral locations of microearthquakes induced by massive hydraulic fracturing in injection well EE-2. Left-hand side presents elevation view, looking north, while right-hand side is plan view, looking down.

not observed. Another large fracturing operation was conducted, this time in the upper well (Dash et al., 1985), but the two stimulated zones did not overlap sufficiently and again no communication was observed. Consequently, in March of 1985 the upper well was sidetracked at a depth of 2.9 km and directionally drilled as shown in Fig. I-3 through the fracture zone created from the lower well. This redrilled well is referred to as EE-3A.

Low flow connections were observed at joints where water flowed into EE-3A during drilling while EE-2 was pressurized to 14.5 MPa. Hydraulic stimulation of the joints near 3.6 km was accomplished by setting a specially developed, high-temperature packer (Dreesen et al., 1986) in EE-3A at a depth of 3.52 km, where the drill hole was reasonably smooth, and then pumping water into the open-hole interval between the packer and the bottom of the hole, which at that time was

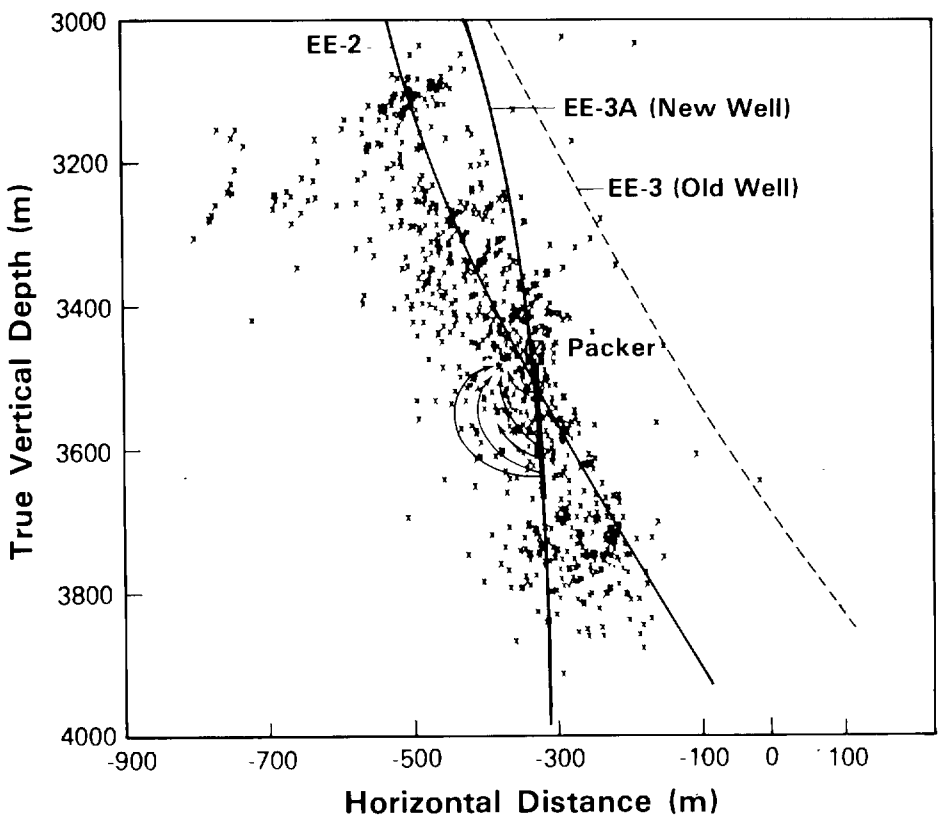

Figure I-3. Elevation view of reservoir, looking north. Packer shown allowed supplementary stimulation of EE-3A, which resulted in low flow resistance connection between EE-2 and EE-3A. The flow paths indicated are inferred from joint locations determined from a temperature survey in EE-3A.

located at 3.72 km. A postconnection temperature survey taken in EE-3A showed that several joints had been stimulated and served as flow entries from EE-3A to the reservoir.

Following this successful connection, the redrilled well was extended to 4 km and additional stimulations were conducted using the open-hole packers. The second stimulation was conducted very deep, at 3.83 km, and failed to result in additional hydraulic communication. The third stimulation, at 3.65 km, a depth about midway between the successful and unsuccessful ones, achieved another hydraulic connection, but the final stimulation, which occurred at 3.76 km, failed to result in additional hydraulic communication.

In March and April of 1986 the new reservoir was readied for preliminary testing by 1) cementing in a liner in well EE-3A, 2) installing a temporary surface piping system, 3) readying the water-to-air heat exchanger used previously for the Phase I reservoir, and 4) hiring a service company to pump water. The Initial Closed-Loop Flow Test was begun May 19, 1986, and completed on June 18, 1986. Cold water was injected into EE-3A, and hot water (as hot as 192°C) was produced from EE-2. The hot water was cooled to 20°C in the heat exchanger before being reinjected, and up to 10 MW_t was produced. Further details are provided in the remainder of this report.

B. Objectives

Experiment 2067, the Initial Closed-Loop Flow Test (ICFT), was designed as a precursor to a long-term energy-extraction experiment in the Phase II reservoir at Fenton Hill. Previous testing in this reservoir consisted of three stimulation experiments conducted in EE-2, Expts. 2018, 2020, and 2032 (the 1983 MHF), that initially created the system and two stimulation experiments during EE-3A redrilling operations, Expts. 2059 and 2062, that resulted in successful fracture connections. Injection parameters of interest from these experiments and the ICFT are summarized in Table I-I. The ICFT sought to prove the feasibility of the Phase II reservoir as an energy producer, determine important reservoir parameters necessary to the design of the final flow loop for the Long-Term Flow Test (LTFT), and evaluate various completion schemes for wellbore EE-3A and repair work on EE-2 (Dreesen and Nicholson, 1985). We envisioned that, at the end of the ICFT, the final

TABLE I-I

SUMMARY OF PERTINENT PHASE II RESERVOIR INJECTIONS

Expt. Number	Date	Injection Wellbore	Open-Hole Interval (m)	Volume Injected (m^3)	Nominal Rate (m^3/s)	Nominal Pressure (MPa)[a]	Connection to Other Well
2018	82/07/19-82/07/20	EE-2	3528-3656	910	0.0315	48.3	no
2020	82/10/06-82/10/07	EE-2	3528-3656	3090	0.0928	46.9	no
2032 (MHF)	83/12/06-83/12/09	EE-2	3528-3550	21 200	0.1140	48.0	no
2059	85/05/27-85/05/28	EE-3A	3516-3719	1590	0.0106	31.7	yes
2062	85/07/18-85/07/20	EE-3A	3651-3825	5770	0.0106	35.9	yes
2067 (ICFT)	86/05/19-86/06/18	EE-3A	3487-3750	37 000	0.0106 0.0185	26.9 30.3	yes

[a] Surface injection pressure.

completion of EE-3A would be accomplished and surface loop design, procurement, and construction could begin. In this section the goals and objectives of the experiment are discussed in more detail, along with a short rationale for each item and a justification of various decisions made in preparation for this flow test.

1. Reservoir Characteristics. All Phase II (wells EE-2 and EE-3A) flow tests to date had been either single-well hydraulic stimulation experiments or very short interwell flow tests after a connection was achieved. Thus, important long-term reservoir information necessary for the design of a permanent flow loop had not been obtained.

2. Flow Splits. Experiment 2059 stimulated a shallower depth of the wellbore by setting the packer at 3.52 km (11 537 ft). A deeper set of fracture connections was created during Expt. 2062 with the packer at 3.65 km (11 976 ft). Information about the relative flow rates and

volumes of the 2059 and 2062 reservoirs would help determine whether to keep the 2059 fractures in the system for the final completion. A chemical tracer experiment would provide a rough estimate of the heat-transfer capacity of this reservoir by comparing the modal volume to previous reservoirs. If the modal volume was less than 150 m^3, then the 2059 reservoir probably had an insufficient heat-transfer capacity and should be isolated from the remainder of the fracture connections in the final completion.

3. Impedance. Since the 2059 and 2062 reservoirs had never been operated in together, we needed to know what the overall impedance would be. Furthermore, impedance was likely to drop during the test, so a longer ICFT would provide a better estimate of long-term flow behavior. These data were of primary importance for pump selection and determination of power requirements for the long-term loop.

4. Water Loss. Pumping at pressures and flow rates sufficient to achieve hydraulic fracturing is obviously of little use in determining water-loss characteristics at closed-loop, recirculating conditions. The ICFT would provide these essential water-loss data. Again, the longer the test, the more relevant the data would be to the permanent system design.

5. Geochemistry. Our estimates of dissolved gases and the possibility of corrosion and scaling in the surface and downhole piping were based entirely on the hydraulic stimulation experiments and the Phase I operations. A circulating loop operated for 30 days should allow the dissolved components (gases and ions) to reach their ultimate values. During the ICFT we planned no major water treatment program. The objective was to monitor the buildup of dissolved species and evaluate the severity of chemical problems both during the ICFT and in future operations. The dissolved CO_2 content at the end of the test would indicate whether a separator was necessary in the final surface system design. Corrosion coupons would be examined periodically since protection of the heat exchanger and rented pumps was imperative for this experiment. Surface piping would be checked for corrosion and solids deposition after the ICFT.

6. Tracer Experiments. Fracture volume and dispersive characteristics can be measured most effectively using tracers. The primary goal

of the tracer tests would be to measure the system residence time, which would indirectly tell us whether the 2059 reservoir had sufficient heat-transfer capacity to be incorporated into the long-term loop. Since more detailed information about fracture geometry is possible with a radioactive tracer, we prepared to run $NH_4{}^{82}Br$. We had also planned, but decided not to run, the first reactive tracer experiment in the Fenton Hill reservoir. Ultimately, this technique could provide a method for rapidly determining the rate of reservoir cooldown, and in the ICFT this test would have been considered to be a baseline experiment to develop the best operational procedures for performing these new tracer tests.

II. SYSTEM DESCRIPTION, OPERATIONS, AND PERFORMANCE

A. Wellbore Configurations

1. Production Well EE-2. The 244.5-mm (9-5/8-in.) production casing in EE-2 was severely damaged in December 1983 during the uncontrolled blowdown that occurred after pumping 21 200 m^3 (5.6 million gal.) of water (Expt. 2032 MHF) into the 3530- to 3550-m (11 580- to 11 648-ft) deep interval extending from the 244.5-mm (9-5/8-in.) casing shoe to a sand and barite plug in the open hole as shown in Fig. II-1. The tubing, the tubing-production casing annulus (backside), and the production casing-intermediate casing annulus were all in direct communication with the subhydrostatic aquifers between 520 and 760 m (1700 and 2500 ft) deep several months after the blowdown.

The damaged 139.7-mm (5-1/2-in.) tubing was removed to a depth of 3268 m (10 722 ft) and the well repaired during the fall of 1984. Two cementing (squeeze) placements behind the production casing at 3170 to 3230 m and 1980 to 2774 m (10 400 to 10 600 ft and 6500 to 9100 ft), using 3.8 m^3 (24 bbl) and 27.8 m^3 (175 bbl) of cement respectively, eliminated the direct communication. The high risk of additional repairs and a limited budget prevented the removal of the remaining tubing and packer below 3268 m. A small drill pipe string was used to clean out through the fish into the open hole below the production casing to a depth of 3548 m (11 640 ft). A second packer and a repaired tubing were installed as shown in Fig. II-1. Slim-hole logging tools

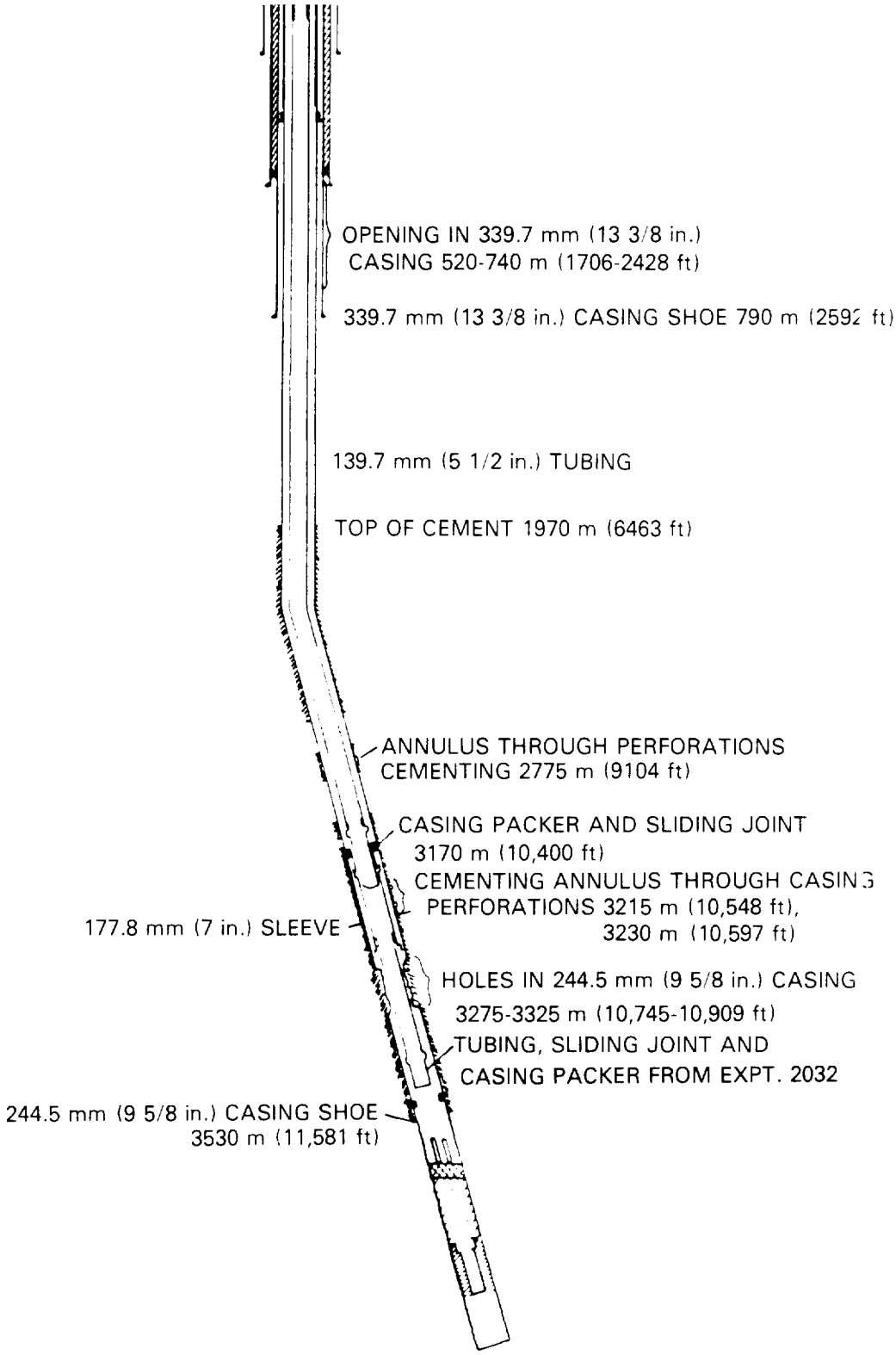

Figure II-1. EE-2 well configuration during the ICFT.

were successfully run into the open hole. An injection test showed that the well remained in pressure communication with an 11.7-MPa (1700-psi) injection zone (possibly Phase I) above the production casing shoe.

EE-2 was first produced during the two connection experiments (Expts. 2059 and 2062). Several weeks before Expt. 2059, EE-2 was cleaned out with a 25.4-mm (1-in.) coil tubing unit to 3473 m (11 394 ft) using 0.35 m^3/s (750 SCF/min) of nitrogen. A large amount of mud was removed. The coil tubing was friction stuck after the mud was unloaded. After cooling the well by circulating soap and cold water, the tubing was removed. Subsequent attempts to log the well with 54.0-mm (2-1/8-in.) o.d. tools encountered an obstruction at 3215 m (10 550 ft), and no further logging below this depth was attempted.

During the second connection stimulation (Expt. 2062), the EE-2 backside began to flow. A small leak between the tubing and the production casing-tubing annulus has been observed intermittently since that flow was first noticed.

2. Injection Well EE-3A. EE-3A was completed in April and May of 1986. The completion followed 10 open-hole packer runs resulting in 6 injection tests in isolated regions of the wellbore. In two of these injection tests, connections to EE-2 were demonstrated: 1) Expt. 2059 injection resulted in injection into four intervals between 3515 and 3712 m (11 532 and 12 180 ft); and 2) Expt. 2062 resulted in injection into four intervals between 3650 and 3749 m (11 975 and 12 300 ft). The packer was stuck in the hole on the final packer run and left at 3750 m (12 300 ft). The configuration of the wellbore at the beginning of the completion operations is shown in Fig. II-2.

Initial completion plans called for a permanent packer, developed in conjunction with Baker Production Technology (formerly Lynes Inc., presently Baker Service Tools), to be set. The packer failed 3 days after it was successfully set and tested at 3560 m (11 685 ft). The packer completion is shown in Fig. II-3.

After fishing out the packer from 3560 m, the wellbore was prepared for a cemented-in liner completion. The bottom of the liner was to be located in an in-gauge wellbore section at 3600 m (11 810 ft), and the well was temporarily plugged back to that depth with sand. A 139.7-mm (5-1/2-in.) liner was run and cemented in using the puddling technique.

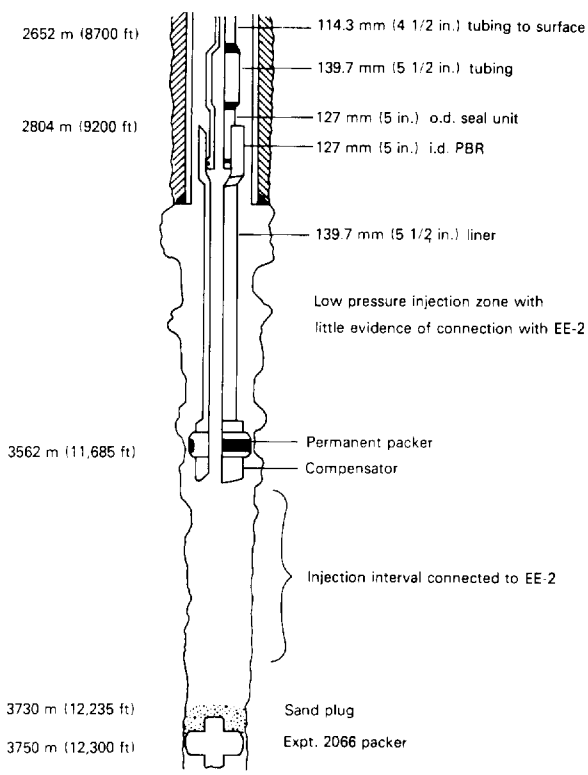

Figure II-3. EE-3A well configuration after installation of a permanent packer at 3560 m (11 685 ft). The packer failed after 3 days and was removed.

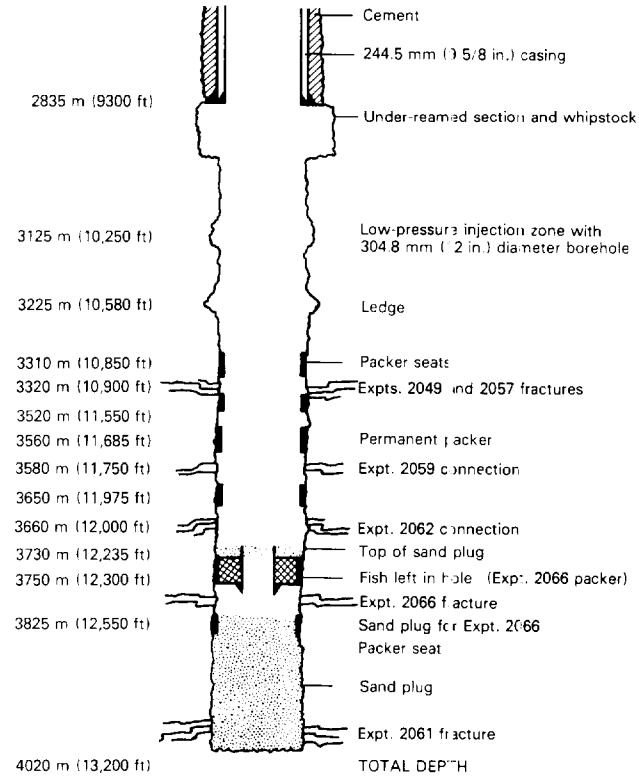

Figure II-2. EE-3A well configuration before the ICFT well completion.

The liner was to have been installed over the main fracture entry point observed after Expt. 2059 at 3580 m (11 750 ft), but an early set of the cement prevented completion of the procedure and the liner bottom was located at 3485 m (11 435 ft). A cement sheath from 3485 to 3600 m remained in the hole after cleanout. A subsequent cement bond log showed that there was good cement behind the liner from 3485 to 3340 m (11 435 to 10 950 ft), and the liner was judged to be satisfactory for the ICFT experiment.

A pressure test of the liner showed that a leak had developed in a threaded connection above the cement top. The liner was backed off in a VAM™ connection at 3530 m (11 590 ft) and the liner was replaced with new VAM™ casing. A screw-in was successful on the first attempt using a machine shop fabricated VAM™ screw-in sub. The liner and open hole were cleaned out to 3729-m (12 235-ft) depth and the well completed with a 127-mm (5-in.) seal assembly, 150-m (500-ft) long 139.7-mm (5-1/2-in.) cushion tubing, and 114.3-mm (4-1/2-in.) tubing as shown in Fig. II-4.

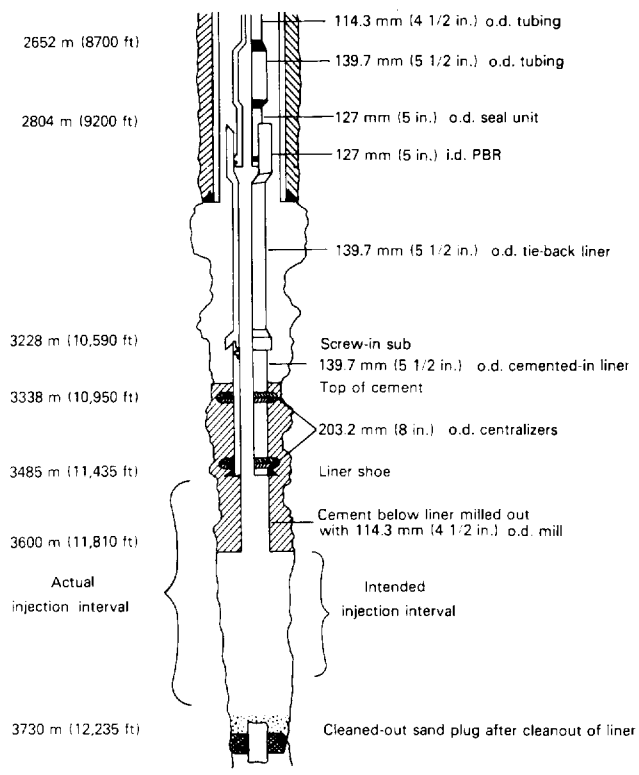

Figure II-4. EE-3A well configuration after installation of the cemented-in liner. This was the configuration of the well for the ICFT.

B. Surface System

A schematic of the surface system is shown in Fig. II-5. This system was constructed as a temporary experimental surface system to meet the needs of the ICFT. The major subsystems were the EE-2 and EE-3A wellheads, the heat-extraction system, the feed-water system, the main circulating pumps, the chemical-sampling system, data acquisition and control, and the seismic system.

The surface piping system may be divided into six segments, according to the pressure rating of each segment. The first segment was the EE-2 wellhead up to the high-low safety valve. This segment consisted of 69-MPa (10 000-psi) API-rated wellhead, master valve, wing valves, 103-MPa (15 000-psi) rated hammer union pipe and pipe fittings, and the 34.5-MPa (5000-psi) rated high-low safety valve. The high-low valve was the key element to protect lower pressure-rated items downstream. This valve automatically shut in the well if the pressure exceeded 4.8 MPa (700 psi) or dropped below 1.7 MPa (250 psi). This segment also contained vent lines to the surface pond through choke manifolds and the low-pressure gas separator.

The second segment of the system was between the high-low valve and control valve CV-1. This was rated at 10.3 MPa (ANSI 1500 psi), which has a 22.6-MPa (3280-psi) working pressure at 204°C (400°F) and a 38.4-MPa (5575-psi) hydrostatic proof pressure. This valve was installed to drop the pressure, if necessary, down to a safe operating value for the third segment of piping. It was used during high-back-pressure experiments and as an isolation valve during the cleaning of the strainer.

The third segment lay between the control valve CV-1 and the back-pressure control valve CV-6. Control valve CV-6 has a 4.1-MPa (ANSI 600-psi) rating, or a cold working pressure of 10 MPa (1450 psi) and a hydrostatic test pressure of 15.3 MPa (2225 psi). The piping in the heat exchanger area, which is part of this third segment, was constructed by the Zia Co. in 1982. The finned-tube, forced-draft, water-to-air heat exchangers have a working pressure rating of 17.2 MPa (2500 psi) at 260°C (500°F) and were hydrostatically tested several times to 19.3 MPa (2800 psi). This third segment of piping was protected by a 38.1-mm by 63.5-mm (1-1/2-in. by 2-1/2-in.) Kunkle pressure relief valve with a

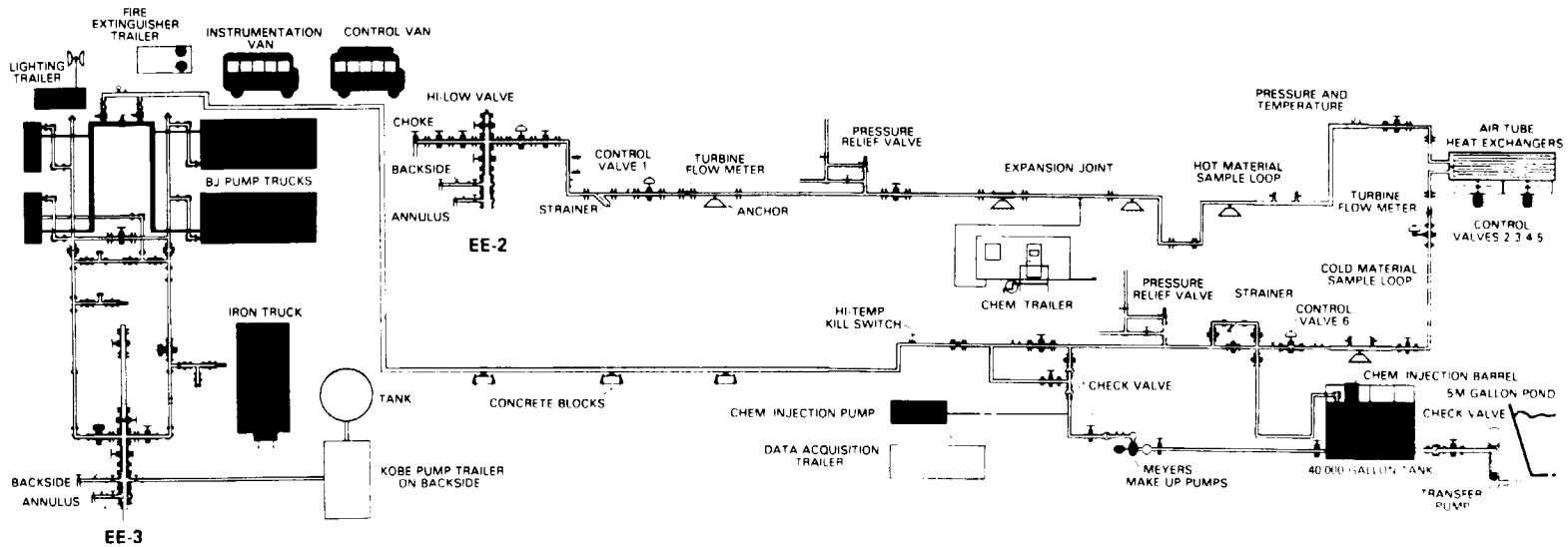

Figure II-5. Schematic of the ICFT surface system.

0.0003245-m^2 (0.503-in^2) nozzle. This valve handled all anticipated flow rates from the EE-2 well, provided that the water was cool. As the water became hotter, there was a tendency for the nozzle to convert to two-phase flow and choke the flow at about 0.00265 to 0.0053 m^3/s (1.0 to 2.0 bpm). This pressure relief valve was set at 4.1 MPa (600 psi) for all of the experiment except for some high-back-pressure experiments where control valve CV-1 was not used.

The fourth segment of piping was downstream of CV-6. It incorporated all of the system downstream of the Meyers makeup pumps and terminated at the suction inlet manifold to the B.J. Titan contract pumps. This section was low pressure, 1.2-MPa (175-psi) normal working pressure, and was protected with a 50.8-mm by 76.2-mm (2-in. by 3-in.) safety relief valve set at 1.7 MPa (250 psi). This relief valve flows 0.0186 to 0.0212 m^3/s (7 to 8 bpm) at its maximum open pressure of 2 MPa (290 psi). This section was plumbed with 101.6-mm (4-in.) schedule 40 and 160 pipe, 76.2-mm (3-in.) schedule 80 and 160 pipe, and 152.4-mm (6-in.) schedule 40 and 80 pipe. The weakest parts of this segment were the two class-150, 101.6-mm (4-in.) check valves downstream of the Meyers pumps, which have a rating of 2 MPa (285 psi) at 38°C (100°F). The rest of the segment was grossly overdesigned with schedule 80 and 160 pipe, which was on hand.

The fifth segment was the 18 900-m^3 (5 million-gal.) pond to the 150-m^3 (40 000-gal.) holding tank. This system was contractor installed, was low pressure [less than 0.3 MPa (50 psi)], and went from open pond to open tank. The suction for the Meyers makeup water pumps came from the 150-m^3 (40 000-gal.) tank.

The sixth and possibly most critical segment of pipe was the high-pressure contract piping that injected the water into the reservoir via EE-3A. This was supplied by the B.J. Titan Co., the oil field pumping contractor that had been selected to provide the high-pressure pumping services on a competitive bid. The specifications for this work had required both pumping services and equipment. The piping was rated at 103-MPa (15 000-psi) working pressure. It consisted of 76.2-mm (3-in.) pipe with hammer unions, valves, etc., feeding our 69-MPa (10 000-psi) API-rated wellhead. The equipment specified for this section was inspected before being accepted.

The B.J. Titan system was assembled around a suction and discharge manifold trailer and four truck-mounted frac pumps, using 12V149 Detroit diesel engines, 8961 Allison five-speed transmissions, and 1300 OPI plunger pumps. Pumps were remotely controlled from a treating van. Pressure, flow, and temperature were monitored and recorded in a second van.

B.J. Titan also provided double 101.6-mm (4-in.) suction and 76.2-mm (3-in.) discharge lines, which were used with remote-operated wing valves on the wellhead. A 50.8-mm (2-in.) vent line was laid to the pond.

Critical parts of the entire surface system piping were anchored with about 40 concrete safety blocks. These blocks were precast by a firm in Albuquerque using 27.6-MPa (4000-psi) concrete. All blocks weighed between 1140 and 1820 kg (2500 and 4000 lb) and were additionally staked to the ground using 25.4-mm (1-in.) diameter stakes. These blocks either sat over the pipe with the pipe running through tunnels precast into the blocks, or the pipes sat on top of the blocks and were anchored with straps that were fastened to anchor bolts cast into the blocks. Further details on the surface system components, fabrication, safety, etc., are contained in Appendix A.

C. Data Acquisition

1. Flow Loop Instrumentation and Recording. Signals from all active transducers, measuring temperatures, pressures, and flow rates, were conditioned and recorded in the Data Acquisition Trailer (DAT). The data from the active transducers were digitized and processed on a Hewlett Packard 9835 computer. These data were recorded on disk, displayed on a large CRT screen, and printed. The computer was programmed to provide a number of options that allowed visual and audible alarm of selected data channels should the measurement exceed either a high or low limit. Data from each channel were averaged over a specified time interval selected by the operator and easily changed through a function key. The data rate for printout was also selectable over a range of once per minute to once per hour. However, if an alarm should occur, the computer would automatically revert to maximum output rate. The program also allowed the operator to select a data channel interrupt to facilitate maintenance such as changing out transducers,

balancing pressure gauges, etc. Some data channels were used primarily for process control and alarm but were not printed out or stored (i.e., air compressor pressure). Data channels for the flow loop were set up as shown in Appendix B (Table B-I).

A remote control panel was designed and installed in the DAT that would allow remote operation of the six control valves used in the system. This control system also provided on-off control for the makeup pumps and heat exchanger fans. Makeup pumps could be cycled from time to time to reduce downtime and increase flow on demand. The system also allowed for manual override at the pump or fan location. The data acquisition and control system remained on-line for the entire flow experiment (May 19 through June 18) and the following extended shut-in to monitor all wellhead pressures and temperatures. The HP9835 computer and associated data acquisition equipment were run off an uninterruptable power supply system (UPS), and the only downtime recorded throughout the experiment was during monitoring of the shut-in when the system was running unmanned.

2. Seismic Coverage Instrumentation. The three separate seismic detection networks were used throughout the interim flow test. Nine surface stations, using the S-13 seismometers, are located on a radius of approximately 3.2 km (2 miles) from the EE-2/EE-3A wellheads. These stations are powered by batteries with solar panels used to maintain sufficient charge during the long-term operations. Data from each station are transmitted to the DAT via FM/FM telemetry. The seismic signal is converted to a VCO frequency that is used to modulate a radio frequency carrier for "line-of-sight" transmission to the receiving system located in the DAT. The frequency response for each seismometer data channel is 100 Hz. The output data are conditioned for interfacing to a MASSCOMP computer system for continuous recording and data storage.

Secondly, three "Precambrian" geophone stations are located on an approximate 1.6-km (1-mile) radius from the EE-2/EE-3A wellheads. The geophones are emplaced in boreholes drilled into the volcanic-Precambrian rock interface at about 610 m (2000 ft). The output signals from each station (PC-1, PC-2, and GT-1) are transmitted to the surface via wireline where the signals are processed in systems identical to the surface network except the data channel frequency response is 300 Hz.

The third seismic detection system was designed to use a triaxial geophone array to be emplaced in deep boreholes adjacent to the EE-2/EE-3A system. The triaxial geophone package was deployed on a seven-conductor armored wireline in EE-1 to a depth of 2865 m (9400 ft). The output microseismic (acoustic) signal detected by each geophone was amplified and transmitted to the surface over the seven-conductor wireline. These data were then conditioned for interfacing to the MASSCOMP. A parallel data link was wired to a digital storage scope (Biomation) for on-line "quick look" analysis to determine the proper operation of the downhole system occasionally.

Figure II-6 shows a block diagram of the recording and data acquisition system for the entire seismic network. Data were also recorded on analog tape recorders used as backups when the MASSCOMP was inoperative. Tape recorder channel assignments are shown in Appendix B (Tables B-II and B-III). The surface seismic stations are coded FNHR, BRLY, etc. The Precambrian stations are coded PC-1, PC-2, and GT-1, and the deep triaxial geophone package nomenclature refers to the EE-1

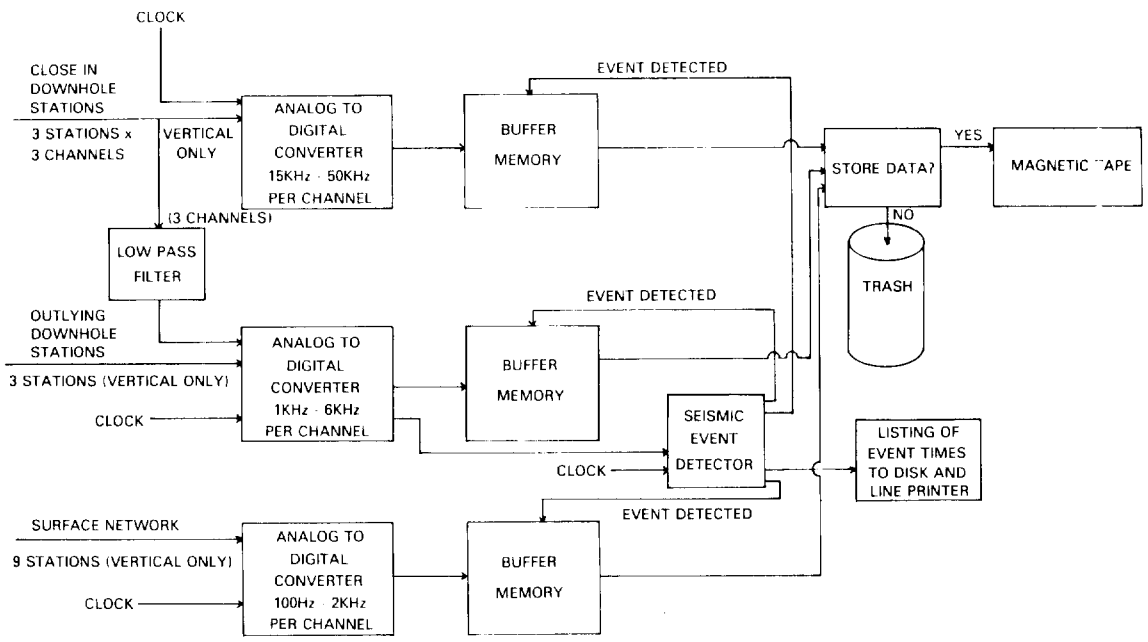

Figure II-6. Schematic of the Hot Dry Rock seismic digital event detecting and recording system.

borehole vertical geophones, upper horizontal geophones, and lower horizontal geophones. Upper horizontal and lower horizontal describes the location of the respective transducers in the geophone cradle forming an orthogonal set.

The overall system performance of the entire seismic/microseismic network performed very well, providing maximum coverage and data collection. The surface seismometer network and the Precambrian geophone array were monitored continuously throughout the experiment except for occasional downtime for maintenance and repair. The triaxial geophone sonde was deployed in the EE-1 wellbore during high-injection pressure tests. During the ICFT the triaxial geophone was deployed at four different intervals of time, the shortest interval being 12 hours and the longest interval being 51 hours. Total time on station in EE-1 was 96.5 hours.

3. Borehole Temperature Measurements. A series of borehole temperature surveys were made in EE-2, EE-3A, EE-1, and GT-2B as an integral part of the ICFT. Background and postexperiment temperature surveys were made using Los Alamos logging equipment. Since the EE-3A wellbore was pressurized above 28 MPa (4000 psi) throughout the pumping experiment, it was not possible to use the Los Alamos logging equipment to run temperature surveys during this time. The high-temperature service cable used by Los Alamos is not well suited for high-pressure service above 17 MPa (2500 psi) and the Bowen packoff for the 11.1-mm (7/16-in.) diameter cable is only rated for a wellhead pressure of about 21 MPa (3000 psi). Therefore, three temperature surveys were made in the EE-3A borehole during the flow test by a commercial oil field service company (Oil Well Perforators) using a high-pressure grease-injector control head and lubricator on the wellhead and a small-diameter cable.

Temperature measurements in the EE-2 production well were made using a slickline (a wireline with no electrical conductors) and a high-temperature Kuster sonde that recorded temperature using a stylus on a metal film driven by a mechanical clock. Four temperature surveys, three obtained during the ICFT and the one made when the flow test was terminated, were run by Tefteller, Inc. The tools were lowered in the wellbore at a rate of 0.25 m/s (50 ft/min) and stopped periodically to

allow complete stabilization of temperature and to verify time-depth correlation. Upon retrieval of the tool from the well, data points were chosen to give definition to any temperature anomalies. Because of the damaged EE-2 wellbore, temperature surveys could not be run below 3185 m (10 450 ft). Results of the wellbore temperature logging are discussed in Section III.

D. Loop Operations

The system was operated 24 hours per day using rotating shifts. Each shift consisted of an experiment manager who was in overall charge of the shift, two electronic technicians who controlled the system from the Data Acquisition Trailer (DAT) and were also responsible for all instrumentation and control, two mechanical technicians who operated out of the operations building and made hourly checks of the surface system, three contract pumping people working out of the B.J. Titan control vans, a chemical technician located in one of the two chemistry trailers, an emergency medical technician located in the operations building, and a security guard. On-site communications were provided by an intercom system, which was backed up by portable radio communication.

The various modes of system operation are listed below:

1. Start-up mode. 100% makeup water into EE-3A; EE-2 in vent mode.
2. Vent mode. All production fluid vented directly to EE-1 pond.
3. Closed-loop mode. Normal operating condition with all production fluid cooled and returned to the injection pumps. Makeup water added as needed.
4. Gas-purge mode. All production fluid cooled and diverted through makeup water-holding tank.
5. Fresh-water-flush mode. 100% makeup water with all production fluid cooled and vented to the EE-1 pond.
6. Shut-in. Both wells shut in but instrumentation left on.

The system operated as follows. Water was transferred from a 18 900-m^3 (5 million-gal.) pond to a 150-m^3 (40 000-gal.) holding tank. Water was drawn from this tank as needed and fed to the high-pressure injection pumps by the makeup/feed-water pumps. Water leaving these pumps was injected into the reservoir via the injection well, EE-3A. After passing through the reservoir, the water returned to the surface through the production well, EE-2. The hot production stream was piped

to the heat exchangers where it was cooled before being combined with the makeup water and returned to the injection pumps.

System operations were started by filling the holding tank with water from the 18 900-m^3 pond and then starting the makeup pumps. After the lines were filled with water, the high-pressure (B.J. Titan) injection pumps were brought on-line and the inflation of the reservoir began. The system was operated by setting the injection flow rate and temperature into EE-3A. The surface pressure of the production well (i.e., the back pressure) was controlled, and the reservoir determined the flow rate and the temperature. When the reservoir was inflated sufficiently, as indicated by a rise in pressure at EE-2, the system was put into vent mode. Once the system was purged of start-up gas, the vent to the pond was valved off, flow was directed to the heat exchangers, and closed-loop operation started.

Throughout the 30-day test the system was operated in various modes as needed. When the dissolved gas content of the water became too high for the chemists to obtain a total gas measurement, the system was run in gas-purge mode (open system operation). For system maintenance, the loop was usually put into vent mode where all of the returns were dumped into the EE-1 pond; on a few occasions the well was shut in. Sufficient excess pumping equipment had been specified to allow for routine maintenance to be accomplished without interruption of the loop. During power failures, all pumping was stopped and the production well was vented to the EE-1 pond. High-back-pressure mode was used during closed-loop operations. EE-2 pressure was increased by simply closing down a control valve. For fresh-water-flush mode, an open system operation, the returns from the production well were first cooled in the heat exchangers and vented to the EE-1 pond. All injection fluid was then supplied by the makeup water system.

The system was shut down by turning off the injection pumps and shutting in EE-3A and EE-2. Pressure instrumentation on both EE-2 and EE-3A was left in place with the data acquisition computer running and recording. Appendix C gives a chronological summary of operations.

E. Borehole Performance

On June 8, the 20th day of the test, a 5100-kg (155 000-SCF) slug of nitrogen was injected during a 30-min interval. The main purpose of

the gas injection was to attempt to clean out the EE-2 production interval. Some sand and mud had previously been removed from EE-2 by surging the well. By gas lifting the production well to increase flow velocity, it was felt debris that was thought to be filling and covering near wellbore fractures could be removed. Although a significant surge of flow occured, little debris was seen. Review of production data showed that the flow rate measurements were inflated because of continuing nitrogen production.

Two radioactive (^{123}I) velocity logs were run in EE-3A, and their results are summarized in Table II-I. The fact that the observed cross flow during shut-in was flowing from the upper zone to the lower zone was surprising based on the original injection pressures measured during Expts. 2059 and 2062. This cross flow may be evidence of a large convection system that was driven by thermal buoyancy and possibly increased by nitrogen left in the reservoir, or by the cooled injection zone. The velocity logs are in good agreement with the temperature logs discussed in Section III.

When temperature logs were run in EE-3A, a collar locator log was run through the lower tubing, seal assembly, polished bore receptacle, and liner. Table II-II shows the results of calculations that check the operation of the PBR/seal assembly expansion joint. From this analysis it appears that the seals were never locked up by scale or debris during the test. The temperature logs and velocity surveys all showed that the liner, the PBR seals, and the screw-in-sub connection were not leaking during or after the ICFT.

EE-3A backside performance is examined in Fig. II-7 where EE-3A backside flow during the ICFT is compared to both EE-3A and EE-2 pressures. A comparison of backside performance to EE-3A frontside pressure (Fig. II-7a, b, and c) indicates a flow response on the backside that lags frontside pressure by approximately 2 days. There are also common pressure inflections between the frontside and backside during the shut-in. However, it seems clear that the leak path between the frontside (tubing) and backside is long and tortuous. A tubing or liner leak would not act this way. A microannulus in the cement or small fractures or porosity in the cement or near-wellbore rock would better explain the pressure flow performance. The shut-in temperature

TABLE II-I

RESULTS OF RA VELOCITY LOGS IN EE-3A

Depth m (ft)	Description	Flow Rate Observed[a] Injection Log 6/16/86 m^3/s (gpm)	Shut-in Log 6/23/86 m^3/s (gpm)
3456 (11340)	Inside liner	0.01735 (275)	0 (0)
3485 (11435)	Bottom of liner	0.01735 (275)	0 (0)
3500 (11484)	Cemented open hole	0.01735 (275)	
3515 (11532)		0.01640 (260)	
3538 (11608)			Fluid entry
3545 (11632)		0.01640 (260)	0.000158 (2.5)
3553 (11658)		0.01356 (215)	
3561 (11682)		0.01136 (180)	
3572 (11718)		0.01136 (180)	0.000189 (3.0)
3584 (11758)		0.00852 (135)	0.000170 (2.7)
3597 (11800)			0.000126 (2.0)
3608 (11838)		0.00852 (135)	0.000095 (1.5)
3620 (11878)		0.00536 (85)	
3625 (11892)		0.00473 (75)	
3630 (11908)		0.00442 (70)	
3634 (11922)		0.00252 (40)	
3639 (11938)		0.00126 (20)	0.000076 (1.2)
3658 (12000)		0.00126 (20)	
3675 (12056)		0 (0)	0 (0)
3729 (12235)	Cleanout TD		

[a] All flows observed were down flows.

log (Fig. III-2, discussed later) would also suggest a long flow path with many small pressure drops between 3320 and 3535 m. The gradually increasing backside flow during the experiment may reflect a slowly expanding pressure field around the main reservoir.

EE-2 pressures (Figs. II-7d and e) at times seem to be related to backside flow at EE-3A. On several occasions the EE-3A backside flow

TABLE II-II

EE-3A EXPANSION JOINT PERFORMANCE

127-mm (5-in.) i.d. Polished Bore Receptacle
127-mm (5-in.) o.d. Molyglass Seal Mandrel

Activity	Date	Average Tubing Temp[a] °C (°F)	Differential Pressure MPa (psi)	Seal Mandrel Position Measured[b] m (ft)	Seal Mandrel Position Calculated m (ft)
Static temp log	5/15/86	116 (240)	0	4.3 (14) initial condition	4.3 (14)
Injection temp log 0.0106 m^3/s (4 bpm)	5/28/86	41 (105)	25.9 (3750)	8.2 (27)	8.9 (29)
Injection temp log 0.0172 m^3/s (6.5 bpm)	6/16/86	33 (91)	31.0 (4500)	8.5 (28)	9.5 (31)
Shut-in temp log 5-day shut-in	6/23/86	91 (196)	12.8 (1850)	5.2 (17)	6.0 (20)

[a] Average temperature calculated using $T_{ave} = \frac{15.5°C + T_{bh}}{2}$ where T_{bh} is the temperature in °C at 3322 m (10 900 ft).

[b] Measurements based on casing collar locator logs with assumed accuracy of ± 0.3 m (± 1 ft). A position of 0 represents a fully closed expansion joint.

appeared to increase a short time after the EE-2 frontside was shut in, though there does not seem to be a consistent pattern. There also appears to be some response in EE-3A to changes in EE-2 backside pressure, but still a clear pattern is not observed.

Figure II-8a shows the EE-2 backside pressure during the ICFT and the first 30 days of the shut-in. For comparison, the EE-2 annulus pressure is shown on Fig. II-8b, the EE-2 frontside (production) pressure is shown on Fig. II-8c, the EE-2 production temperature on Fig. II-8d, and the EE-3A frontside (injection) pressure on Fig. II-8e. From these plots it is concluded that the EE-2 backside is in intermittent pressure communication with the EE-2 tubing (frontside) with no observable time delay. Failure of the EE-2 casing packer was later

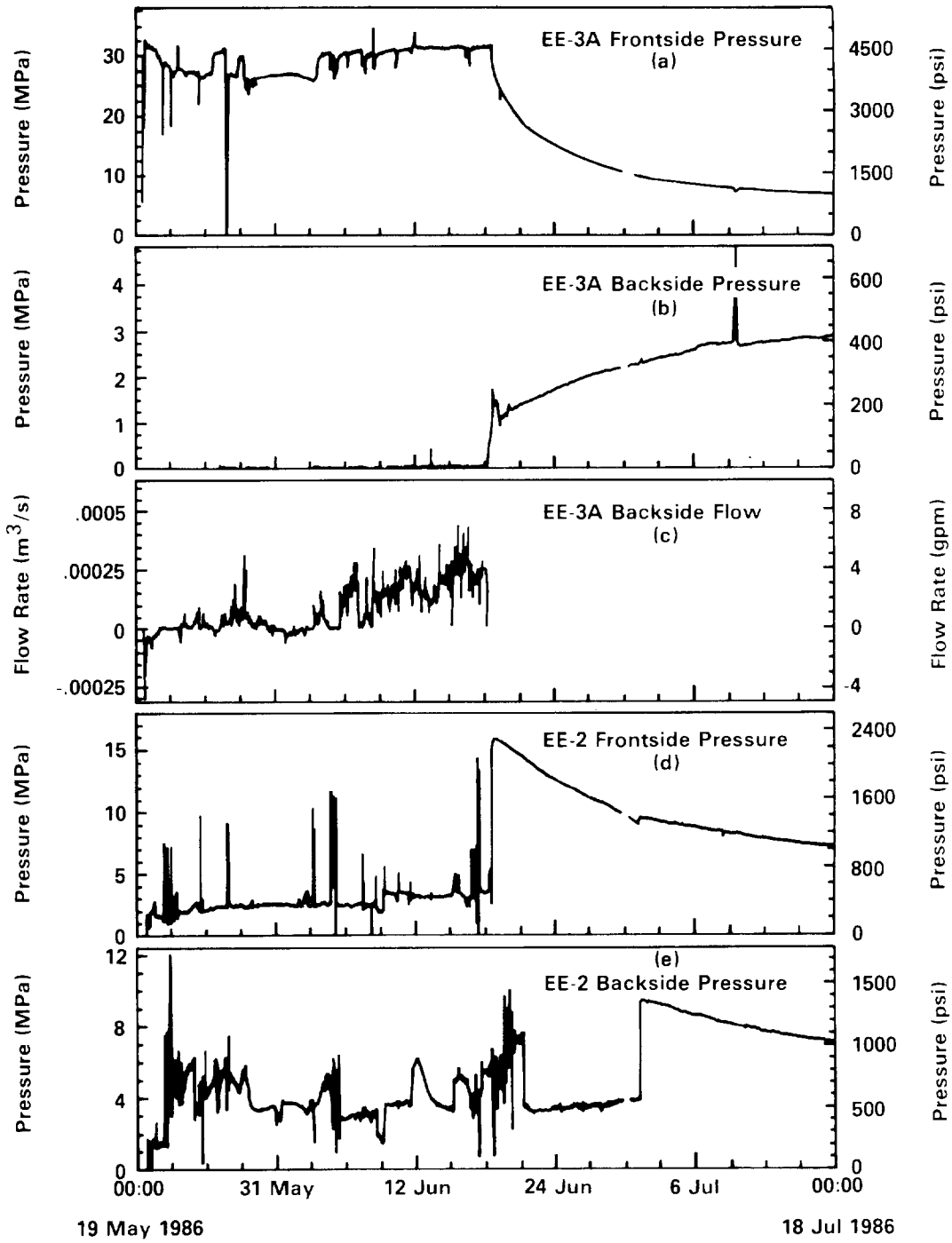

Figure II-7. EE-3A backside flow compared to EE-3A and EE-2 pressures: a) EE-3A frontside pressure, b) EE-3A backside pressure (there is some evidence of a 2-day response on the backside to pressure changes on the frontside), c) EE-3A backside flow data (negative flow occurred as the well was cooled and liquid was added to the backside to make up for fluid contraction), d) EE-2 frontside pressure, and e) EE-2 backside pressure.

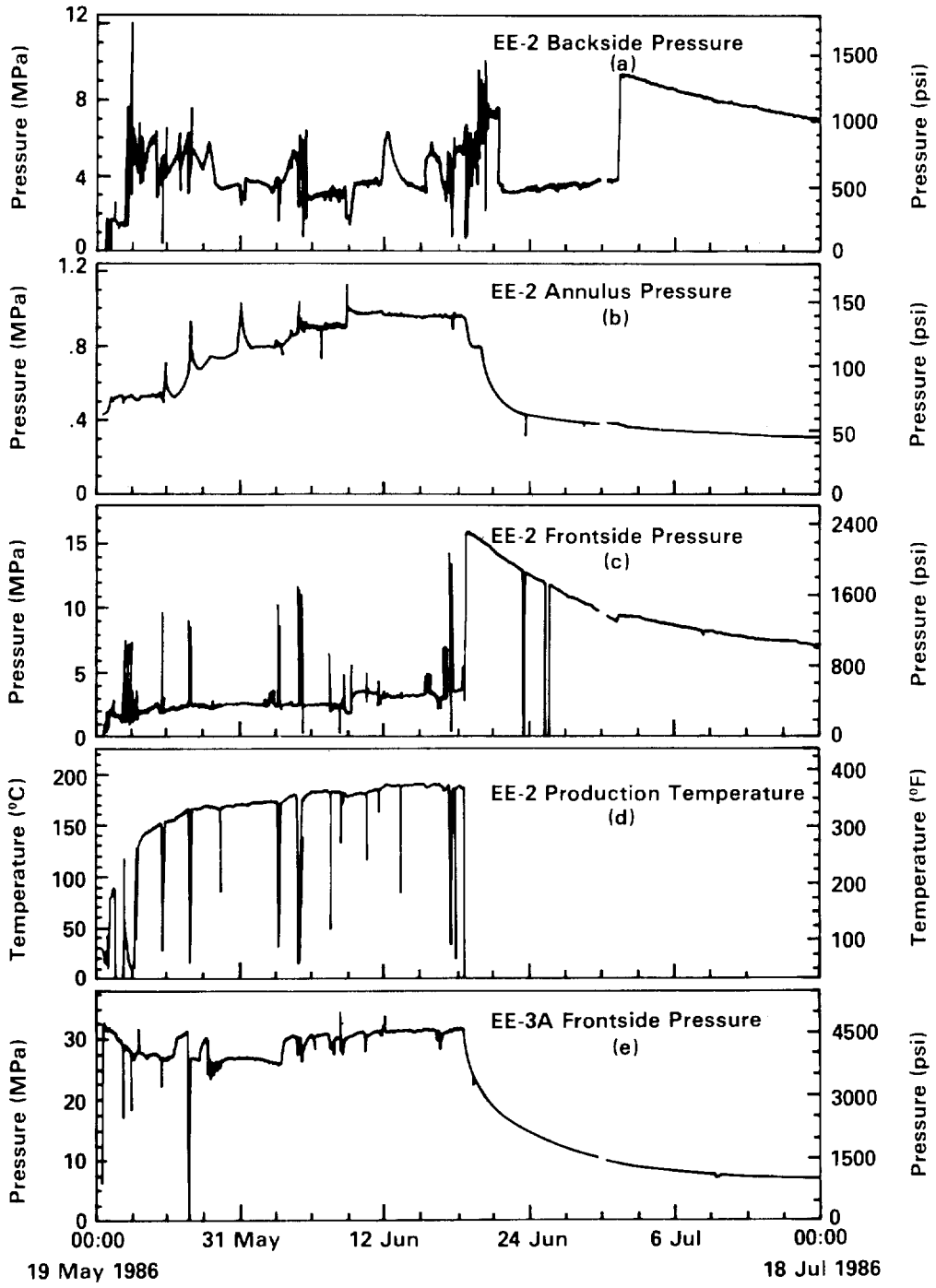

Figure II-8. EE-2 backside pressure (a) compared to b) EE-2 annulus pressure, c) EE-2 frontside pressure (an intermittent connection from the frontside to the backside is indicated), d) EE-2 surface production temperature (backside pressure intermittently responded to temperature changes in the tubing, indicating the leak on the backside was occasionally sealing off), and e) EE-3A frontside pressure (the reservoir connection is evident but subtle).

shown to be the cause. Communication commences with a sudden increase in frontside pressure (Fig. II-8c). EE-2 backside is in communication with the EE-3A frontside (Fig. II-8e) with a 3-hour delay. The communication path observed with the EE-3A frontside is most likely the main reservoir connection through the EE-2 frontside.

The EE-2 backside at times appears to become isolated from the EE-2 frontside and acts like a closed pressure vessel. During these periods, the backside pressure indicated good thermal communication between the tubing and annulus (Figs. II-8d and b).

III. THERMAL BEHAVIOR

A. Temperature Measurements

Temperature measurements were an integral part of Expt. 2067. Injection and production temperatures were measured at the EE-3A and EE-2 wellheads, respectively. Inlet and outlet temperatures were also measured across the heat exchangers. In addition, a series of borehole temperature surveys were made in both the Phase II and Phase I Fenton Hill wells.

1. EE-3A Borehole Temperature Measurements. A background temperature survey was conducted in injection well EE-3A on May 15, 1986, before pumping into the Phase II system (Fig. III-1). Since the EE-3A wellbore was pressurized above 25 MPa (4000 psi) throughout the pumping experiment, temperature surveys of the EE-3A borehole were run by a commercial service company, Oil Well Perforators (OWP). Three high-pressure logs were run by OWP (Fig. III-2), two during ICFT injection, May 28 and June 16, and one 5 days after shut-in, June 23. Two additional post-ICFT temperature surveys were run in EE-3A on August 5 and August 28, 1986 (Fig. III-1).

The OWP temperature logs (Fig. III-2) show that a well-distributed injection interval was established between 3535 and 3660 m (11 600 and 12 000 ft) with two major entry zones, one above and one below the 3600- to 3630-m (11 800- to 11 900-ft) zone, which was the intended bottom of the liner and actually the bottom of a cement sheath remaining after cleanout. Possible discrete fractures noted at 3540 m (11 620 ft), 3580 m (11 750 ft), and 3640 m (11 950 ft) correspond to fractures first

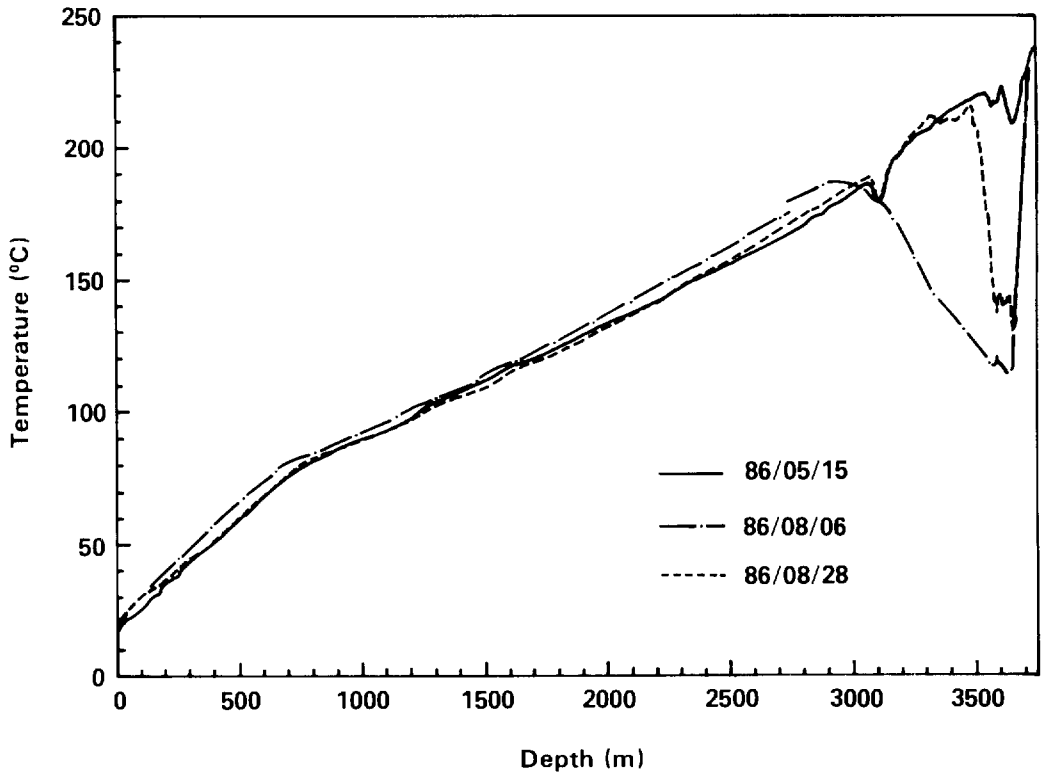

Figure III-1. Pre- and post-ICFT temperature surveys of EE-3A run by Los Alamos.

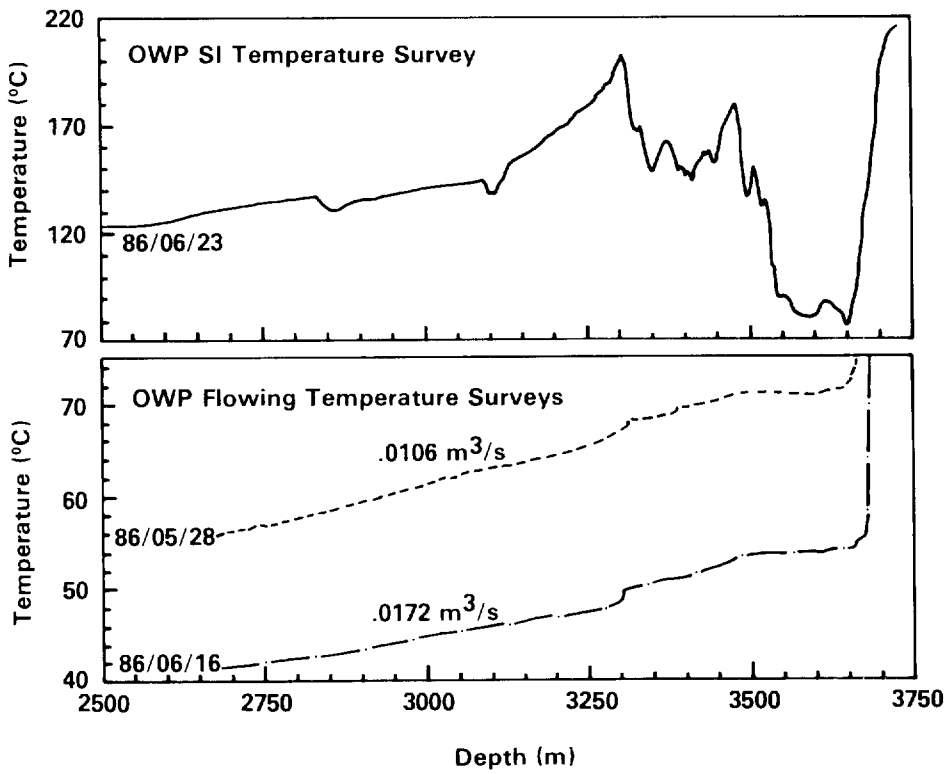

Figure III-2. High-pressure temperature surveys of EE-3A run by OWI.

stimulated in Expt. 2059 and later during Expt. 2062. The thermal anomalies between 3300 to 3510 m (10 825 to 11 520 ft) on the shut-in log are consistent with the flow observed on the EE-3A backside. The appearance of these anomalies suggests a near-wellbore leakage path that is long and tortuous. It is estimated that about 0.0004 m^3/s (6 gpm) is entering behind the liner and flowing up the well, with about 0.0001 m^3/s (2 gpm) leaving the wellbore region at 3125 m (10 250-ft, low-pressure zone) and 0.0003 m^3/s (4 gpm) at the surface. The postexperiment temperature surveys are compared to the background run made on May 15 (Fig. III-3) and show the thermal recovery of the wellbore with time.

2. EE-2 Temperature Measurements. During the ICFT, 3 temperature surveys of the EE-2 production well were obtained and a fourth survey was made 10 days after the flow test was terminated (Fig. III-4). These measurements were with the Kuster recorders (a downhole mechanical recording system). The first three surveys made on May 28, June 4, and

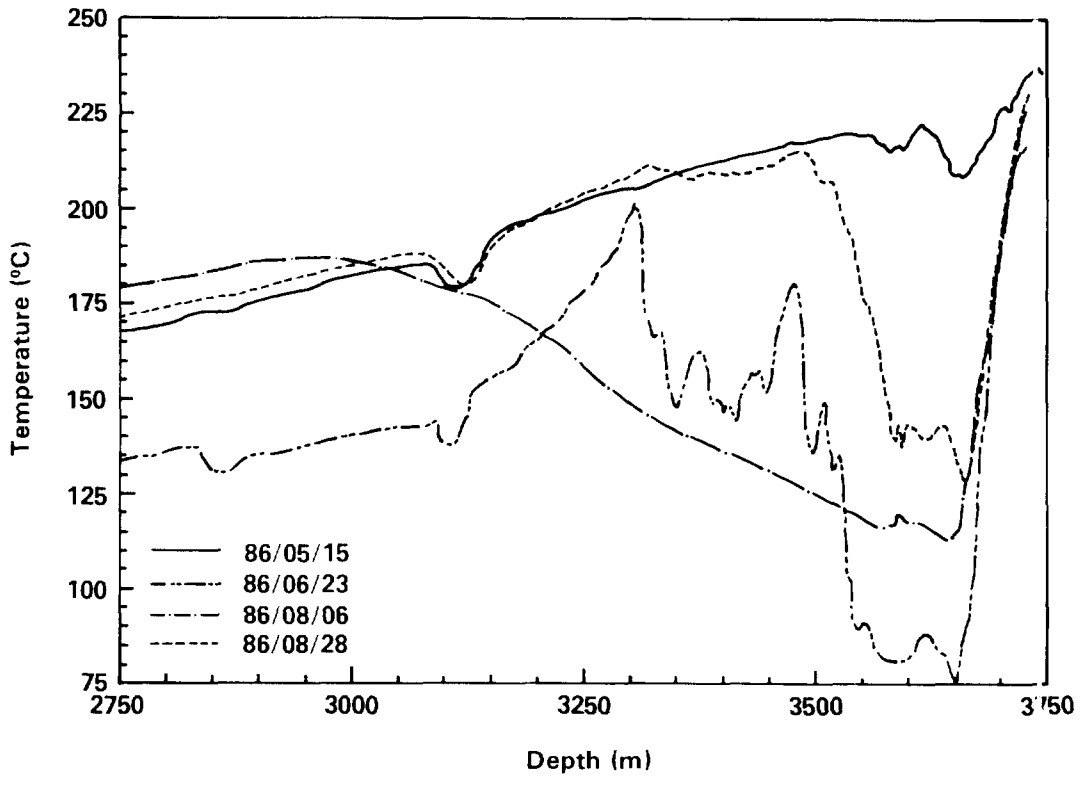

Figure III-3. Comparison of the pre-ICFT survey with post-ICFT surveys showing thermal recovery of EE-3A with time.

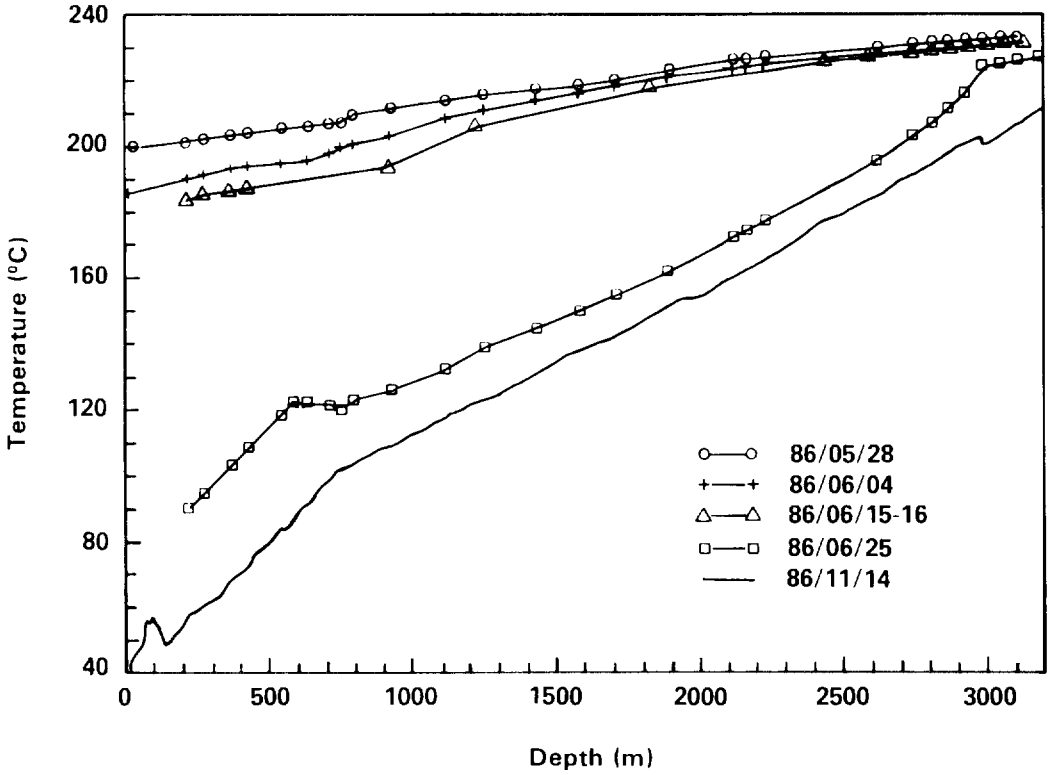

Figure III-4. Kuster temperature surveys of EE-2 during the ICFT compared to a post-ICFT temperature survey.

June 15 show the progressive heating of the entire wellbore throughout the experiment. A temperature survey run on Los Alamos equipment on November 14, 1986, (also shown on Fig. III-4) when compared to the fourth Kuster survey (June 28, 1986) shows the temperature recovery of the wellbore. Because of the damaged EE-2 wellbore, temperature surveys could not be run below 3185 m (10 450 ft).

Figure III-5 shows a calculated boiling pressure curve, based on EE-2 production temperature, compared to the pressure measured in the EE-2 244.5- to 339.7-mm (9-5/8- to 13-3/8-in.) casing annulus. At the beginning of the test the annulus pressure was 0.4 to 0.5 MPa (62 to 75 psig), well above the boiling point. Once the increase in EE-2 production temperature caused the calculated boiling pressure to exceed 0.5 MPa (75 psig), the annulus pressure followed the boiling curve until a pressure of 1 MPa (140 psig) was reached and then declined slowly until cooling occurred at shut-in. It is assumed that the fluid level

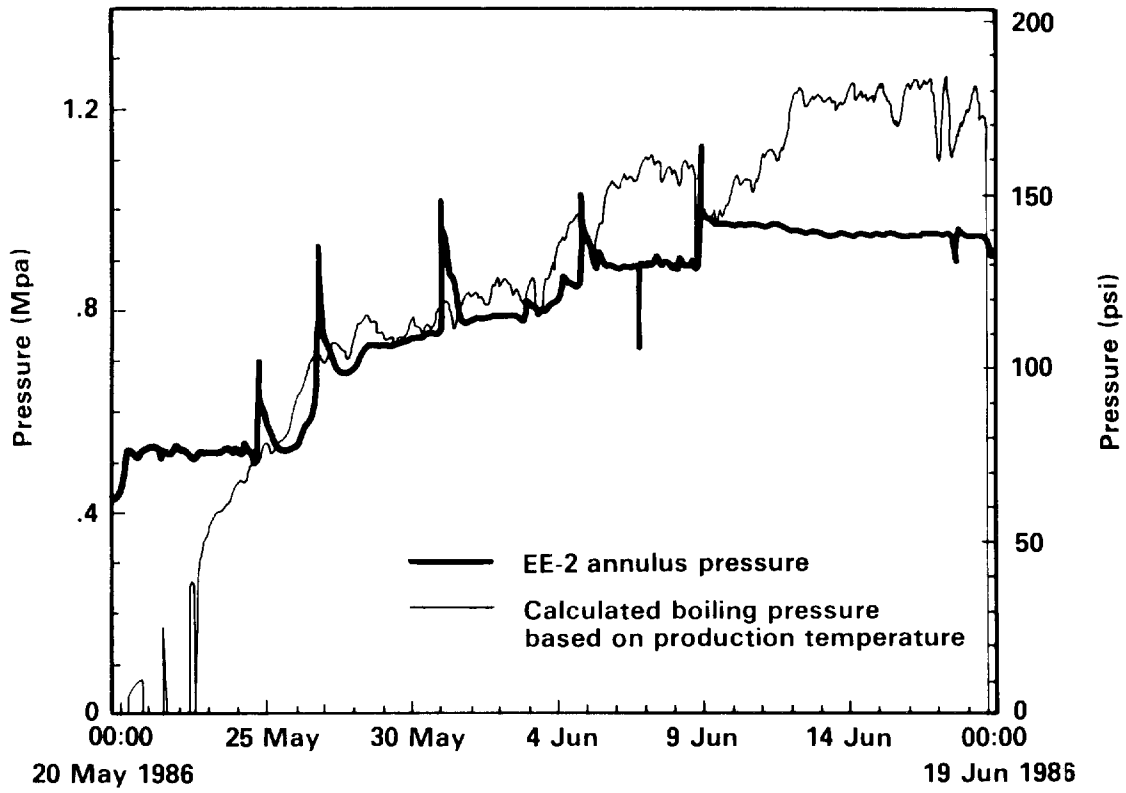

Figure III-5. A calculated boiling pressure curve (based on the EE-2 surface production temperatures) compared to the EE-2 annulus pressure data.

in the annulus was lowered as the pressure followed the boiling pressure curve. The fluid, displaced by steam, was pushed out into the aquifers through the damaged 339.7-mm (13-3/8-in.) o.d. casing (damaged during drilling) below 536 m (1760 ft). The pressure leveled out at 1 MPa (140 psi) when the fluid level reached the first aquifer that would accept all of the steam being produced in the annulus. The temperature anomalies on the Kuster production surveys (Fig. III-4) between 245 and 915 m (800 and 3000 ft) were quite pronounced, while the annulus pressure followed the boiling pressure curve but had almost disappeared once the annulus pressure deviated from the boiling curve.

An active cross-flow region between 640 and 790 m (2100 and 2600 ft) was observed on the Kuster log following shut-in (June 28, 1986). This corresponds to an aquifer near the transition of the sediments and Precambrian basement rock. This thermal anomaly might also be

attributed to changes in thermal conductivity in the different geologic formations. The possibility of a small leak in this area should not be ignored. Another, deeper anomaly was noted in the temperature gradient on the shut-in temperature log. The gradient is quite flat from 2990 to 3185 m (9800 to 10 450 ft) indicating some flow behind the casing believed to be the top of a cross flow between the main HDR reservoir and the Phase I low-pressure system. It is estimated a small amount of fluid, about 0.0019 m^3/s (30 gpm), was still entering the wellbore below 3185 m after EE-2 was shut in and flowed up the well and out into the rock at 2990 m. On Fig. III-6 an interpretation of cement bond log amplitude shows cemented regions behind the 244.5-mm (9-5/8-in.) casing that resulted from the squeeze work done to "repair" EE-2 in 1984. The existence of this cross flow would indicate a deterioration of the squeeze cement between 3215 to 3230 m (10 550 to 10 600 ft). The cement placed above the 2775-m (9100-ft) squeeze perforations appears to be in good condition based on the temperature logs.

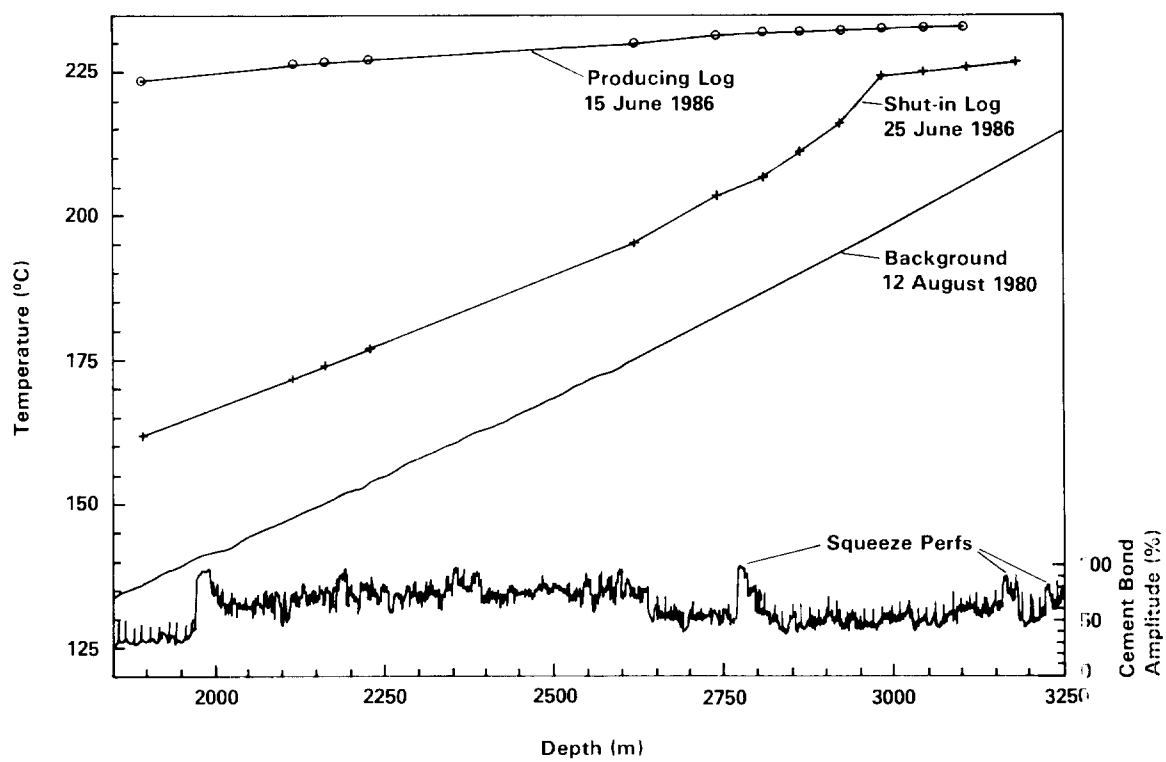

Figure III-6. EE-2 temperature logs with interpretation of the 1984 cement bond log amplitude shown. The bond log was run following the squeeze cement jobs conducted during the 1984 EE-2 repair.

3. Phase I Wells. Background temperature surveys were made in EE-1 and GT-2B on May 13 and May 14, 1986, respectively, before the start-up of the ICFT. Throughout the experiment, the EE-1 and GT-2B wellheads were monitored. A small amount of fluid was noted flowing from GT-2B on June 12, 1986. When this wellbore was shut in, a pressure increase at the wellhead was noted and recording of both EE-1 and GT-2B pressures commenced. On July 31, 1986 (about 43 days after the pumping into EE-3A was terminated), a second survey was run in EE-1. The data from the three temperature surveys are shown in Fig. III-7. The effects of the warming of the EE-1 borehole via the leakage into the old Phase I system are clearly defined.

B. Modeling Thermal Performance

Following completion of the ICFT, simulations of both EE-3A and EE-2 performance were made to match the data collected during the experiment using a wellbore heat transfer (WBHT) code (Dash and Zyvoloski, 1982). The WBHT model solves the basic 2-D radial equations

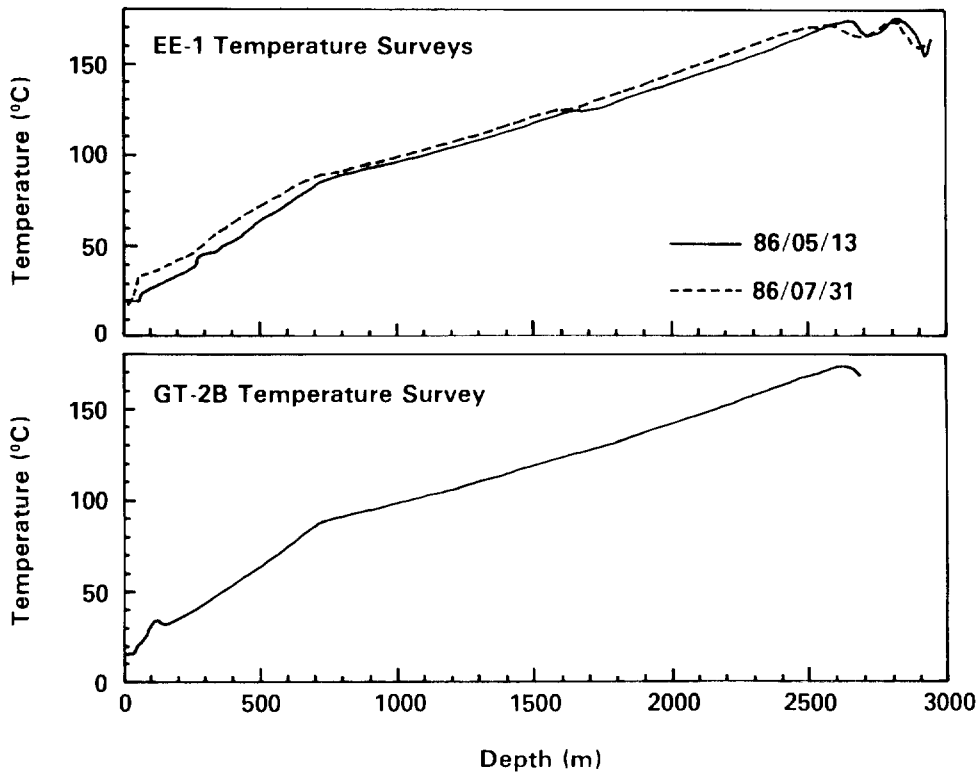

Figure III-7. EE-1 and GT-2B temperature surveys.

for heat transfer and accounts for forced convection in the wellbore and annulus and for conduction to the surrounding rock mass.

1. EE-3A WBHT Simulation. EE-3A injection was modeled using an approximation to the measured flow rates (Fig. III-8) and a constant inlet temperature of 20°C, which corresponds to the average injection temperature over the course of the experiment. The resulting bottom-hole temperature versus time is given in Fig. III-9. WBHT-calculated wellbore temperature profiles are compared to corresponding OWP temperature surveys in Fig. III-10. The EE-3A simulation profiles are in good agreement with wellbore cooldown during injection and postinjection thermal recovery. The model used, however, is not sufficiently complex to model flow into the reservoir. The simulation also provided information that allowed estimation of bottom-hole injection pressures.

2. EE-2 WBHT Simulation. EE-2 production was modeled using a reservoir outlet temperature of 232°C, which corresponds to the original rock temperature at 3535 m (11 600 ft) and flow rate as measured at EE-2

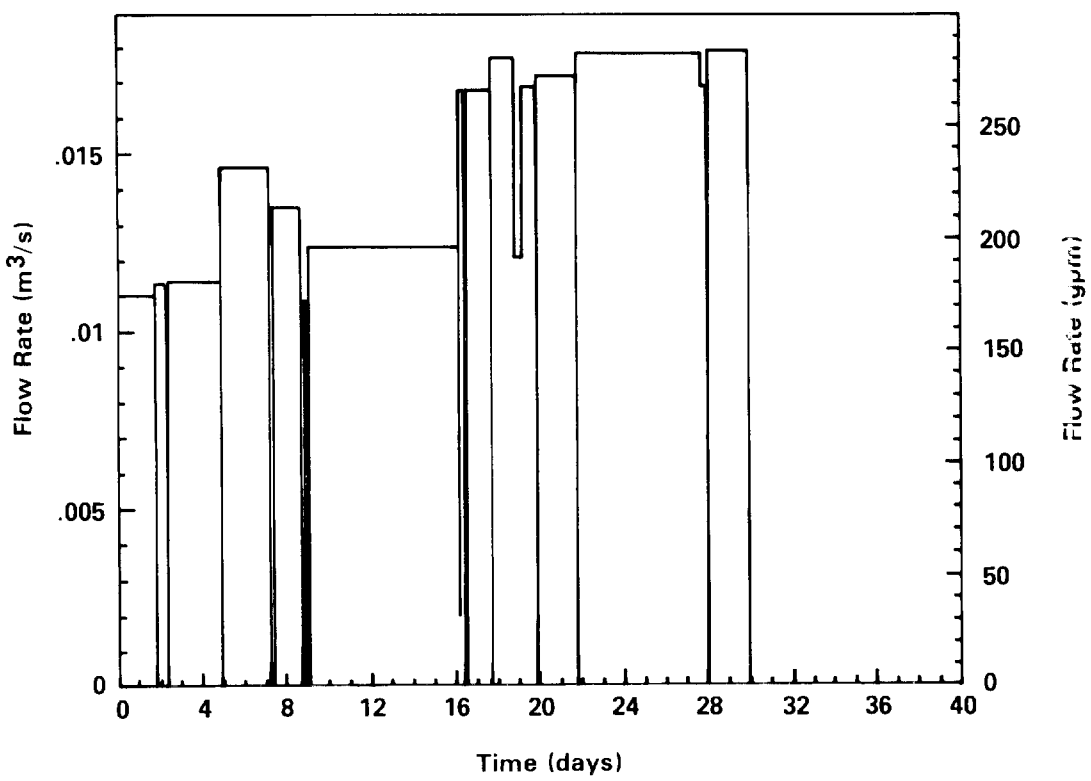

Figure III-8. EE-3A injection flow rate versus time.

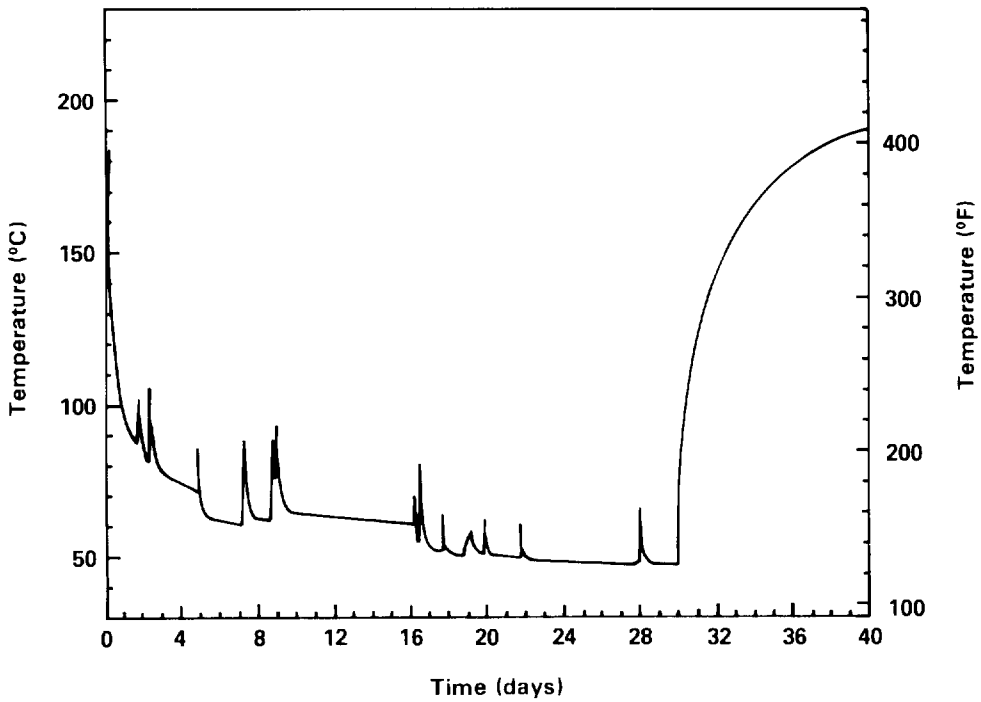

Figure III-9. WBHT projection of EE-3A bottom-hole temperature.

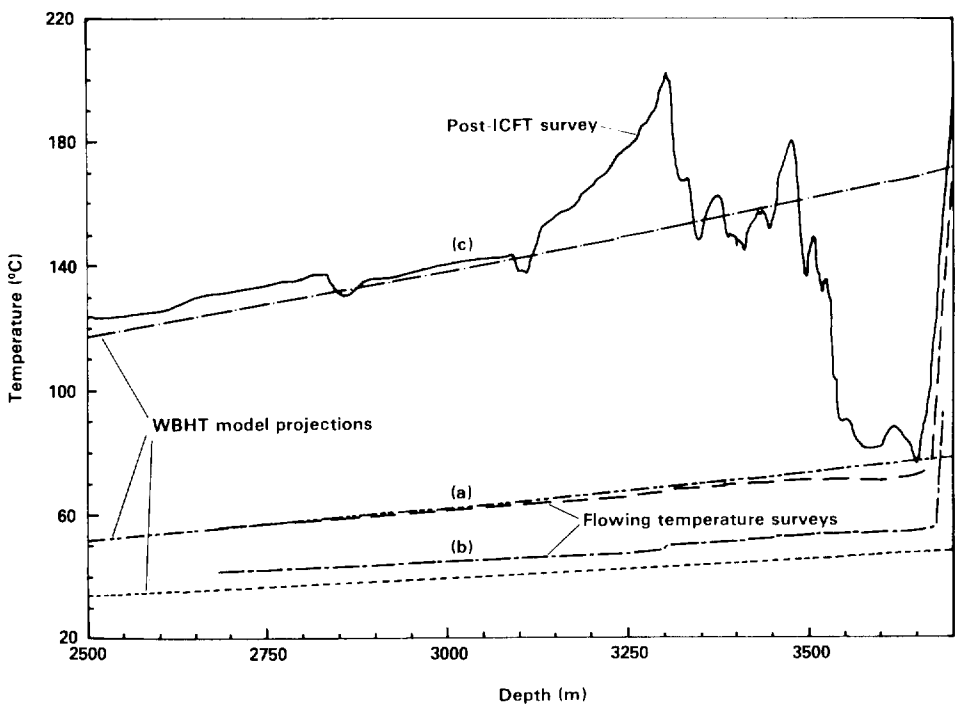

Figure III-10. WBHT projection of EE-3A temperature surveys compared to OWP surveys: a) OWP survey 86/05/28; b) OWP survey 86/06/16; and OWP survey 86/06/23.

wellhead (Fig. III-11). The production temperature projected by the model as a function of time is given in Fig. III-12 and compared with measured production temperatures. These temperatures are in good agreement during the first 9 days of the ICFT. At that time the temperature predicted by the model exceeds that measured by about 5 to 10°C. Around the 20th day of the simulation, this difference has increased to 20°C. In general, the discrepancies correspond with the appearance of more gas in the production fluid; in particular, the largest discrepancies correspond to an experiment in which nitrogen was introduced into the system on June 8. The same discrepancies can be noted between the downhole Kuster measurements and WBHT wellbore temperature profiles (Fig. III-13).

Because of the increasing error in predicted production temperature, the model was rerun using a production rate derived from summing the flow rates through the heat exchangers (Fig. III-11). During the early part of the test, EE-2 wellhead and heat exchanger flow rate measurements were consistent, but a difference in the measurements of

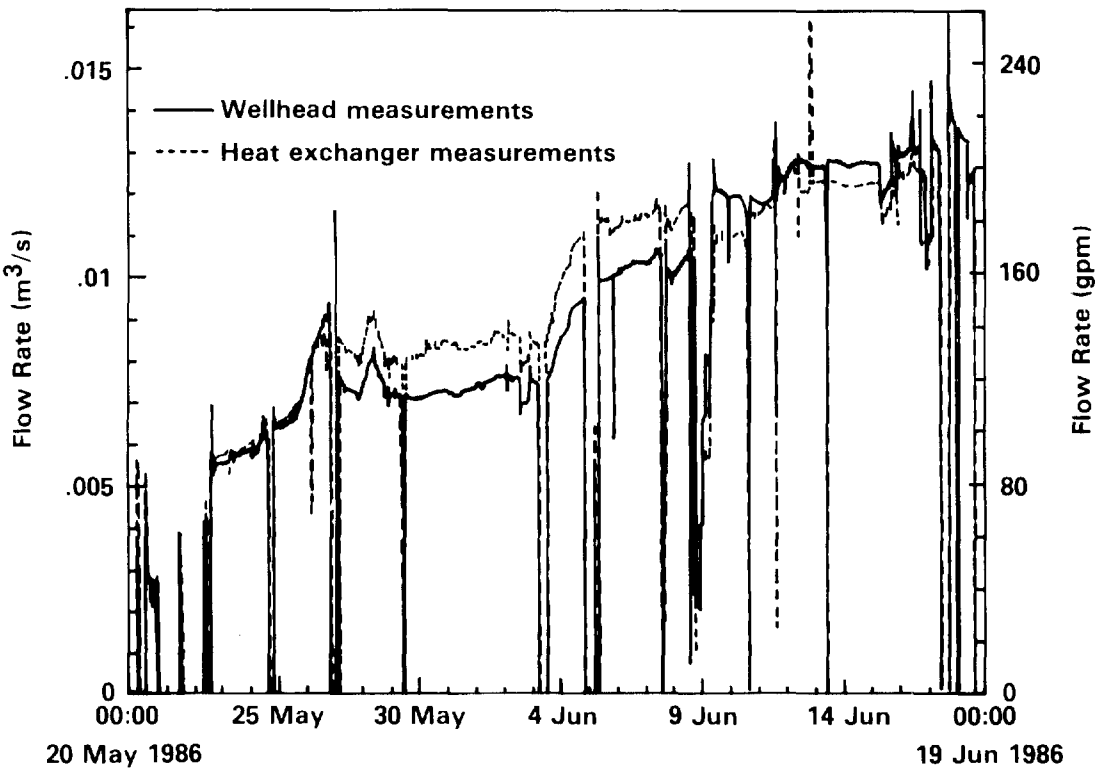

Figure III-11. EE-2 production flow rate.

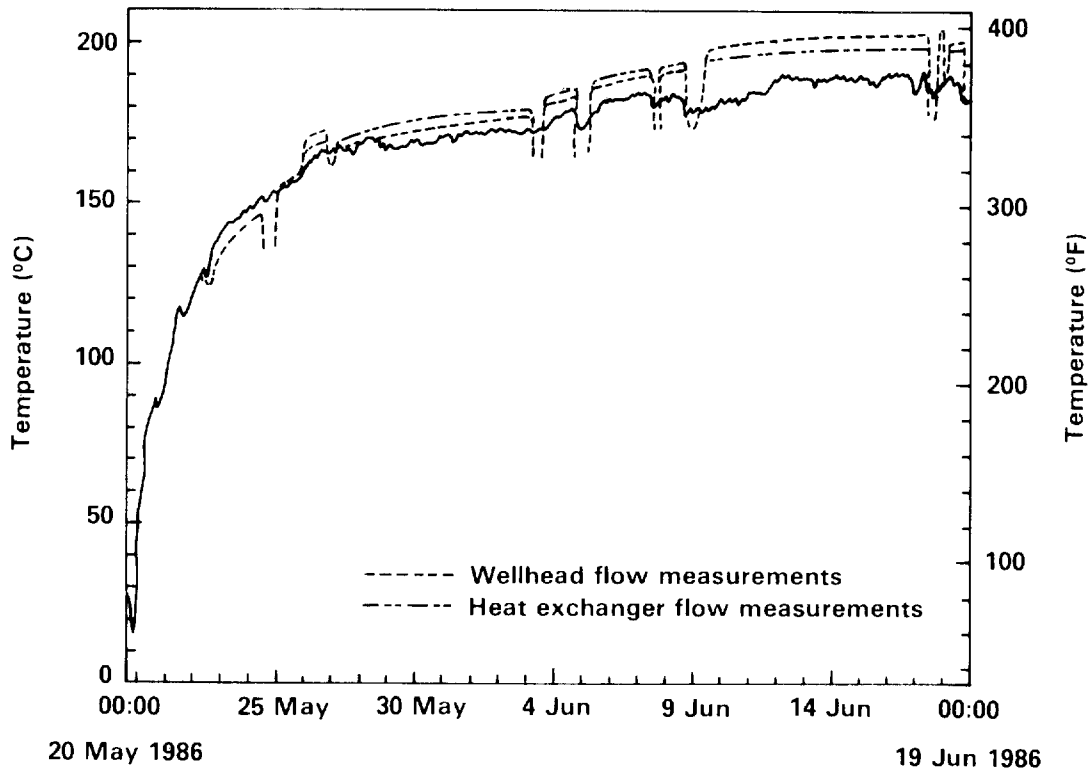

Figure III-12. EE-2 wellhead production temperature compared to WBHT projection of production temperature using wellhead measured flow rates and using heat exchanger rates.

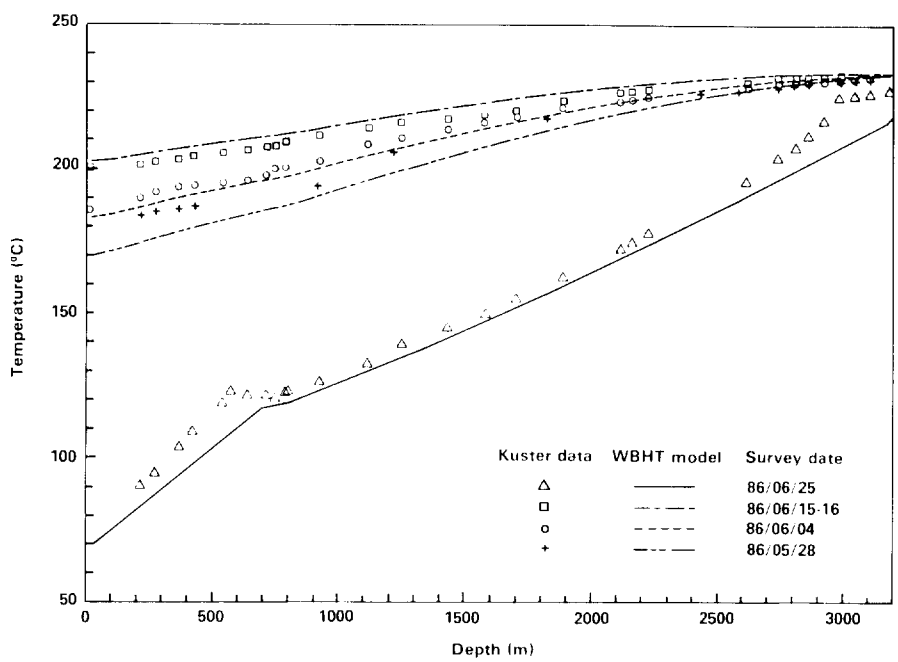

Figure III-13. EE-2 Kuster temperature surveys compared to WBHT projections using wellhead flow rates.

flow rate was noted after about 8 days. This deviation between wellhead and heat exchanger flow rates occurred at about the same time the strainer in front of the wellhead flow meter required cleaning owing to severe clogging, suggesting some debris may have affected the wellhead flow meter. To determine which flow rate measurements were more reliable, a cross check was made by estimating flow using the difference between injection and makeup flow meters (Fig. III-14). The values obtained consistently match the heat exchanger flow rates when the system was not being run in gas-purge mode. Therefore, it is believed that the heat exchanger flow rates provide the most reliable values. Projections of production temperature using the heat exchanger flow rates, although still high (about 5 to 10°C), are in much better agreement with experimental results (Fig. III-12). Downhole Kuster measurements and WBHT wellbore temperature profiles compared in Fig. III-15 are also in much better agreement.

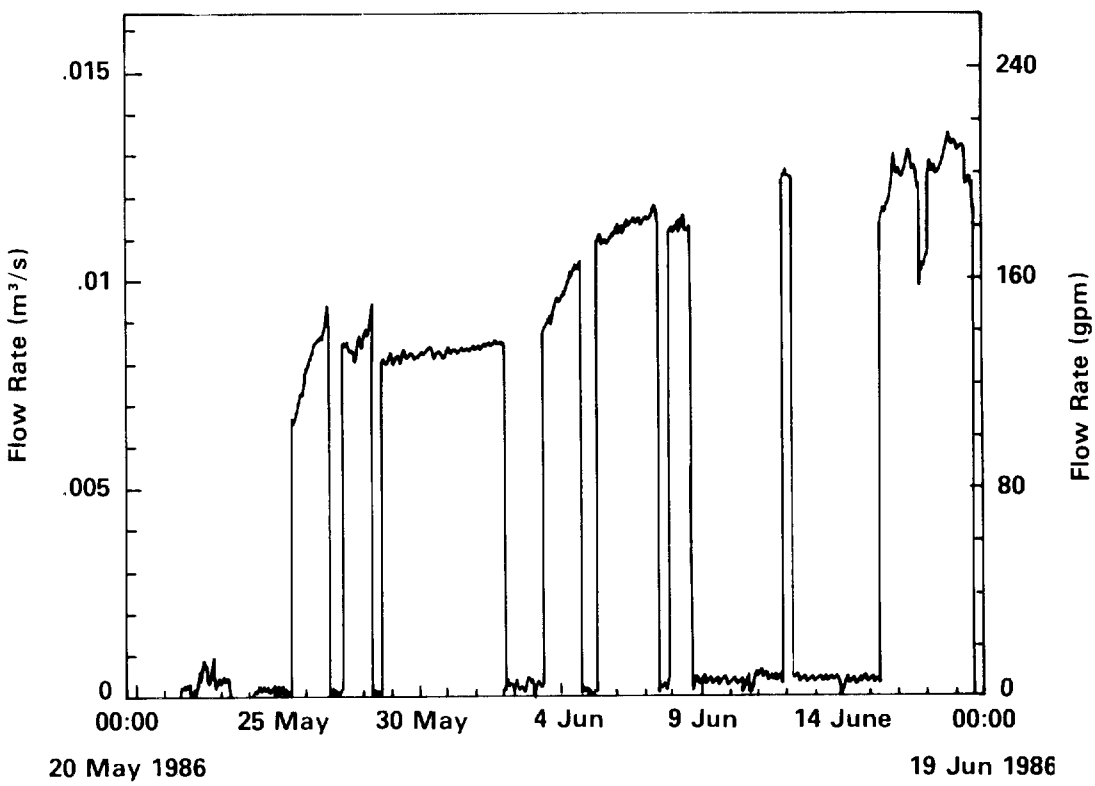

Figure III-14. EE-2 production flow rate estimated from difference between makeup flow and injection flow measurements.

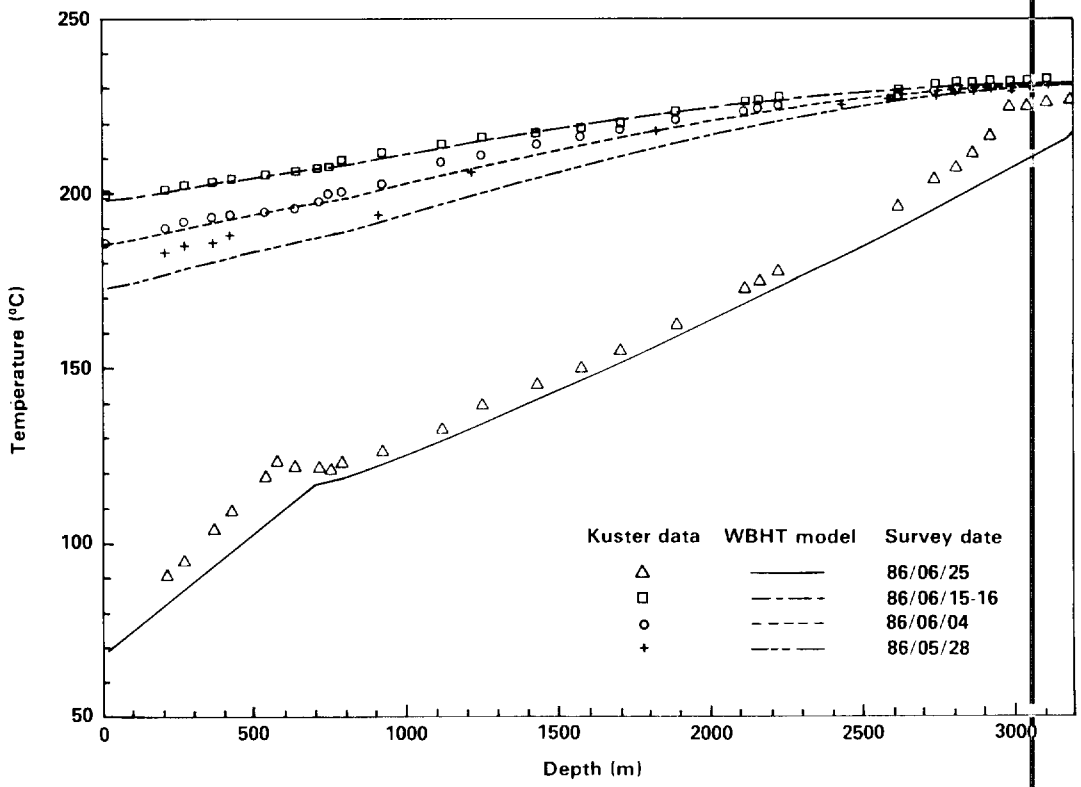

Figure III-15. Kuster measurements with WBHT projections of downhole temperature using heat exchanger flow rates.

C. Estimation of Thermal Power Production

Thermal power production was estimated for the ICFT using the measured production temperature at the EE-2 wellhead, the injection temperature at EE-3A, and production flow rate. First calculations used the production flow rate measured at the EE-2 wellhead; later calculations used the flow rates measured at the heat exchangers (Fig. III-16). Using the wellhead measurement of flow, a peak power of 10.5 MW_t was estimated; however, with the lower flow rates measured at the heat exchangers, this peak was slightly under 10 MW_t. A model projection using a sustained flow rate of 0.0126 m^3/s (200 gpm), which is close to the rate maintained over the last 7 days of the test, results in a power production of 10 MW_t.

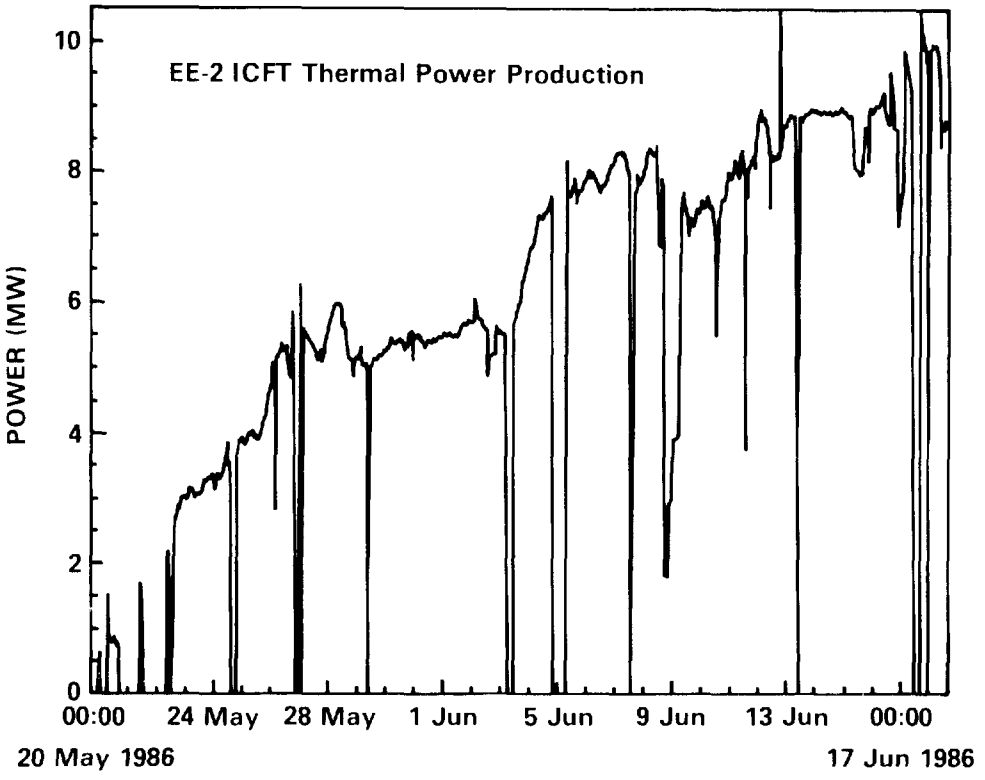

Figure III-16. Thermal power production during the ICFT estimated using heat exchanger flow rates.

IV. RESERVOIR HYDRAULICS

A. Pressure Rate Response

Many hydraulic reservoir tests were conducted within the ICFT that included shut-ins, vents, and pressure and flow rate variations. These experiments provided information about reservoir and well characteristics and the changes caused by water circulation during the ICFT.

1. Analysis of EE-3A Data.

a. Introduction. Figure IV-1 shows the EE-3A pressure and flow rate (averaged every 15 min) on a condensed time scale; Table IV-I lists the many shut-ins of the injection well during the ICFT along with the estimated instantaneous shut-in pressure for each shut-in. A short step-rate test was conducted at the start of the ICFT, followed by a nominally steady injection at 0.0114 m^3/s (180 gpm) for 6 days. The injection pressure decreased from 32.1 MPa (4650 psi) to 27.6 MPa (4000

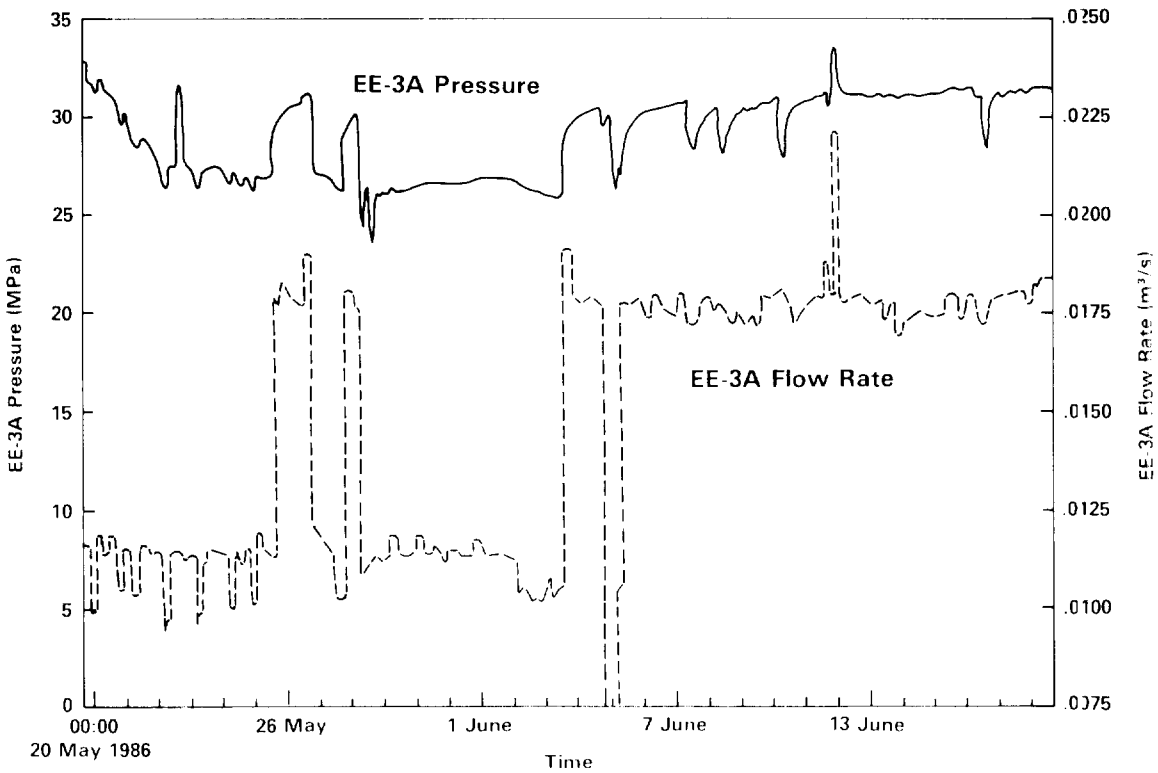

Figure IV-1. EE-3A pressure and flow rate.

psi) during the first 3 days of injection, leveling off to 26.9 MPa (3900 psi) later in the test. Following the 6 days of steady injection, there were two short intervals with elevated rates: one at 0.0180 m^3/s (286 gpm) for 28.2 hours beginning at 1620 hours on May 25, and one at 0.0174 m^3/s (276 gpm) for 12.9 hours beginning at 2008 hours on May 27. Both caused the surface injection pressure to increase quickly to approximately 31.0 MPa (4500 psi), reflecting a very small increase in the bottom-hole pressure. The 4.1-MPa (600-psi) rise in surface pressure was due mainly to increased pipe friction. The injection rate was then dropped back to 0.0113 m^3/s (180 gpm) for 5 days and further down to 0.0107 m^3/s (170 gpm) for 2 days. After this, the injection rate was increased to 0.0180 m^3/s (285 gpm) and held to the end of the ICFT except for a short pump of 0.0265 m^3/s (420 gpm) at 2325 on June 11 and several shut-ins. There are two especially noteworthy facts from these data:

TABLE IV-I

EE-3A SHUT-INS

Date	Time	P_o (MPa)	P_{ISIP} (MPa)	Q (l/s)
5/19/86	1651	0.0	27.9	4.4
5/19/86	1811	0.0	29.8	8.5
5/19/86	1922	0.0	30.2	10.7
5/19/86	2042	0.0	32.6	19.1
5/21/86	0941	17.8	26.9	11.4
5/22/86	0027	19.4	26.1	11.5
5/24/86	1209	22.7	26.2	11.4
5/28/86	0810	24.1	25.3	11.9
5/28/86	1513	23.6	25.1	11.1
6/04/86	1953	27.5	28.5	17.8
6/05/86	0328	26.8	28.0	10.4
6/06/86	0820	27.7	28.6	18.0
6/07/86	1244	27.9	28.9	17.7
6/08/86	1255	27.6	28.4	11.0
6/08/86	1737	27.2	28.1	17.5
6/10/86	0937	28.1	29.5	18.0
6/16/86	1053	27.7	29.5	17.9
6/18/86	1601	28.6	29.6	10.1

1) The bottom-hole injection pressure changed only slightly in response to large changes in injection rates.
2) The pumping pressure at a given pumping rate stayed fairly constant.

It is concluded from this behavior that the fractured region began to "inflate" with fluid soon after injection began.

b. Early Time Data. Figures IV-2 and IV-3 show the injection pressure versus time plot for the initial step flows of 0.0044 m^3/s (70 gpm) and 0.0085 m^3/s (134 gpm), respectively. During the initial pressure rise in both buildups, water was being stored in the wellbore and the rapid pressure increase is due to fluid and wellbore compressibility. Figures IV-2 and IV-3 indicate that the wellhead

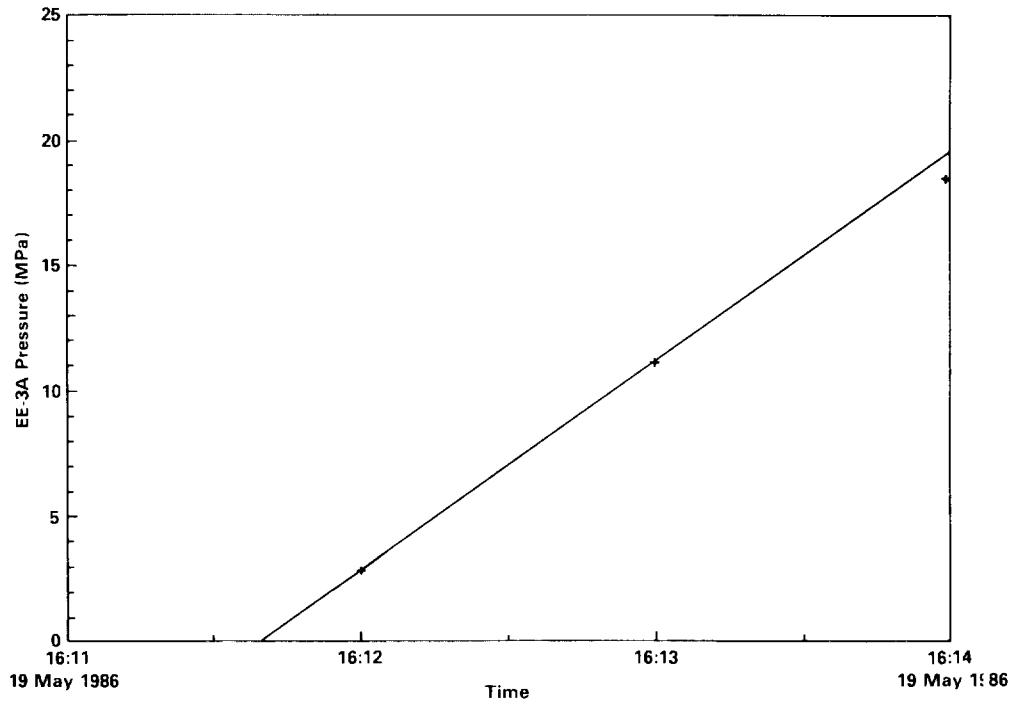

Figure IV-2. EE-3A pressure buildup during first step-rate test.

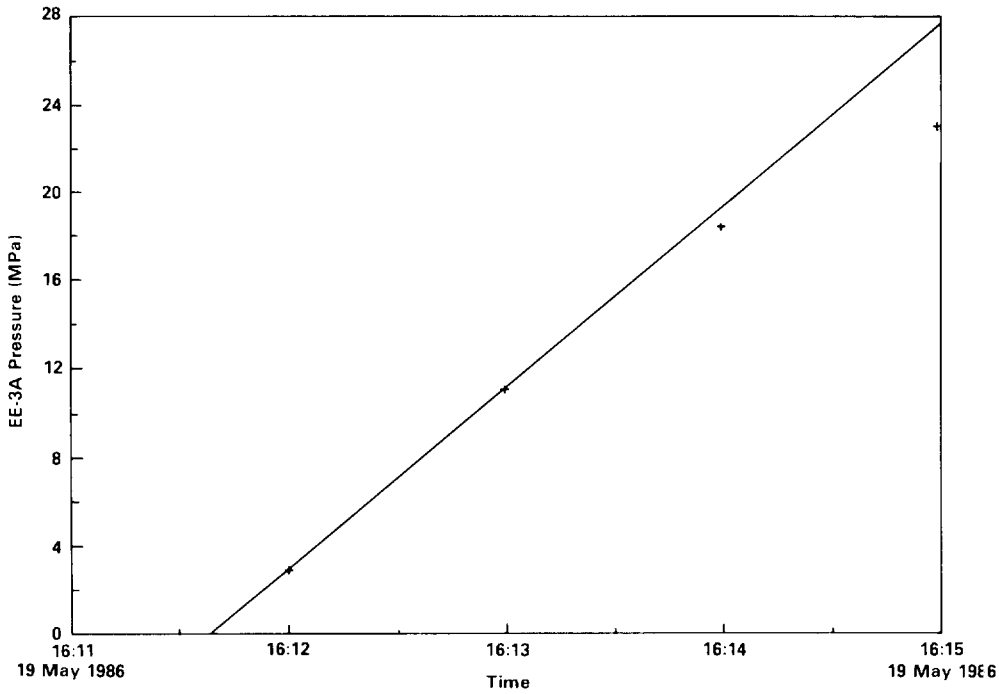

Figure IV-3. EE-3A pressure buildup during second step-rate test.

pressure starts deviating from straight-line behavior at about 17.2 MPa (2500 psi), indicating the threshold pressure at which fluid began to flow into the formation. This value agrees with the previous findings listed in Table IV-II. From the initial slope of these curves, the wellbore compressibility is estimated to be between 6.5×10^{-4} MPa^{-1} and 7.0×10^{-4} MPa^{-1} (4.5×10^{-6} psi^{-1} and 4.8×10^{-6} psi^{-1}).

c. Fracture Closure Stresses. The EE-3A wellhead pressure, injection flow rate, surface temperature, and estimated bottom-hole temperature and pressure are given for several different times in Table IV-III. The bottom-hole values were calculated using the WBHT code, which accounts for heat transfer with the formation as well as for variations in fluid density, viscosity, pipe friction, and hydrostatic head.

Bottom-hole pressures are plotted versus the square root of their flow rates in Fig. IV-4 for several previous experiments and the ICFT. A linear relationship in these coordinates is expected based on the assumption of turbulent flow through a fracture parallel with an opening, or aperture, which varies linearly with pressure excess over the fracture closure stress. Extrapolated back to zero flow rate, these curves yield the theoretical bottom-hole fracture closure pressures for each experiment. In the case of this experiment (2067, or ICFT), two sets of data were used, one grouping the initial pumps of 0.0044,

TABLE IV-II

COMPARISON OF EXPERIMENT 2067 RESULTS WITH PREVIOUS TESTS

	Initial Pump Data		Shut-In Data	
Experiment Number	Compressibility (MPa^{-1})	Deviation from Straight Line (MPa)	ISIP (MPa)	Slope ($MPa/min^{1/2}$)
2049	3.9E-4	22.8	29.6	1.4
2057	10.2E-4	13.8	29.9-31.7	1.7-2.2
2059	6.4E-4	8.3	34.5	2.0
2061	5.1E-4	<6.9	38.4	0.43
2062	7.4E-4	8.3	29.5	0.97
2067	(6.5-7.0)E-4	13.8-17.2	29.8	0.12

TABLE IV-III

ESTIMATED EE-3A BOTTOM-HOLE PRESSURES AND TEMPERATURES

Time (hours)	Flow Rate (l/s)	$P_{surface}$ (MPa)	$T_{surface}$ (°C)	T_{bottom} (°C)	P_{bottom} (MPa)
0.33	4.4	25.9	9.5	235	61.7
2.0	8.5	30.2	10.0	222	65.0
3.0	10.7	29.6	11.5	227	64.9
96.0	11.4	27.6	12.5	74.2	62.8
120.0	14.6	27.6	12.0	69.8	62.3
290.4	12.3	26.2	16.0	62.4	61.3
559.2	27.3	33.1	20.0	45.0	65.5
590.4	17.6	31.0	17.5	47.9	65.3

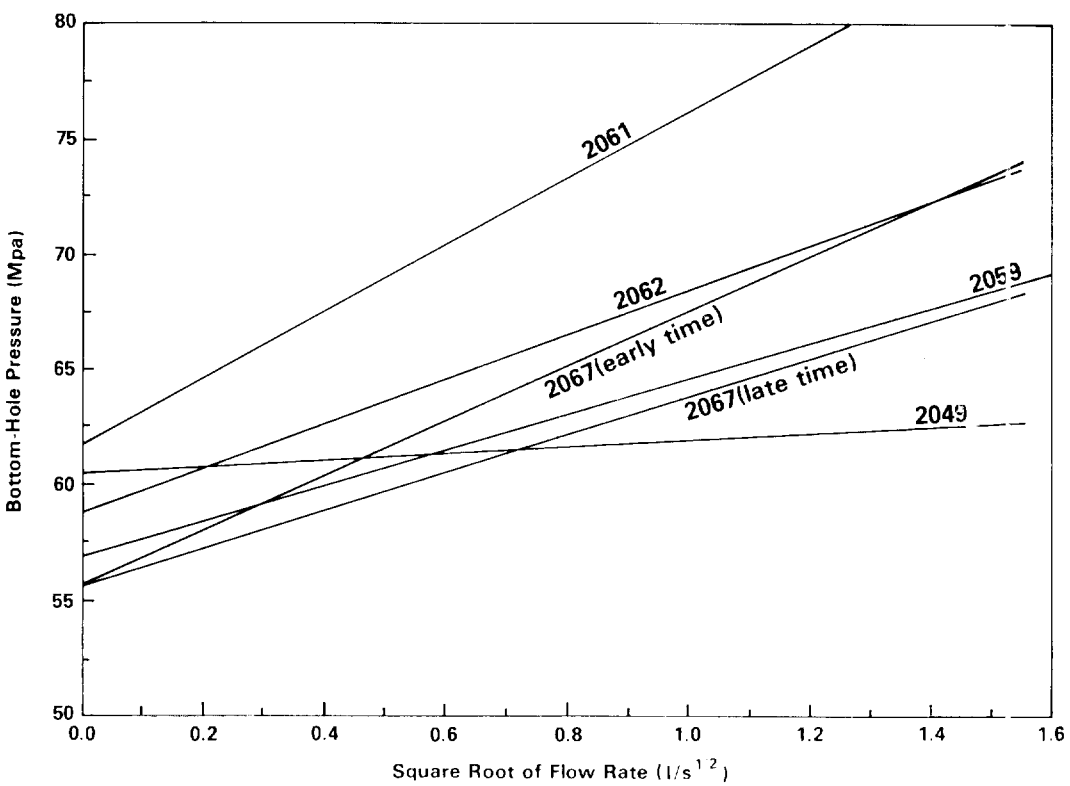

Figure IV-4. Bottom-hole fracture closure pressure for five experiments.

0.0085, and 0.0107 m^3/s (70, 134, and 170 gpm), and another consisting of data obtained during later steady flows. Although the slopes for these two data sets are different, they indicate approximately the same bottom-hole fracture closure stress of 55.6 MPa (8070 psi), or 19.7 MPa (2850 psi) at the surface. This value is about 3 MPa (435 psi) lower than that obtained in Expt. 2062 and is quite close to that obtained from Expt. 2059. This indicates that significant volumes of water went into the connections created previously by these two experiments.

d. Shut-Ins. The final shut-in occurred after 30 days of pumping at various rates. At the injection well (EE-3A), the surface pressure transient exhibited the expected sudden drop of 2 MPa (290 psi) because of wellbore friction followed by a more gradual decay. Assuming that the pressure drop is caused by a discharge of wellbore fluid into the formation through fracture faces, with no tensile fracture extension (i.e., the fluid pressure is below the closure stress), the estimated initial shut-in pressure (ISIP) using the square-root-of-time method is 29.8 MPa (4318 psi), as shown in Fig. IV-5. The slope of this curve is 0.1 $MPa/min^{1/2}$ (18 $psi/min^{1/2}$). This is about an order of magnitude less than values obtained during past tests (Table IV-II).

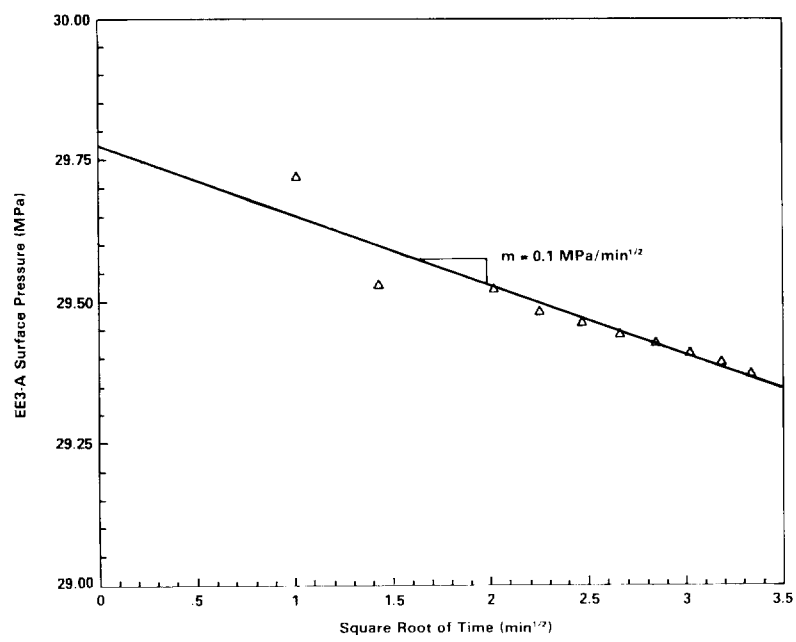

Figure IV-5. Shut-in curve for the final shut-in.

With the hope of spotting some orderly trend to explain this discrepancy, the slopes of the linear regions of all the shut-in curves were plotted versus the total volume of injected water to the time they occurred (Fig. IV-6). A sharply decreasing trend is noted in this figure, with the curve leveling off around 0.1 - 0.2 MPa/min$^{1/2}$ after the injection of about 8000 m^3 (2.1 million gal.). As shown in Fig. IV-7, the qualitative character of the shut-in pressure response also changes during injection. This suggests that perhaps the standard method (Hickman and Zoback, 1983) of determining ISIP is not valid after a large amount of fluid (i.e., approximately 3800 m^3, or 1 million gal.) is pumped into a reservoir. The reason for the decreasing slopes is thought to be due to the inflation of the reservoir. As more and more fluid is pumped into the formation and the reservoir approaches a pseudo steady state, local pressure gradients decrease, leading to reduced flow.

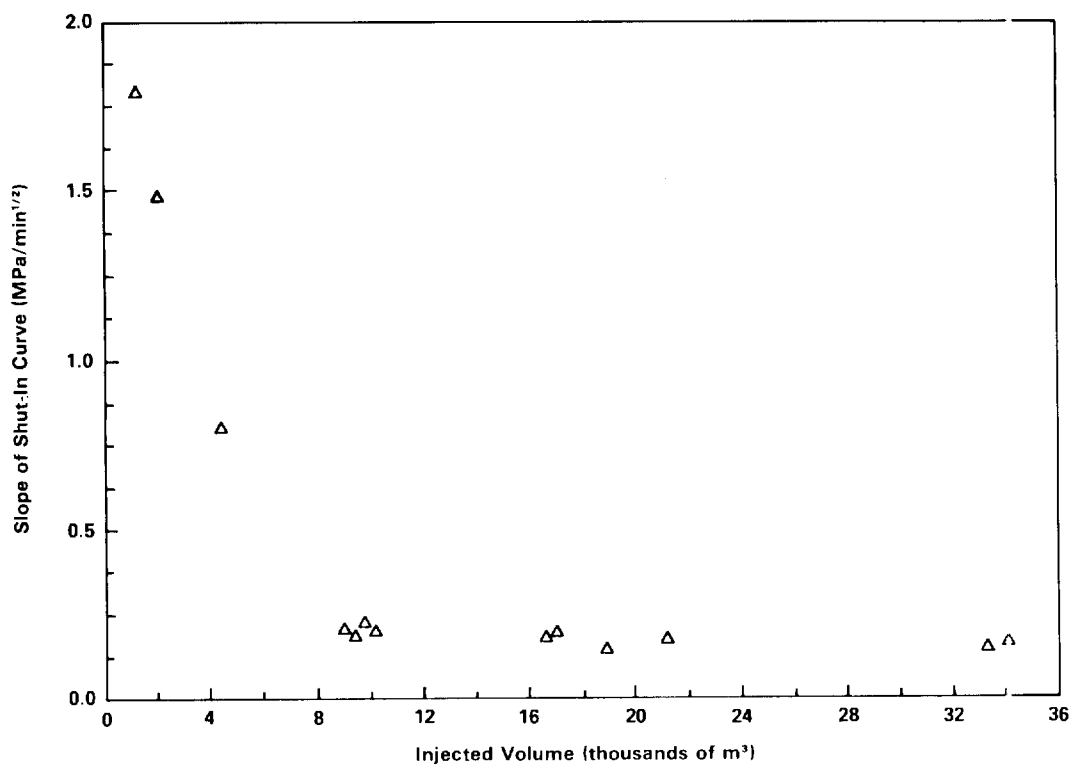

Figure IV-6. Slope of shut-in curves versus volume injected for EE-3A falloffs.

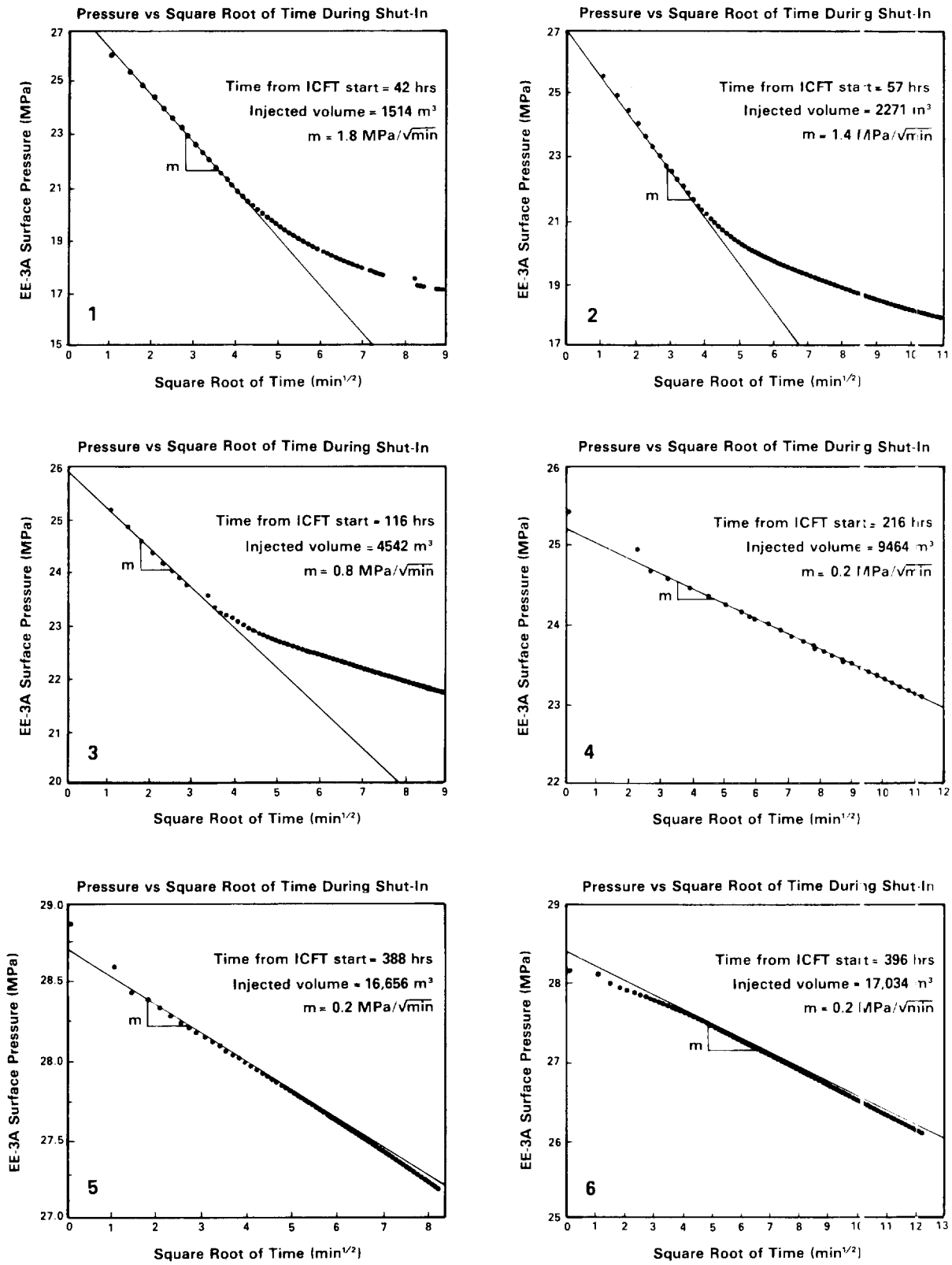

Figure IV-7. Six different shut-in curves during the ICFT.

Figures IV-8 and IV-9 are Horner curves for the wellhead pressures at EE-3A and EE-2, respectively. Assuming an injection zone of 150 m (492 ft) in height, the average permeability near EE-3A is 30×10^{-15} m^2 (30 md) and the skin factor is about -1. Around EE-2, the data were more ambiguous. Again assuming a 150-m production zone, the average permeability varied between 2×10^{-15} to 3×10^{-15} m^2 (2 to 3 md) and the skin factor varied between -3 to -2. The variability of results is due to little or no wellbore storage effect, making the location of a linear region rather arbitrary. The negative skin factors denote the expected presence of fractures, and the range of permeabilities is of the expected order of magnitude.

Another use for the fall-off curve is to identify the equilibrium pressure of the reservoir after a long shut-in (often denoted as p^*). Figure IV-8 shows that, on the surface, p^* of the Phase II reservoir is 29.0 MPa (4200 psi), or about 64.8 MPa (9400 psi) bottom hole. Using an overall compressibility of 3×10^{-5} MPa^{-1} (2×10^{-7} psi^{-1}) and a water-loss volume of 13 680 m^3 (3.61 million gal.), a total reservoir volume of 16.3×10^6 m^3 (4300 million gal.) can be derived. This volume compares well with that of a sphere of radius 150 m (492 ft). Looked at another way, a p^* of 29 MPa (4206 psi) leads to a fracture volume porosity of 0.08%.

Fracturing pressures are summarized in Table IV-IV, comparing the values obtained during the ICFT with those of the 1985 redrilling campaign. Figure IV-10 shows that the new values follow the same general trend with depth, falling around a pressure gradient of about 19 MPa/km (0.8 psi/ft). Also, the fracture closure stress obtained from the shut-in data is lower than that extrapolated from the ISIP method, again remaining consistent with previous results.

2. Analysis of EE-2 Data. EE-2 production pressures and rates were controlled by maintaining a fairly constant back pressure on the well. The wellhead pressure was generally maintained between 1.4 and 3.4 MPa (200 and 500 psi) so as to have single-phase flow from the well and through the heat exchangers. Notable exceptions to this occurred during various shut-ins, vents, gas kicks, and the nitrogen experiment. The pressure and flow rate data are summarized in Fig. IV-11 and compared with EE-3A in Figs. IV-12 and IV-13. The percentage of injection

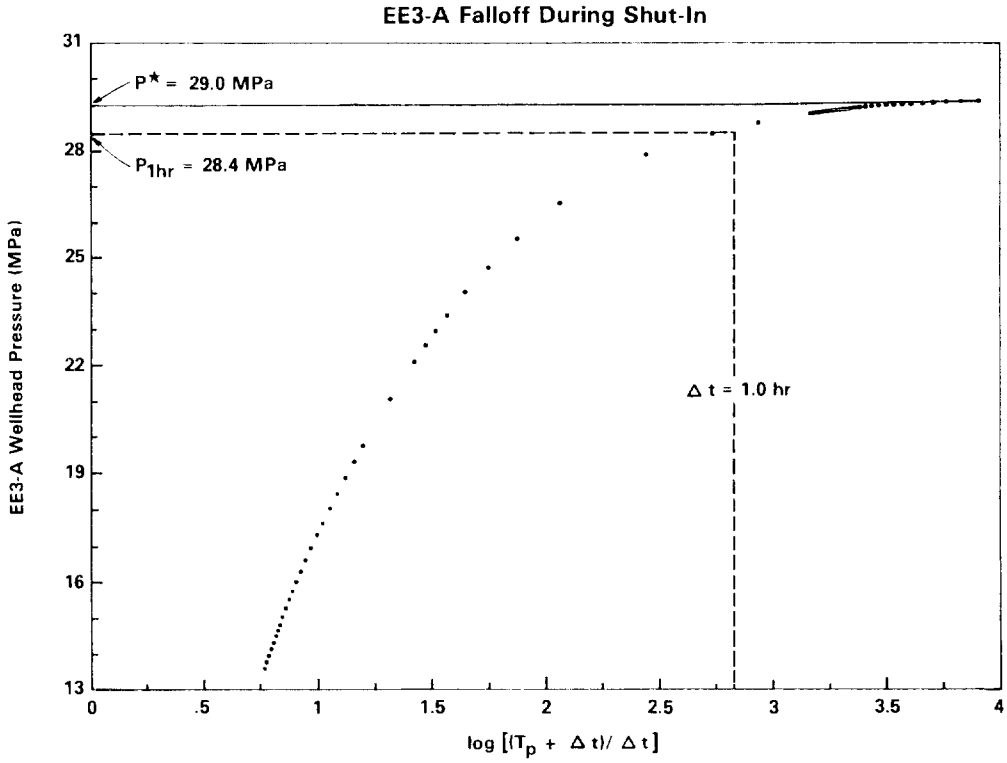

Figure IV-8. Horner curve for EE-3A wellhead pressure.

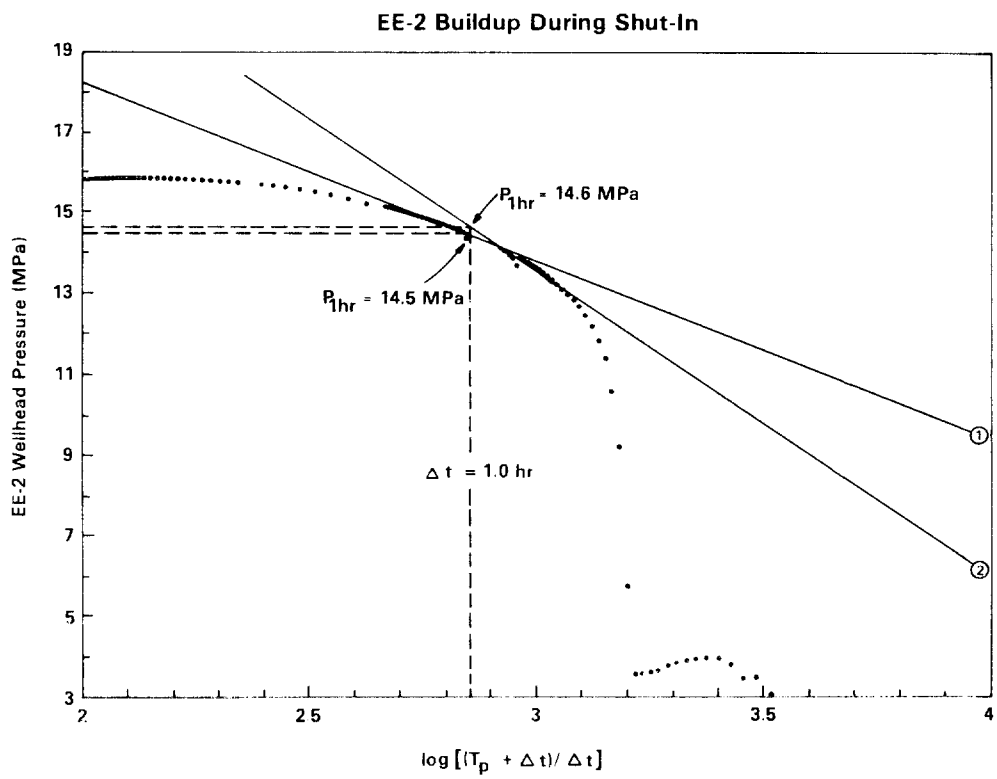

Figure IV-9. Horner curve for EE-2 wellhead pressure.

TABLE IV-IV

EE-3A FRACTURING PRESSURE COMPARISON WITH 1985 DRILLING CAMPAIGN

Expt. Number	Injection Interval (m along wellbore)	Fracturing Pressures (MPa) ISIP ($t^{1/2}$ method)	Extension Press. ($Q^{1/2}$ method)	Comments
2049	3301-3316		61.0	5.3 l/s
		60.2		10.6 l/s
		60.3		15.9 l/s
			61.8	5.3,10.6,15.9 l/s
2057	3301-3316	60.6		5.3 l/s
		62.7		15.9 l/s
2059	3516-3719 (most taken @ 3600)	69.6	56.7	connection
2061	about 4020	77.8	61.4	
2062	about 3660	64.9	59.0	connection
2067	about 3660	65.8	55.6	

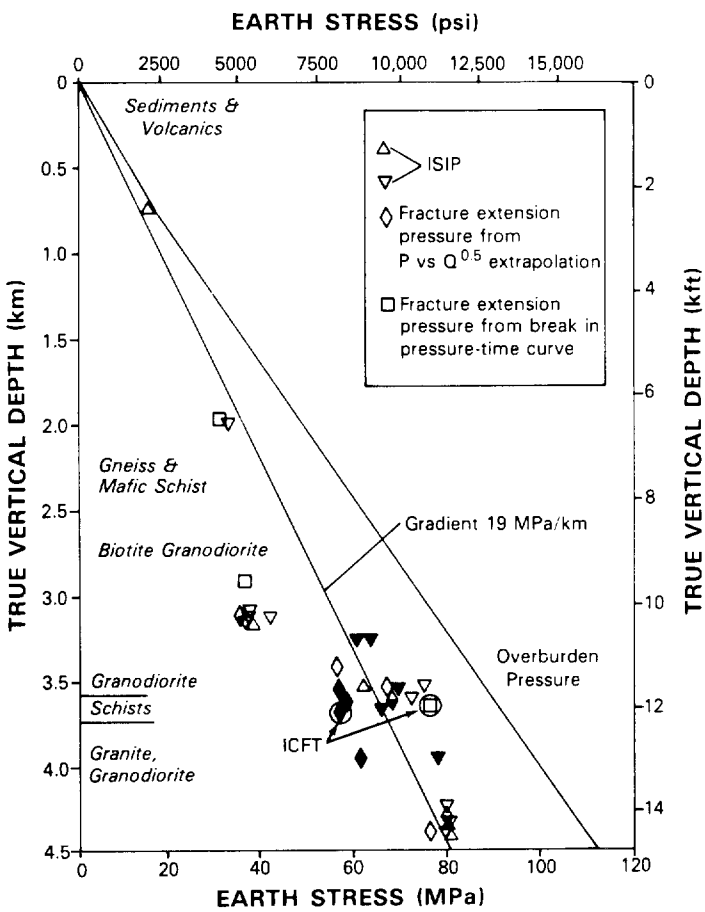

Figure IV-10. Fracture closure pressure versus depth for several experiments.

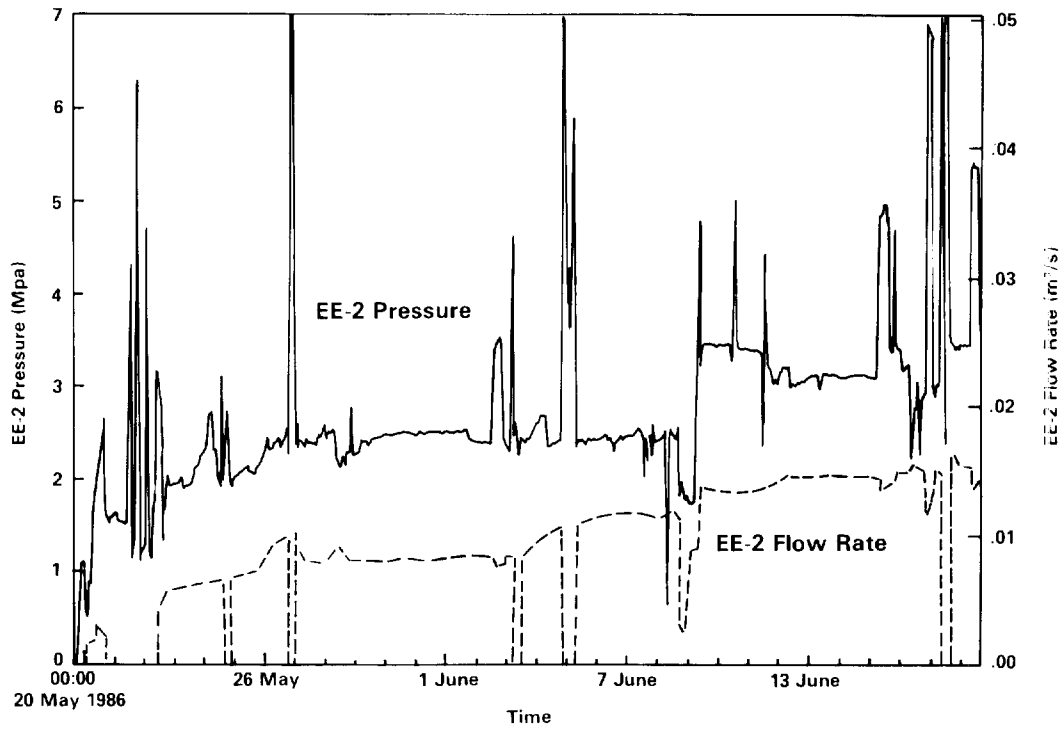

Figure IV-11. EE-2 pressure and flow rate.

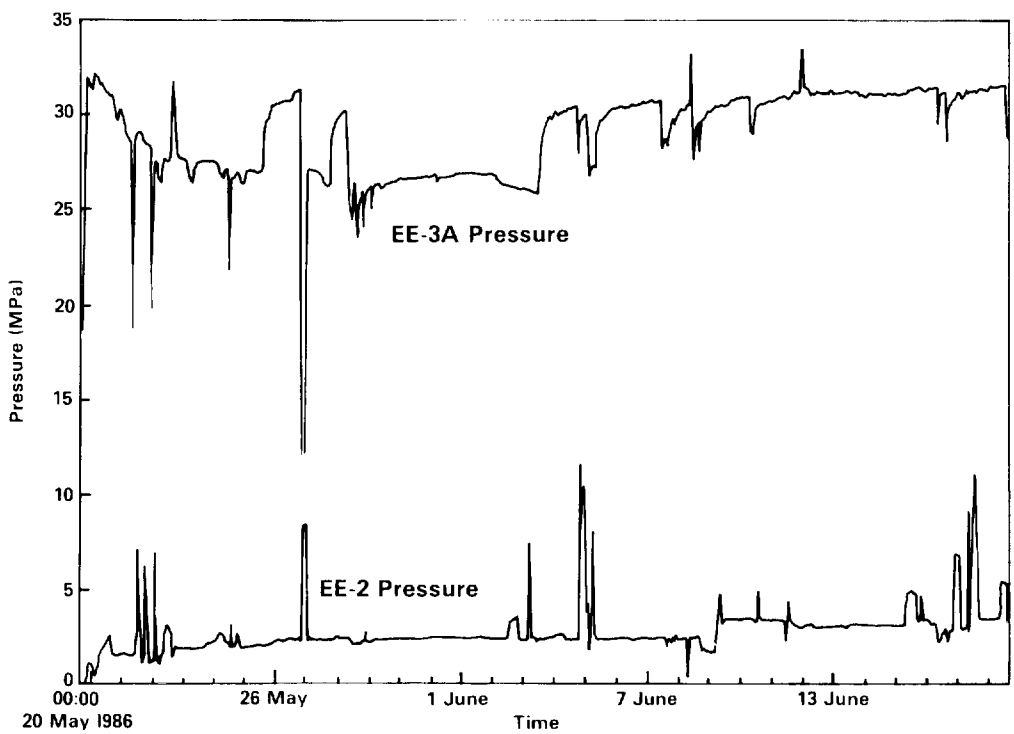

Figure IV-12. EE-2 and EE-3A pressure.

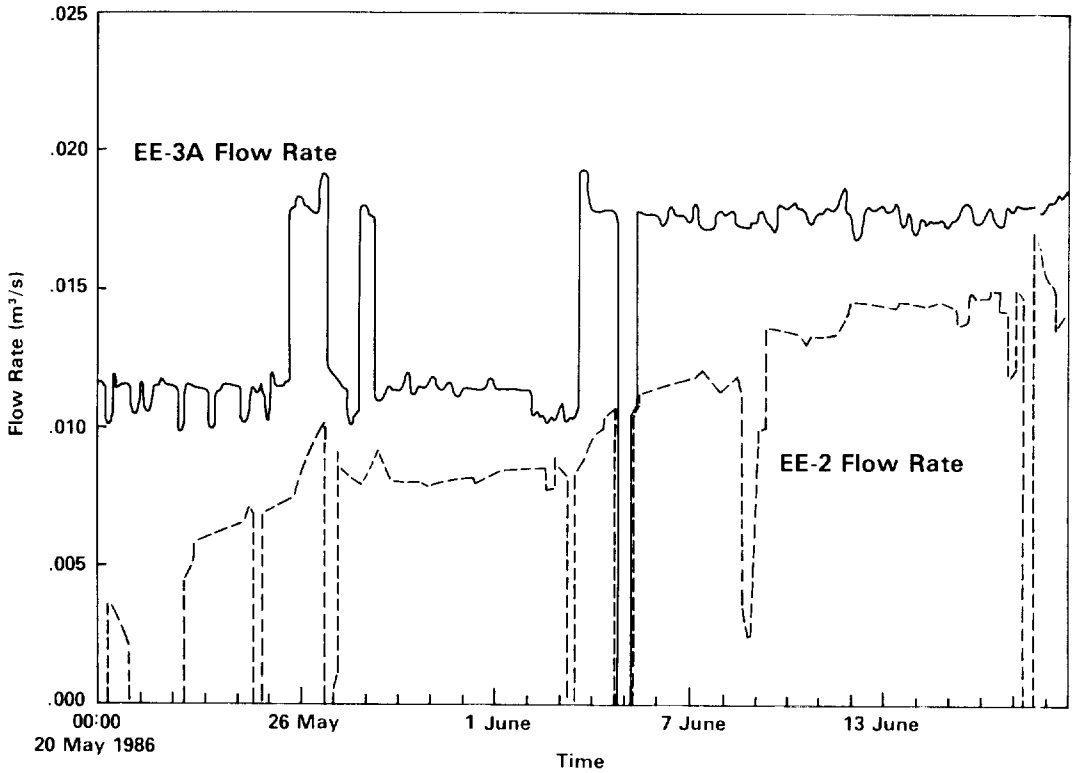

Figure IV-13. EE-2 and EE-3A flow rate.

flow that returned through the production wellbore increased throughout the flow test as the reservoir inflated to a quasi steady-state size.

Figure IV-14 shows the response of EE-2 pressure during the first 8 hours of pumping while EE-2 was shut-in. It took approximately 4.25 hours after the start of injection into EE-3A to observe a significant pressure response in EE-2. After this, the pressure increased at a rate of 1.6×10^{-4} MPa/s (1.4 psi/min).

3. Pressure Response at Phase I Wells. A flow connection from the Phase II reservoir to the Phase I reservoir, a pre-existing fractured region, was noted during the ICFT. Figure IV-15 shows that after 28 days of pumping into EE-3A while flowing EE-2, the two Phase I wells, EE-1 and GT-2B, experienced a pressure rise from atmospheric to 0.15 MPa (22 psi). The pressure increased steadily to 0.83 MPa (120 psi) 12 days after the final shut-in, a total increase of 0.68 MPa (98 psi).

The pressure rise in the Phase I wells was modeled by representing the fractured rock in the region previously mapped by microseismic events as a spherical region of constant pressure embedded in an

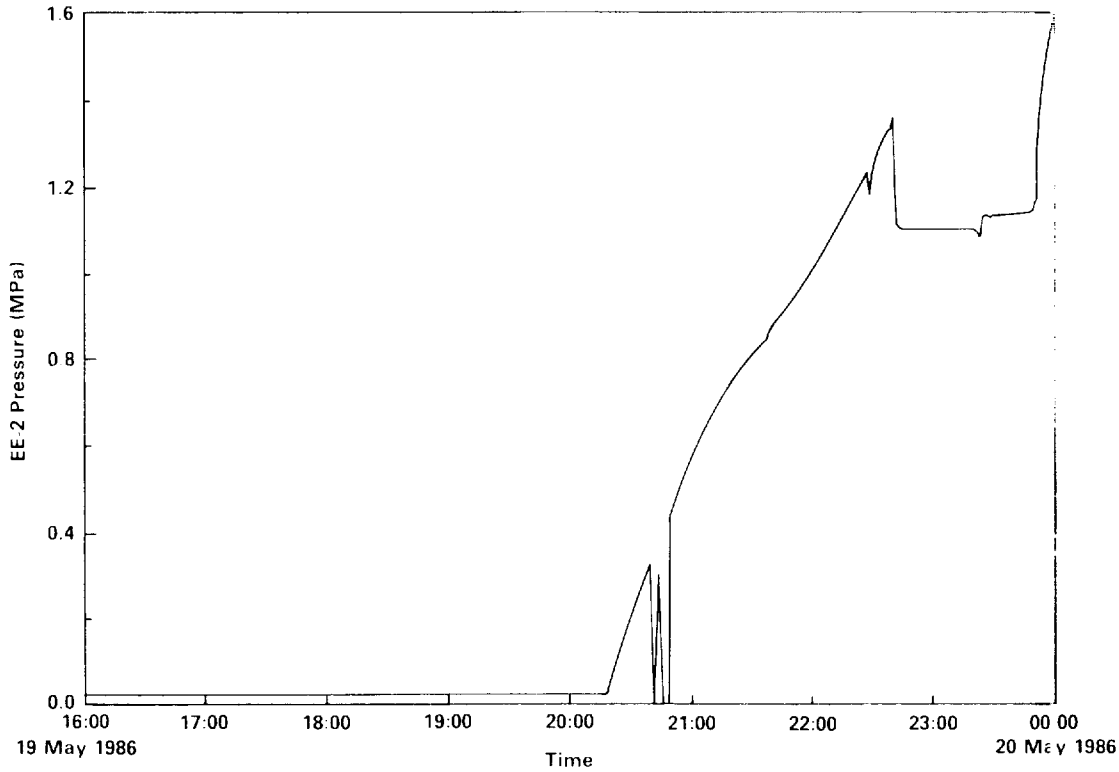

Figure IV-14. EE-2 pressure during the first 8 hours of the ICFT.

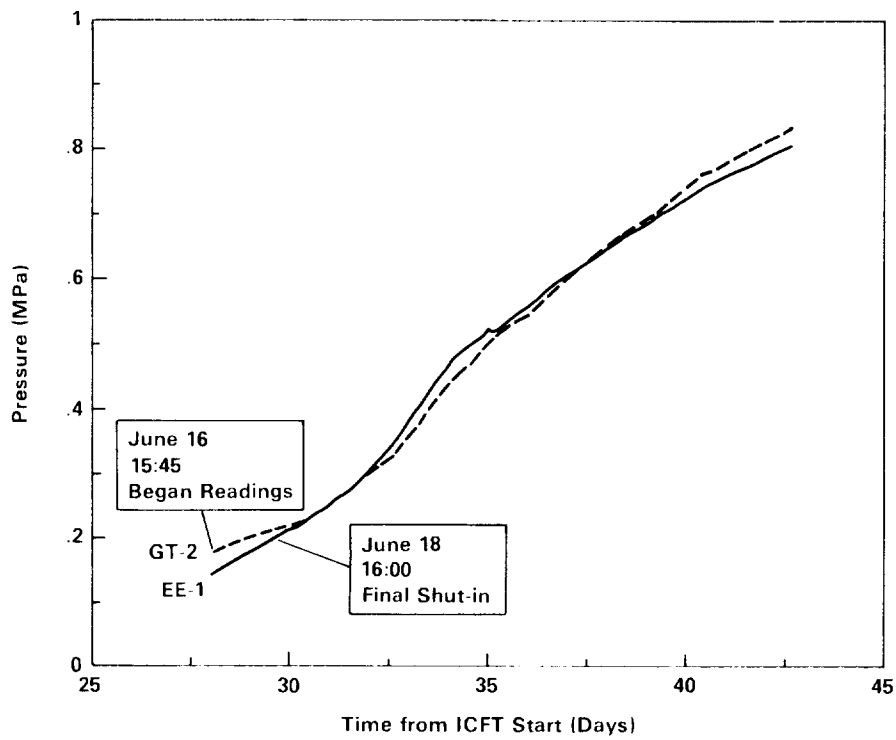

Figure IV-15. EE-1 and GT-2B response to the ICFT pressurization.

infinite homogeneous medium (Malzahn, 1986). Using an overall compressibility of $3x10^{-5}$ MPa^{-1} ($2x10^{-7}$ psi^{-1}) given by Murphy et al. (1977), preliminary results indicate a regional permeability of $18x10^{-18}$ m^2 (18 μd). This compares well with Fisher's (1980) estimations of $5x10^{-18}$ to $10x10^{-18}$ m^2 (5 to 10 μd).

B. Impedance

Impedance is a measure of the ability of a formation to transmit fluid and is analogous to electrical resistance. It is determined by simply dividing the pressure drop across a segment by the flow rate exiting the segment.

Reservoir impedance, calculated by removing the wellbore effects from the data, differs from overall impedance because of correction of the pressure drop for buoyancy and pipe friction, thereby eliminating the effects of depth and the pumping system. Figure IV-16 shows that the reservoir impedance decreased throughout the ICFT, going from 7 $GPa \cdot s/m^3$ (64 psi/gpm) to 2 $GPa \cdot s/m^3$ (18 psi/gpm) over the 30-day test with the most rapid decrease occurring during the first week of injection. This is due to hydrothermal stimulation along the fracture surface, especially near the injection wellbore.

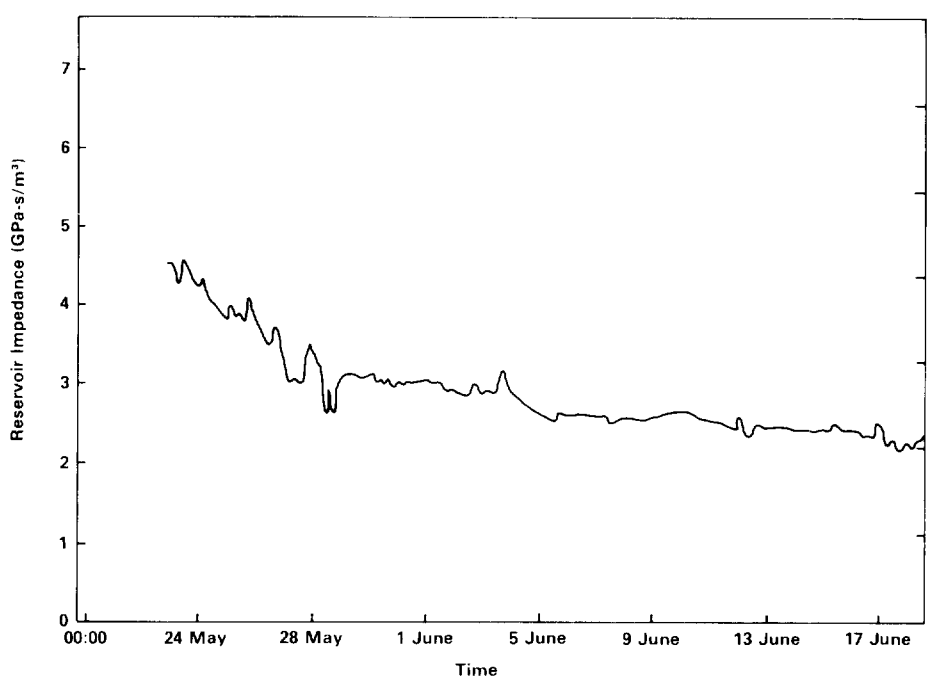

Figure IV-16. Overall reservoir impedance.

Near-wellbore impedance describes the part of the reservoir impedance immediately surrounding the wellbore and is found by subtracting the surface pressure from the instantaneous shut-in pressure, correcting this amount for buoyancy and friction, and then dividing by the surface flow rate immediately before the shut-in. Figure IV-17 shows that the EE-3A injection well impedance dropped rapidly during the first half of the test from 0.7 GPa·s/m^3 (6.6 psi/gpm) to 0.002 GPa·s/m^3 (0.02 psi/gpm), while the decrease at the production well, EE-2, was much more gradual. This may indicate that the EE-2 wellbore is damaged or otherwise restricted, e.g., by the short open-hole reach below the casing shoe and/or the casing restriction at 3200 m (10 500 ft).

C. Water Loss

There were four mechanisms of water loss operating during the ICFT: 1) reservoir extension indicated by microseismic activity; 2) reservoir inflation of the active reservoir and the static regions of several previous fracture experiments; 3) flow into the Phase I system; and 4)

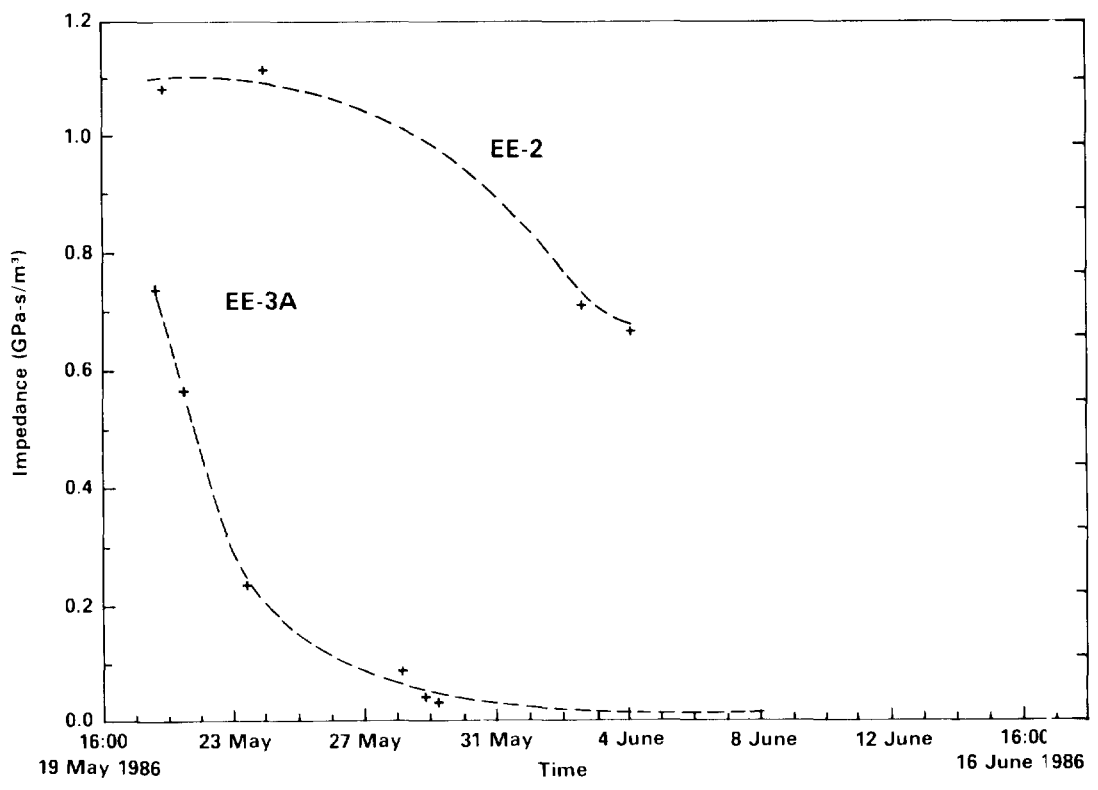

Figure IV-17. Wellbore impedance for EE-3A and EE-2.

leakoff into secondary porosity (i.e., into the country rock surrounding the fracture).

To calculate the cumulative water loss, the difference between the cumulative injection, 36 950 m^3 (9.76 million gal.), and the cumulative production, 23 270 m^3 (6.15 million gal.), was used as a first estimate giving 13 680 m^3 (3.61 million gal.). This does not account for the times that the production well, EE-2, was being vented to the EE-1 pond. An estimated 950 m^3 (0.25 million gal.) of water was vented based on log book records and data observations of the length of the vent and the previous flow rate from EE-2. This leaves approximately 12 730 m^3 (3.36 million gal.) of water lost during the experiment.

As shown in Fig. IV-18, the largest water loss occurred near the beginning of the ICFT, as the formation inflated. As the reservoir approached a quasi equilibrium, water loss averaged 30% of the injected volume, with a low of 26%. At this point, loss was due to reservoir extension, loss to the Phase I system, and leakoff into the surrounding rock.

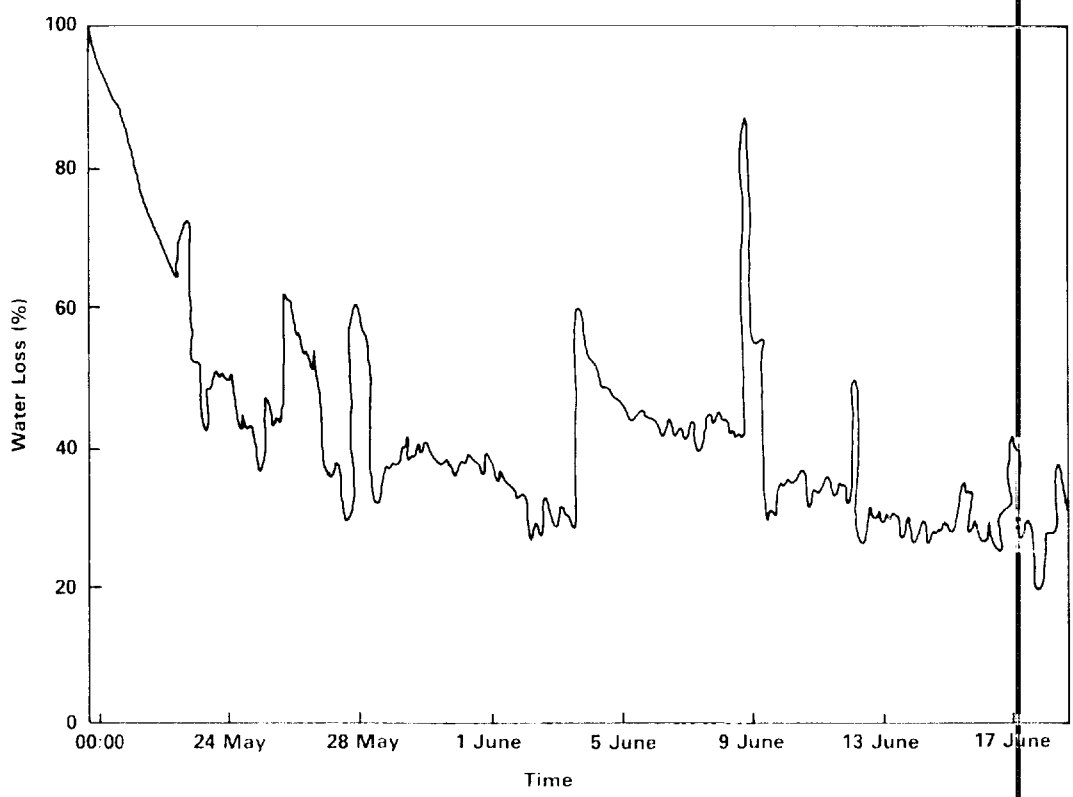

Figure IV-18. Percent water loss.

V. GEOCHEMISTRY AND TRACERS

A. Geochemistry Data

1. Sampling Apparatus and Procedures. The apparatus used to collect produced fluid gas and liquid samples is shown in Fig. V-1. Hot, pressurized fluid from a side stream off the production wellhead flowed to a small chemistry laboratory containing this equipment. The fluid was cooled under pressure in a heat exchanger and directed to the various apparatus in the figure either manually or automatically, depending on the sample being collected. Filtered and unfiltered liquid samples were collected manually through the ports labeled 1 and 2. Alternatively, fluid passed through an instrumented manifold kept at a pressure sufficient to prevent degassing. The eH, pH, and electrical conductivities of the fluid were recorded automatically in this manifold. The gas separation equipment on the right side of the figure supplied gas samples for the gas chromatographic and radon analyses. This separator was operated continuously, with gas samples directed

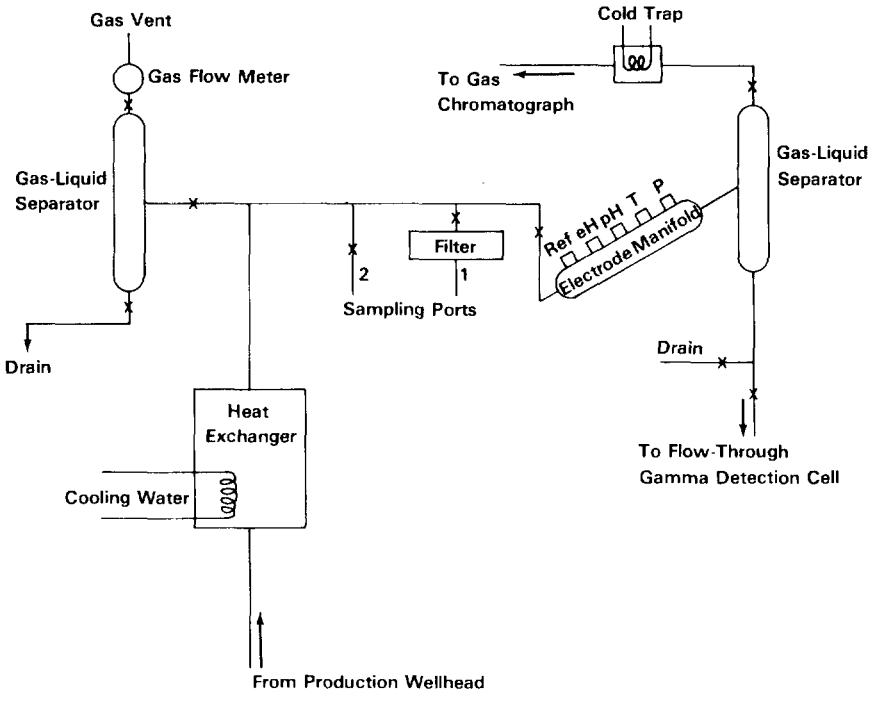

Figure V-1. Schematic of the sampling apparatus for production fluid liquids and gases.

periodically to the gas chromatograph after passing through a cold trap to remove any remaining moisture. In addition, the liquid effluent from this separator was directed to the gamma counter during the radioactive tracer experiments.

The other gas separation unit was used to measure gas and liquid flow rates simultaneously to obtain the gas mass fraction in the produced fluid. The separator was manually adjusted to achieve a constant liquid level and gas flow rate, and the gas and liquid flow rates were measured simultaneously. Since the gas was predominantly CO_2, the concentration of CO_2 (in weight percent) in the produced fluid was determined directly.

The procedures employed at Fenton Hill for analyzing gas and liquid samples for dissolved anions, cations, gas concentrations, suspended solids, and other species are described in detail by Trujillo et al. (1987).

2. Major Dissolved Species. Figure V-2 shows the concentration-time behavior of the major dissolved anions and cations in the produced fluid. Table V-I shows the concentrations in a sample collected 6 days

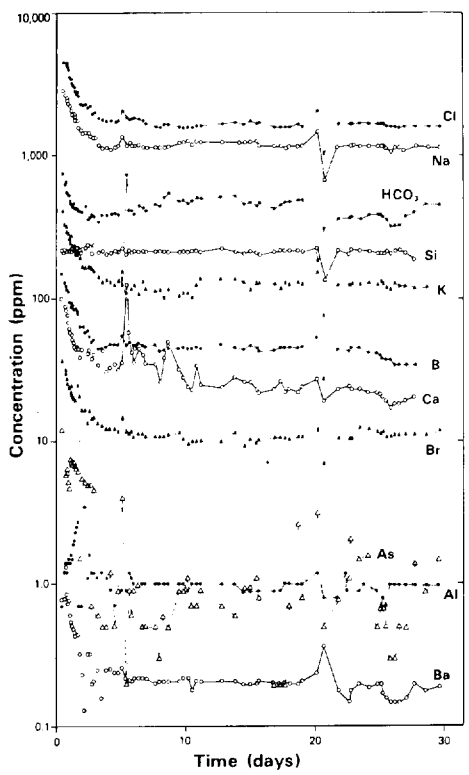

Figure V-2. Concentration-time behavior of the major dissolved species in the production fluid.

TABLE V-I

TYPICAL ION CONCENTRATIONS
(Sample Collected on Day 6)

Component	Concentration (ppm)
As	0.6
B	48
Br	11.5
Ca	42
Cl	1814
F	10.4
Fe	2.1
HCO_3	408
K	114
Li	23.4
Na	1180
pH	5.79
SiO_2	452
SO_4	183
TDS	4300 (I = 0.05 m)

into the flow test, after the geochemical behavior had reached a quasi steady state. The concentrations of most species are two to three times higher than in previous reservoirs, probably because of higher reservoir temperatures and a larger contribution from the *in situ* pore fluid. The total dissolved solids value of 4300 ppm, equivalent to ionic strength I = 0.05 m, is low enough that major brine-handling problems are not expected.

3. Noncondensable Gas Analyses. Gas analysis consisted of total gas flow rate (Fig. V-3) and gas chromatograph analysis of the dry gas composition. After the initial transient in the first few days of the flow test, the average gas flow rate was about 0.2% CO_2 by weight. Dismissing the high gas flow rates during a nitrogen injection experiment on day 20, the highest values were observed during the experiment

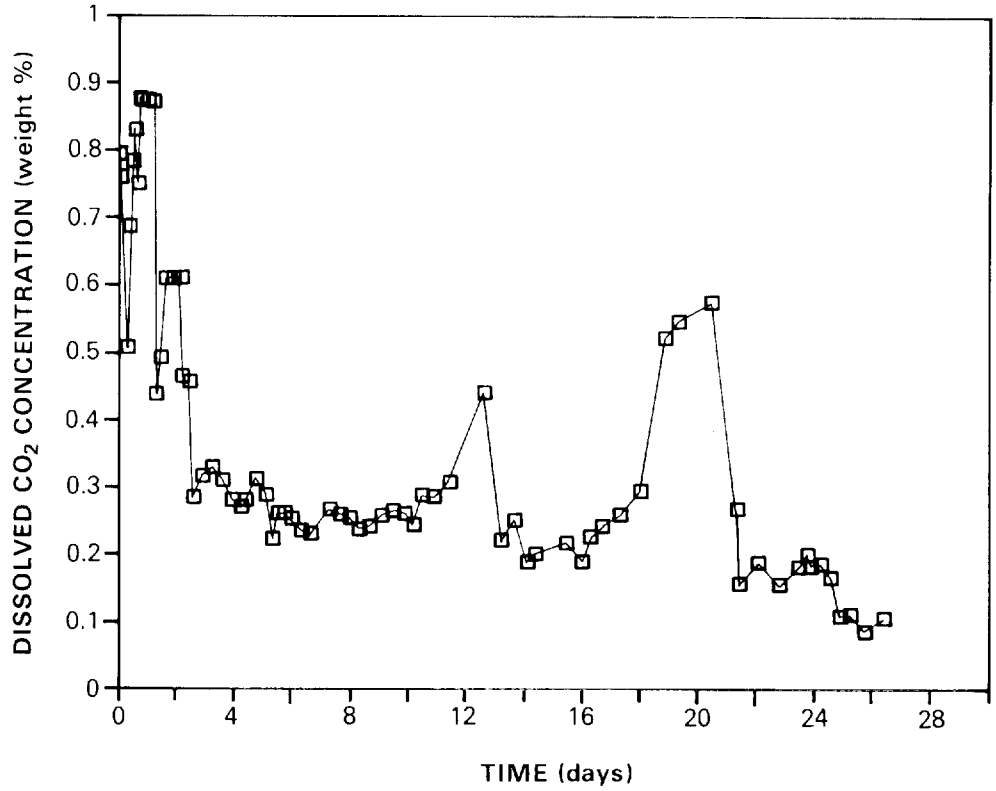

Figure V-3. Dissolved CO_2 concentration in the production fluid.

start-up. The high value of 0.9% is the best estimate of the CO_2 concentration in the pore fluid. Higher gas concentrations may have been present during periods of two-phase flow, but our sampling apparatus did not enable us to obtain a representative sample of the fluid during two-phase flow.

Gas chromatograph analyses determined the dry gas to be predominantly CO_2 (typically 90-95%), with lesser quantities of N_2, minute amounts of H_2S, O_2, and occasionally CH_4 and C_2H_6.

B. Interpretation of Geochemistry

1. Time-Dependent Behavior. When fluid of different concentration than the underground pore fluid is injected into a circulating HDR reservoir, the resulting produced fluid geochemistry behavior will be governed by three mechanisms: 1) displacement of the downhole fluid by the injected water; 2) rock-water dissolution, precipitation, or alteration reactions; and 3) adsorption of chemical species on the reservoir rock. Throughout most of the flow test, the downhole, injection, and

makeup fluids were all at similar concentrations (approximately those listed in Table V-I). However, early in the test the inlet and outlet concentrations were different and can be interpreted most effectively by defining a nondimensional concentration C* (Grigsby, 1983):

$$C^* = \frac{C - C_{in}}{C_o - C_{in}} \quad ; \qquad \text{(V-1)}$$

where C_{in} is the injection concentration and C_o is the initial produced fluid concentration, which is the true downhole concentration of the component if the sample is collected immediately after the wellbore fluid is displaced. (A summary of geochemistry nomenclature is provided in Appendix D.) The most common behavior is that of an inert, nonadsorbing species, which behaves like a tracer for a negative step change in injection concentration. Injected fluid gradually sweeps the concentrated underground pore fluid from the reservoir until the produced fluid concentrations approach the injection values (Fig. V-4).

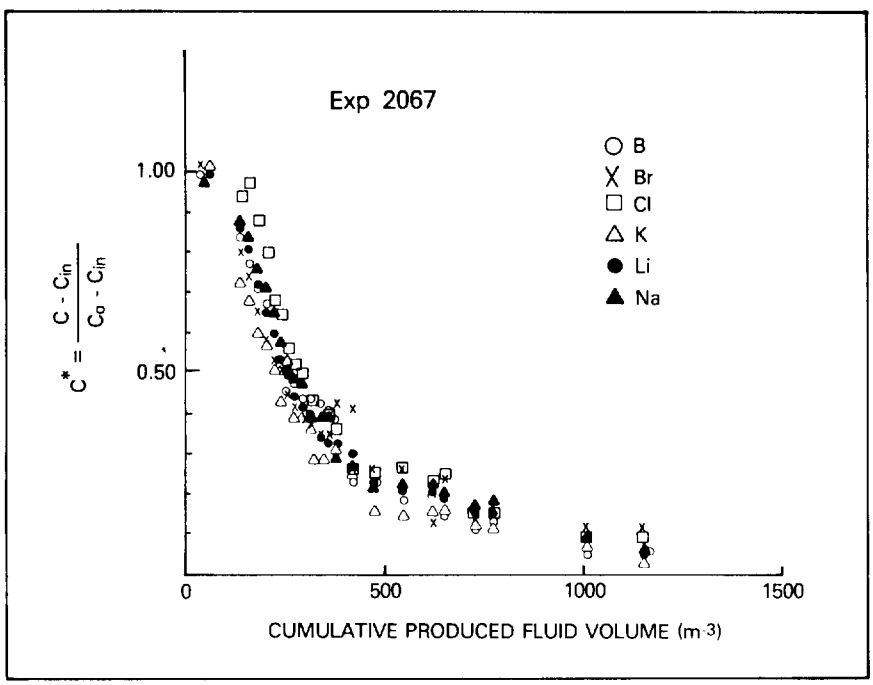

Figure V-4. Dimensionless concentration versus produced fluid volume for inert species during initial reservoir operation. Concentrations start at high downhole values and decline to injection fluid concentration.

Chloride ion, Cl, as well as B, Br, K, Li, Na, electrical conductivity, and total dissolved solids all fall in this category.

Two other characteristic concentration-time responses are exhibited in Fig. V-5. The dissolved silica concentration remained constant during the initial sweep of pore fluid from the reservoir and throughout the entire 30-day test. Quartz dissolution supplies a constant source of silica to the undersaturated injection fluid, allowing the solution to reach equilibrium in one pass through the reservoir. The third type of time-dependent behavior is for species whose concentration decreases to a value below the injection value. This result implies consumption of the component, either by adsorption on the rock surface or precipitation reactions. Divalent cations such as magnesium clearly show a propensity to adsorb on granite, and, as shown in the figure, fall into this third category. Calcium, bicarbonate, and iron also exhibit this behavior, although the mechanisms for these three components are as yet unclear. Finally, a few species such as Ba, Mn, and SO_4 exhibit anomalous time dependences, which have not been explained.

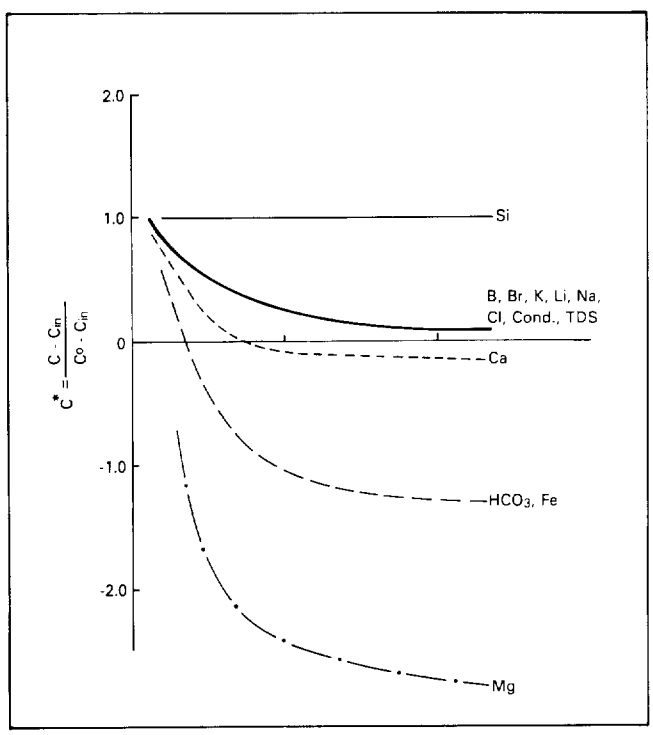

Figure V-5. Different types of concentration-volume behavior observed during initial reservoir operation.

2. Sources of Dissolved Species. The origin of dissolved species in hot dry rock geothermal fluids has been treated by Grigsby et al. (1983). The two primary sources of dissolved species are displacement of downhole pore fluid and dissolution of minerals. Current models postulate a continuous extraction of the original pore fluid from the fractured rock mass over long periods of time. The most compelling argument supporting this theory is the presence and continued supply of chemically inert species such as boron and chloride, which are not found in the reservoir granite and hence are not supplied by a dissolution reaction.

Since most reservoir fluid samples are composed of the original downhole fluid after dilution with injected fluid, true values of the pore fluid concentrations are difficult to obtain. Grigsby (1983) has demonstrated that even when the pore fluid is diluted, the ratios of ions in solution should remain constant for conservative species supplied only by pore fluid rather than by mineral dissolution or alteration. When the concentration of one component is plotted directly against another, the data should fall on a single straight line if the source of the pore fluid is the same. Figure V-6 is a plot of boron

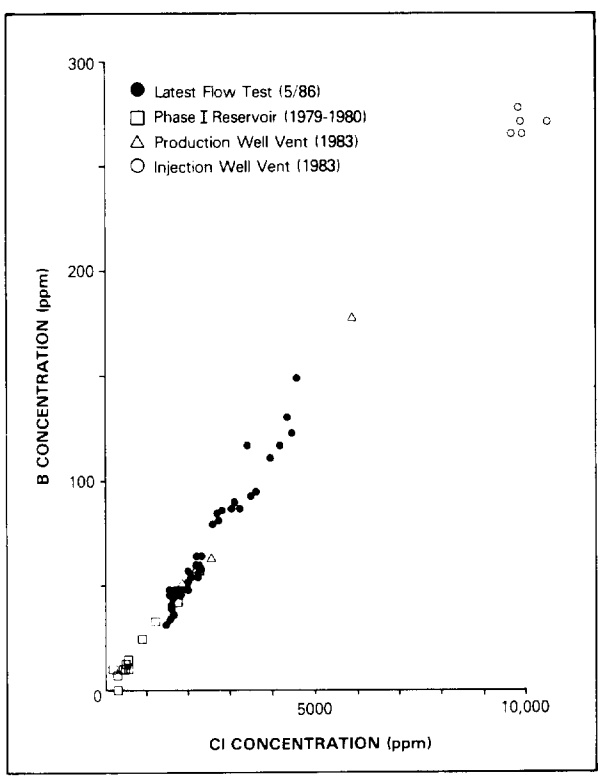

Figure V-6. Boron versus chloride for fluid samples collected in the Fenton Hill HDR reservoir over the past 6 years.

versus chloride for the ICFT and previous Fenton Hill circulation experiments and vents of the past 6 years. The new data all fall on the same straight lines as those for other fluid samples collected at Fenton Hill. The evidence now even more strongly supports the pore fluid hypothesis and suggests that a single underground fluid supplies the conservative species found in fluid samples at the Fenton Hill site.

Rock-water reactions are also important in the production or consumption of some species. For example, quartz dissolution controls the concentration of dissolved silica in the production fluid. The constant concentration measured during the flow test implies that the kinetics of quartz dissolution were rapid enough for the fluid to reach saturation in one pass through the system. Robinson (1982) measured the rate of quartz dissolution as a function of temperature and rock surface area and determined the following relation:

$$\ln \Phi = \ln \left[\frac{C^{\infty} - C}{C^{\infty} - C_{in}}\right] = -ka^{*}t \quad ; \qquad \text{(V-2)}$$

where a* is the quartz surface area to fluid volume ratio ($2f_q/b$ for a flat fracture, where b is the fracture aperture and f_q is the fraction of quartz present in the granite), C^{∞} is the saturation concentration, and k is the rate constant for dissolution. To obtain a minimum value for a*, or a maximum value for the average fracture aperture, the following values were used:

Φ = 0.1 (equivalent to the dissolution reaction reaching 90% of its equilibrium value),

t = 10 hours (the residence time at the peak tracer response),

k = 4.13×10^{-8} m/s at 250°C (Robinson, 1982), and

f_q = 0.3.

These assumptions yield a* = 1550 m^{-1}, or b = 0.4 mm. In other words, the average aperture encountered by fluid should be no greater than about 0.4 mm and quite possibly less in order for the system to reach saturation with respect to quartz in one pass through the reservoir. Future models for the permeability and tracer behavior of the reservoir must be consistent with this information.

Another set of reactions affecting the produced fluid chemistry is the dissolved carbon dioxide-bicarbonate equilibrium reactions, which are coupled to the calcite dissolution reaction. Carbon dioxide is present in the underground pore fluid and is produced along with other pore fluid elements. If calcite (calcium carbonate, $CaCO_3$) is present, its solubility is also affected by the presence of dissolved CO_2. For a CO_2-rich fluid in equilibrium with calcite, the following chemical reaction applies:

$$CaCO_3 + H_2O + CO_{2(g)} \leftrightarrow Ca^{2+} + 2HCO_3^- \quad , \tag{V-3}$$

with equilibrium constant K_{eq} equal to

$$K_{eq} = \frac{\gamma_{Ca}\ \gamma^2_{HCO_3}\ [Ca][HCO_3]^2}{P_{CO_2}} \quad . \tag{V-4}$$

The concentrations are in mol/l and the activity coefficients, γ, are related to ionic strength and temperature using a modified Debye-Huckel model (Henley et al., 1984). The partial pressure of CO_2, P_{CO_2}, is given by

$$P_{CO_2} = K_H\ x_{CO_2} \quad ; \tag{V-5}$$

where K_H, the Henry's law constant for CO_2, is a function of temperature, and x_{CO_2} is the fraction of CO_2 in the liquid. Using the measured values of all concentrations, and expressions supplied by Henley et al. (1984) for K_H and the γ's, we may iteratively calculate the equilibrium temperature at which these dissolved species were produced. For the 75 samples analyzed, the average calculated temperature was 211°C, with a standard deviation of 16°C. These temperatures are in reasonable agreement with the measured downhole production temperature of about 232°C, suggesting that for a given downhole P_{CO_2}, calcite dissolution is governing the equilibrium between dissolved CO_2, bicarbonate ion, and Ca. As significant changes in downhole temperatures occur due to thermal drawdown or exposure of hotter fluid

flow paths, corresponding changes in these concentrations should also occur. However, to use these equilibrium reactions to evaluate reservoir temperature patterns, further refinements of the calculations will be required to explain the 20°C discrepancy between the actual and average calculated temperatures.

3. Geothermometer Readings. Since rock-mineral dissolution or alteration reactions are temperature dependent, the concentrations of certain dissolved species will depend on temperature. The calculations just presented are one example. Two more commonly used chemical geothermometers that exploit this temperature sensitivity are the quartz and Na-K-Ca geothermometers. These two measurements are shown for samples collected throughout the flow test in Fig. V-7. The recorded geothermometer temperature for quartz dissolution of about 250°C agrees fairly closely with the actual downhole temperature. The reactions governing the Na-K-Ca geothermometer do not reach equilibrium in short times, however. Thus, since the produced fluid is a mixture of the

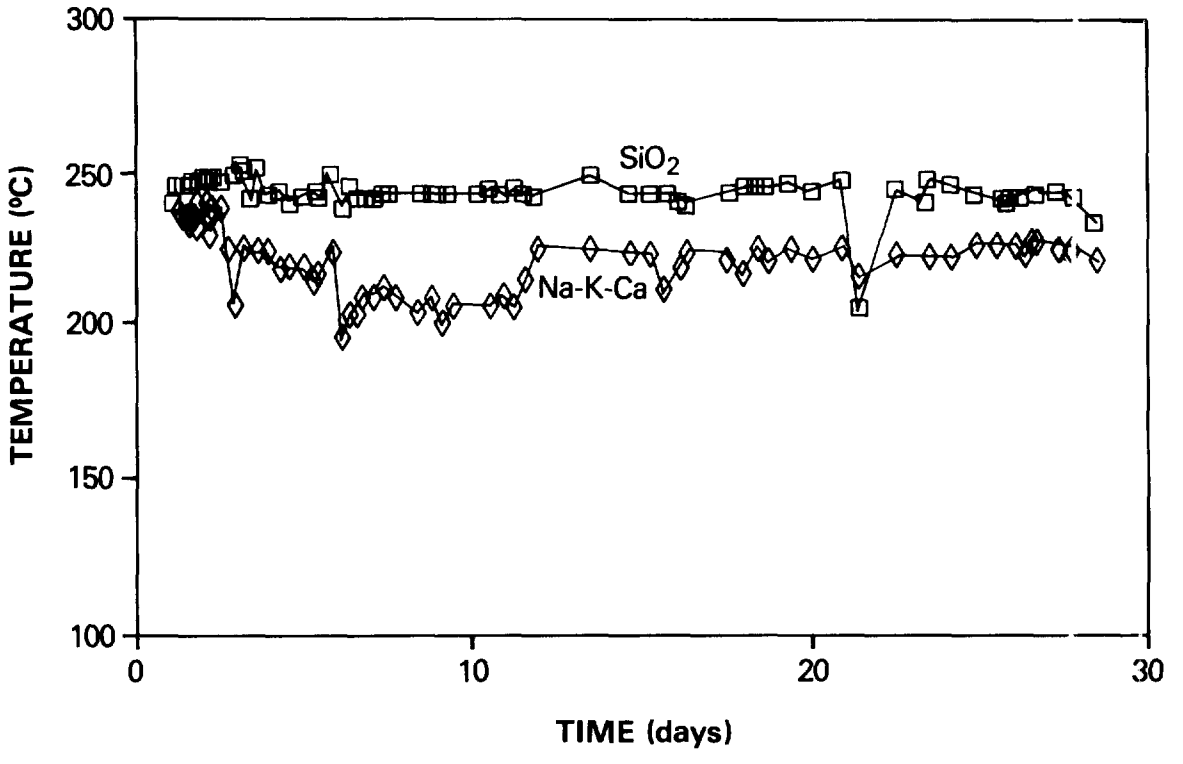

Figure V-7. Silica and Na-K-Ca geothermometer temperatures.

injection fluid and underground pore fluid, these geothermometer readings are not as precise. The Na-K-Ca temperatures decrease from essentially the known rock temperature to a somewhat lower value. In future work we will model this behavior, as well as the carbon dioxide-bicarbonate equilibrium reactions, as the mixing of fluids of different concentrations and temperatures to attempt to determine what concentrations and flow fractions are required to match the results.

C. Chemical Effects on Operations

1. Corrosion Studies. Because of the large number of metal hardware failures attributed to metallic corrosion during the drilling of the injection and production wellbores, corrosion monitoring was performed during this flow test. Of greatest concern are the high temperatures, gas concentrations, and concentrations of corrosive ions such as Cl^-. This 30-day flow test provided data for future surface loop design.

Corrosion coupons were placed on side streams off the main-stream flow on both the hot and cold sides of the heat exchanger. Each station contained two coupons attached to a coupon holder of sufficient length that the coupons were exposed to a representative sample of the fluid. The coupons were oriented parallel to the fluid flow to minimize erosion. Shutoff valves placed at both stations allowed the coupons to be removed periodically. Pressure taps were placed at the entrance and exit points of the side-stream piping to direct the fluid flow to the coupons. The coupons were analyzed periodically for corrosion rate (by measuring coupon weight loss over a specified time, typically 150 hours), type of corrosion, and scale formation.

The corrosion rates at various times during the flow test are presented in Fig. V-8. The more rapid corrosion rates occurring on the hot side of the heat exchanger are due to the higher temperature, which increases the attack of metal hardware by elemental species present in the production fluid. The highest corrosion rate of 15 mils per year (mpy), occurring with the second set of coupons, will be used as the design criterion for the surface equipment for future tests. In the final set of coupons, the dramatic decrease in hot-side corrosion rate is attributed to equipment malfunctions that prevented liquid flow from reaching the coupons.

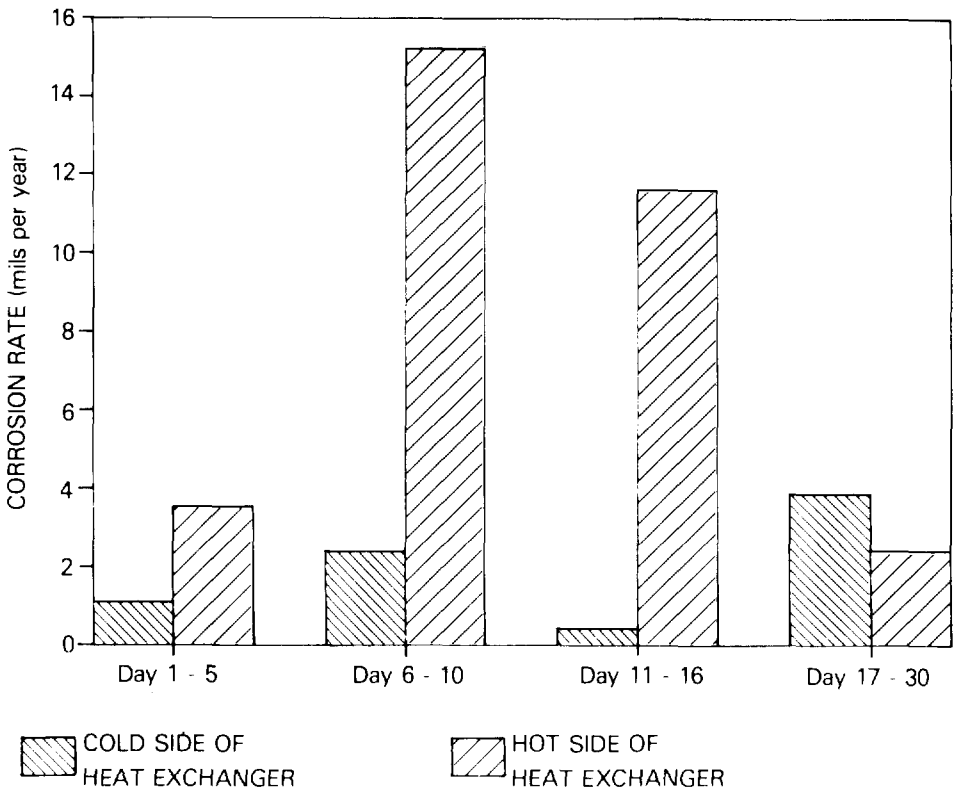

Figure V-8. Corrosion rates measured on the hot and cold sides of the heat exchanger. Each value is obtained from a determination of weight-loss for a coupon exposed to fluid during the times labeled.

The type of corrosion observed on both sample stations was generalized and uniform. This behavior is typical of metal exposed to acidic fluid under flowing conditions. The only deviation from this pattern was in the final set of coupons on the cold side, where the corrosion rate increased and extensive pitting was observed. This anomalous behavior is probably due to the increase in dissolved oxygen observed at this time in the experiment.

When assessing the potential for corrosion damage in geothermal systems, the type of corrosion may be more important than the rate of metal dissolution. A high concentration of Cl^- or dissolved O_2 induces pitting, which increases potential equipment failures dramatically. The lack of heavy pitting on our corrosion coupons suggests that materials will not be subjected to severe corrosive attack. Nonetheless, surface hardware durability and performance in future flow tests can be enhanced

with appropriate corrosion treatment. Alternatively, corrosion-resistant materials or heavy-walled pipe could be used, but in our case the cost advantages of light carbon steel equipment outweigh the possible benefits of these approaches, particularly if dissolved gases are handled properly. To minimize pitting corrosion during longer periods of operation, dissolved oxygen in the injection fluid will be kept low (in the parts per billion range) by injecting an oxygen scavenger such as ammonium bisulfite or hydrazine.

2. Gas Handling. To keep a geothermal fluid containing dissolved CO_2 a single phase, the total system pressure must be greater than the sum of the partial pressures of CO_2 and water:

$$P > P_{CO_2} + P_w \quad . \tag{V-6}$$

This expression is valid for a closed system not open to the atmosphere. The partial pressure of water, P_w, is approximately equal to its vapor pressure. The term P_{CO_2} is a function of the concentration of CO_2 in the liquid phase and its Henry's law constant K_H, as given by Eq. (V-5). The constant K_H and P_w are both functions of temperature. Figure V-9 shows the minimum pressure required to keep the solution a single-phase liquid for different temperatures and concentrations of dissolved CO_2.

During most of the flow test, dissolved CO_2 remained in the liquid phase and was reinjected after energy extraction. A simple calculation or use of Fig. V-9 shows why this was possible. The dotted line in Fig. V-9, representing the pressure-temperature behavior of fluid in the surface loop, shows that only fluids with dissolved CO_2 concentrations greater than 0.7% will cause flashing. For the typical value of 0.2 - 0.3%, the mixture will remain a single phase. Occasionally, new regions of the reservoir were accessed and a transient period of high CO_2 concentration occurred. Phase separation in the production wellbore prevented us from collecting a representative sample, but Fig. V-9 shows that the CO_2 concentration must have been about 1% or greater. For future operations we will install a high-pressure, high-temperature gas separator to handle these occasional gas surges.

3. Scale Deposition. The two types of scale deposition that were of greatest concern before the flow test were silica and calcite

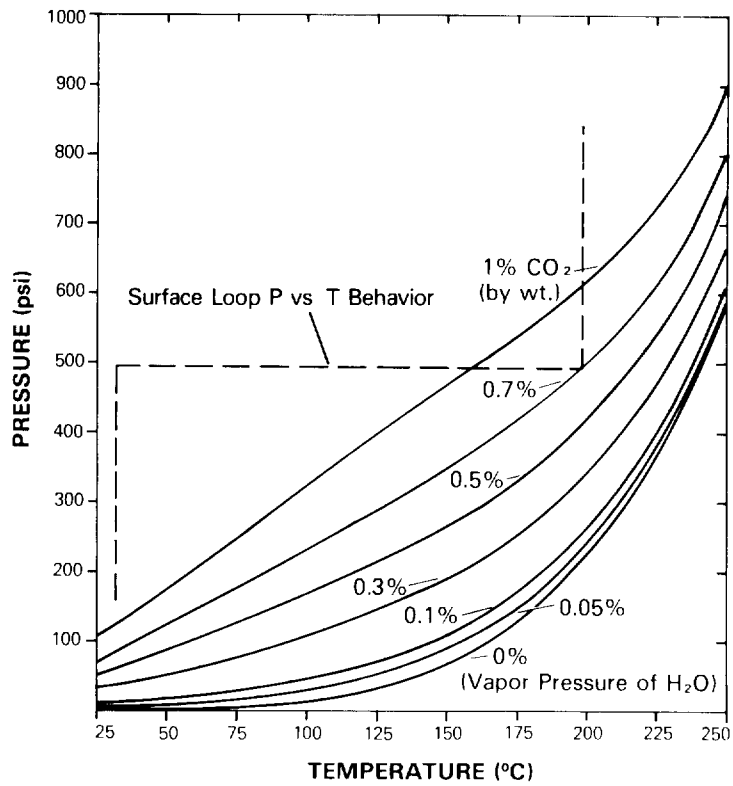

Figure V-9. Pressure required to keep CO_2 - H_2O solution single phase for different CO_2 concentrations and temperatures. Dotted line is a typical (P,T) curve for an element of fluid passing through the surface loop equipment.

precipitation. When water saturated with respect to quartz at reservoir temperatures is cooled, it becomes supersaturated with respect to all forms of silica. Hence a driving force for silica scaling is present. Calcite precipitation occurs for a different reason. Flashing of CO_2 from solution creates disequilibrium which, according to elementary chemical thermodynamics, will cause the reaction of Eq. (V-3) to proceed to the left to reachieve equilibrium. Thus, calcite ($CaCO_3$) is deposited.

Despite these potential mechanisms, very little scale deposition was uncovered in a postexperiment examination of the surface loop, and this scale did not adversely affect the performance of the equipment. Only a small amount of calcium carbonate scale was found on a pipe leading to the heat exchanger, while no silica deposits were found. However, some magnetite scale was detected in the inlet manifolds of the heat exchangers, although we cannot determine whether it was deposited

during this or a previous flow test. In addition, a yellowish precipitate containing about 4% arsenic was detected on the corrosion coupons on the cold station of the heat exchanger and in the heat exchanger itself.

D. Tracer Experiments

1. Procedures. Two radioactive tracer experiments, the first on day 10 and the second on day 25, were carried out using an irradiated form of the water soluble salt, ammonium bromide, NH_4Br. The tracer, ^{82}Br, a gamma-emitting radionuclide with a half-life of 35.3 hours, has been used as a conservative (nonreacting, nonadsorbing) tracer at Fenton Hill for several years (Robinson and Tester, 1984). In each tracer experiment a sample was irradiated in the Los Alamos Omega West nuclear reactor, assayed, and transported to the Fenton Hill site. Accounting for radioactive decay during the transportation, the injected pulse strengths were 61.9 mCi and 70.2 mCi. Measurements of gamma activity as a function of time were obtained in the mobile chemistry laboratory by flowing a liquid side stream through a continuous flow cell equipped with a NaI scintillation counter.

2. Results. To obtain a residence time distribution (RTD) curve from a pulse injection tracer experiment, the background radioactivity must be subtracted and the resulting value corrected for radioactive decay. Then, the RTD f(V) is given by

$$f(V) = \frac{C(V)}{m_p} \quad ; \qquad \text{(V-7)}$$

where C(V) is the corrected concentration at produced fluid volume V, and m_p is the mass of the tracer pulse.

When the produced fluid is recirculated, as in the first test, the concentration-time response must also be corrected for the reinjection of radioactive fluid using a mathematical deconvolution technique (Robinson and Tester, 1984). This calculation was performed for the first experiment, while the second test was conducted in the open-loop injection mode with production fluid returns temporarily vented to a holding pond. Thus in the second test the true RTD was obtained directly from Eq. (V-7).

The RTD curves for the two experiments are shown in Fig. V-10. The most striking difference from tracer tests in past Fenton Hill reservoirs is the low recovery of tracer. The ^{82}Br tracer experiment is limited to 2-3 days owing to its half-life, so the low tracer recoveries actually imply that a larger percentage of the fluid has residence times longer than 3 days. According to current models of tracer flow through fractured reservoirs, the present system must contain flow paths of large volume that conduct at least half the fluid. In addition, the modal volume (produced fluid volume at the peak of the response curve), a standard correlating parameter for estimating the heat-transfer capacity of a fractured HDR reservoir (Robinson and Tester, 1984) is larger by roughly a factor of 2 than previous Fenton Hill reservoirs at a similar stage of operation. Hence we expect a longer-lasting reservoir with more gradual production fluid temperature drawdown than in the past.

Comparing the two tracer curves, the response is shifted to larger volumes, and less tracer was recovered in the second test. This result

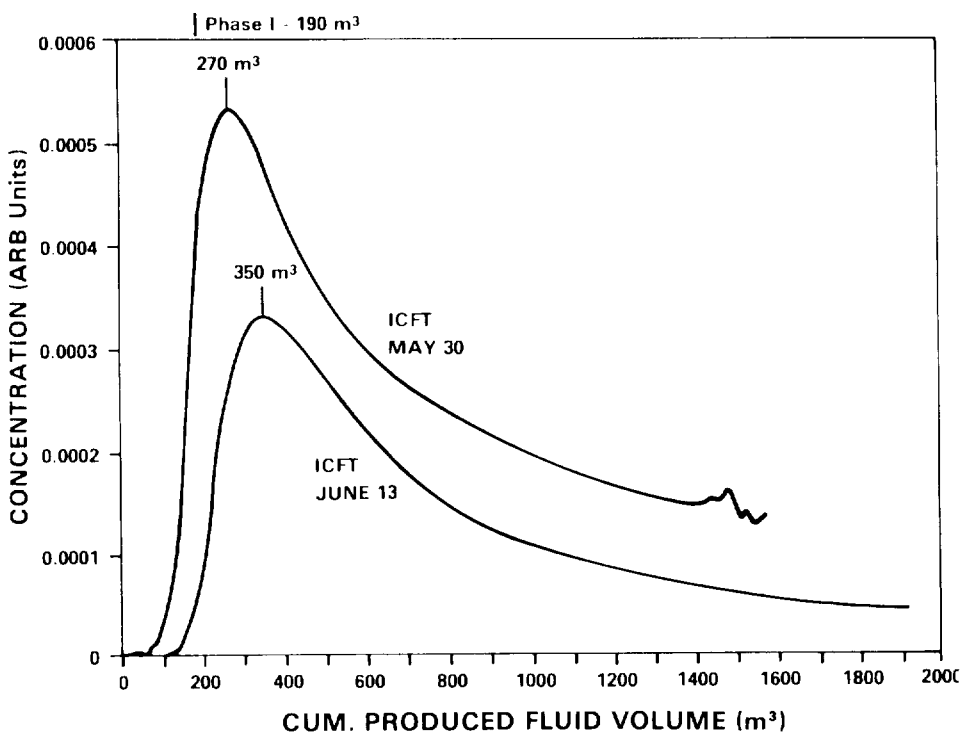

Figure V-10. Residence time distribution curves obtained from the two radioactive tracer experiments.

is due to the transient state of the reservoir during the flow test; throughout the test, the difference of the inlet and outlet flow rates, commonly thought of as water loss, was in large part going into charging the reservoir. Thus a dramatic increase in the integral mean volume (the volume of all fractures connecting the two wellbores, regardless of residence time) from 2180 to 8440 m^3 was observed. The postexperiment vent of the reservoir supports the idea that the observed water loss was caused by the need to fill the fracture system. Of the total of 12 000 m^3 net water lost to the fracture system, 6400 m^3 returned during the vent. Both of these values are in rough agreement with the fracture volume of 8440 m^3 measured in the second tracer test.

The fracture volume estimates aid in the development of conceptual models of the flow system. Assuming a homogeneous fracture network of known porosity, fracture volumes may be used to calculate the swept rock volume. The value of fracture porosity may be bounded between 0.0004 - 0.004, based on measurements of seismicity and reservoir compressibility calculations. For a fracture porosity of 0.003, the rock volumes calculated from the second tracer experiment correspond to a sphere of diameter 150 m. Although the value of porosity is inexact, the resulting sphere diameter is of the same order of magnitude as the wellbore separation distance of 110 m. Thus the conceptual model of flow through a large network of fractures with a point source and sink is a reasonable first approximation.

VI. SEISMOLOGY

A. Data Collection and Processing

Seismic sensors were deployed at 17 sites during the ICFT (Fig. VI-1, Table VI-I). Nine of these were the Fenton Hill surface network stations. These were augmented by four three-component MIT remote digital recorders. These four temporary stations were located very close to the site in order to study anisotropy that should cause shear wave "splitting" because of vertically oriented structures such as cracks. Unfortunately, little data were obtained from the remote digital recorders. Precambrian stations PC-1, PC-2, and GT-1 ran continuously throughout the experiment, while the three-component EE-1

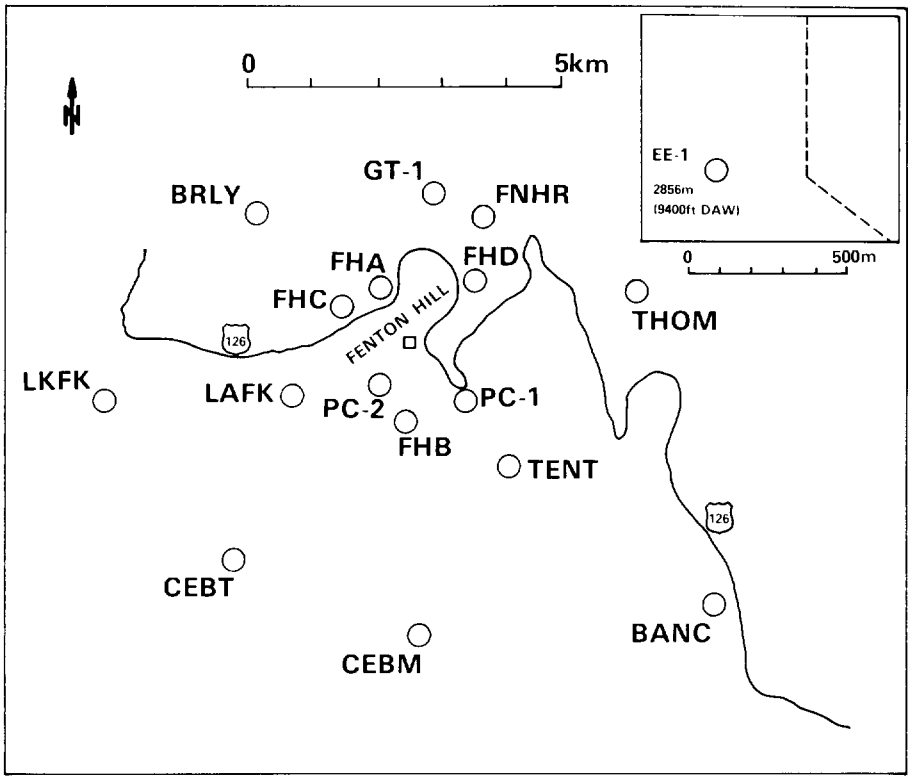

Figure VI-1. Seismic stations used during the ICFT.

tool was deployed intermittently (Table VI-II). The PC-2 station proved to be quite noisy, so a 100-Hz low-pass filter was applied. This remedied the situation but also produced a lower frequency pulse that degraded the quality of the arrival time determination.

The new MASSCOMP digital seismic data acquisition system was employed to perform real-time, on-line event detection and digitizing. The system employed three digitizers that were operated at software selectable digitizing rates. One of the digitizers was run at a relatively slow rate, 500 samples per second per channel, and digitized data from the 9-station surface seismic network. A second digitizer operated at 5000 samples per second and digitized data from the 4-station Precambrian network. The third digitizer was only used when the triaxial geophone was downhole in EE-1. This digitizer was set at a rate of 50 000 samples per second per channel. In addition to the channels of seismic data, a time signal was sent to each digitizer.

TABLE VI-I

FENTON HILL SEISMIC STATION LOCATIONS AND CORRECTIONS

	Location[a]			Correction[b]	
	North	East	Depth	P-wave	S-wave
EE-1	-480.82	-562.26	2854.60	0.6	2.3
GT-1	1976.63	-229.82	804.98	-0.5	10.9
PC-1	-954.44	613.53	741.88	4.6	10.2
PC-2	-925.93	-1358.80	577.94	30.0	0.0
FNHR	1483.0	774.0	-21.0		
BRLY	1393.0	-2967.0	24.0		
CEBM	-4312.0	-464.0	54.0		
CEBT	-3630.0	-3290.0	77.0		
BANC	-4456.0	4204.0	172.0		
LAFK	-1113.0	-2178.0	55.0		
THOM	218.0	3047.0	139.0		
TENT	-2411.0	1035.0	11.0		
LKFK	-1302.0	-5273.0	81.0		

[a] Locations in meters, relative to reference at latitude 35.855°, longitude -106.6687°, elevation 2651.76 m.

[b] Station corrections in milliseconds.

TABLE VI-II

EE-1 TRIAXIAL GEOPHONE DOWNHOLE (MDT)

On		Off	
Date	Time	Date	Time
5/19/86	2220	5/20/86	1450
5/27/86	1850	5/28/86	1000
6/03/86	1036	6/05/86	1305
6/11/86	2141	6/12/86	1000

All data were written temporarily to disk so that data before event declaration (described below) were always stored; data from time periods that did not correspond to events were discarded and the disk space reused. Because of this scheme, total system throughput was limited by the speed of the disk. The maximum achievable aggregate digitizing rate (from all digitizers and channels) was about 400 000 samples per second.

While the data were being digitized, a real-time event detector operated in the CPU of the system. The event detector analyzed data from the medium-speed (5000 samples per second) digitizer to determine the occurrence of a seismic event. The procedure used was to perform long- and short-term averages of each channel of the seismic data. If an event occurred, the short-term average would rise faster than the long-term average because of the increase in signal level. When the ratio of the short- and long-term averages exceeded a specified value, a flag was set at the station. If enough other stations also triggered on the ratio test, an event was declared and all digital data from the event were stored.

Tables VI-III and VI-IV list setup and trigger parameters used during times that EE-1 was in operation. Parameters are described in detail in the Raven user's manual (written by NEWT, Inc.). The only problem that occurred with this setup was that an occasional P-wave was lost at station EE-1. This is most likely the result of a late event declaration; perhaps P-waves were missed and an S-wave provided the decisive trigger. This can be rectified in the future by extending the pre-event memory (if possible), at most by the S-P time at the most distant Precambrian station.

During the ICFT the MASSCOMP data collection system ran from May 19 to June 20 with occasional downtime, primarily because of power outages. Downtime was not logged completely as problems often occurred when seismologists were not present. A list of times that the analog tapes were run as backup appears in Table VI-V; these times represent a liberal estimate of downtime. Perhaps an automatic system of logging downtime can be devised for the LTFT; this would involve the addition of an internal clock that will not be affected by a crash.

TABLE VI-III

SETUP PARAMETERS

Parameter	Digitizer 1	Digitizer 2	Digitizer 3	Description
nch	4	5	10	number channels
bufalloc	580	96	16	total buffer size (kB)
nbufs	6	8	8	number buffers
trate	50000	5000	500	digitizing rate
tpem	450	900	2000	pre-event memory (ms)
max-evlength	2	10	20	max-event length (buffers)

TABLE VI-IV

TRIGGER PARAMETERS

Parameter	Value	Description
ntrig	5	number of stations to compute trigger
nstatrig	3	number of station flags to declare event
nppsta	300	data points per short-term average
ltadiv	8	long-term average constant
enumer	12	sensitivity constant: numerator
edenom	8	sensitivity constant: denominator
equiet	6	quiet station constant
trigmin	58	min duration of trig; multiples of STA
trigmax	20	max duration of trig; multiples of buffers
decimate	5	decimation for trigger algorithm
trig-reset	1	max-event length reset of STA to LTA

TABLE VI-V

ICFT MAGNETIC TAPE BACKUP TO MASSCOMP (MDT)

On		Off	
Date	Time	Date	Time
5/22/86	1253	5/22/86	1324
5/25/86	1037	5/26/86	1220
5/27/86	1535	5/27/86	1614
5/27/86	1814	5/27/86	2206
5/29/86	1626	5/29/86	1841
6/03/86	1627	6/03/86	1856
6/03/86	2341	6/04/86	0717
6/06/86	0907	6/06/86	1450
6/06/86	1611	6/08/86	1255
6/13/86	1205	6/13/86	1408

Microearthquake locations were determined using arrival-time data from the Precambrian stations and EE-1. The station corrections used are listed in Table VI-I. When EE-1 was downhole, microearthquake locations were normally based on P- and S-wave arrival times at EE-1 and GT-1 and P-wave arrival times only at PC-1 and PC-2. When EE-1 data were not available, S-wave times at PC-1 had to be added in order to obtain high-quality locations. PC-1 S-wave arrival times were often difficult to determine. Hence, we investigated the possibility of systematic biases between locations obtained with and without EE-1 data. To do this, a number of ICFT events were re-located by adding PC-1 S-wave data while ignoring the EE-1 P- and S-wave data. Nine events were assigned "A" quality locations in both cases; results are shown in Fig. VI-2. RMS differences in the locations are only 10 m in the horizontal directions and 20 m in depth. No systematic differences were noted. These small differences give us confidence that those "A" quality events that occurred while EE-1 was not operating were reliably located. Of course, the total number of located events increased when the EE-1 tool was operating as a result of the addition of high-quality data.

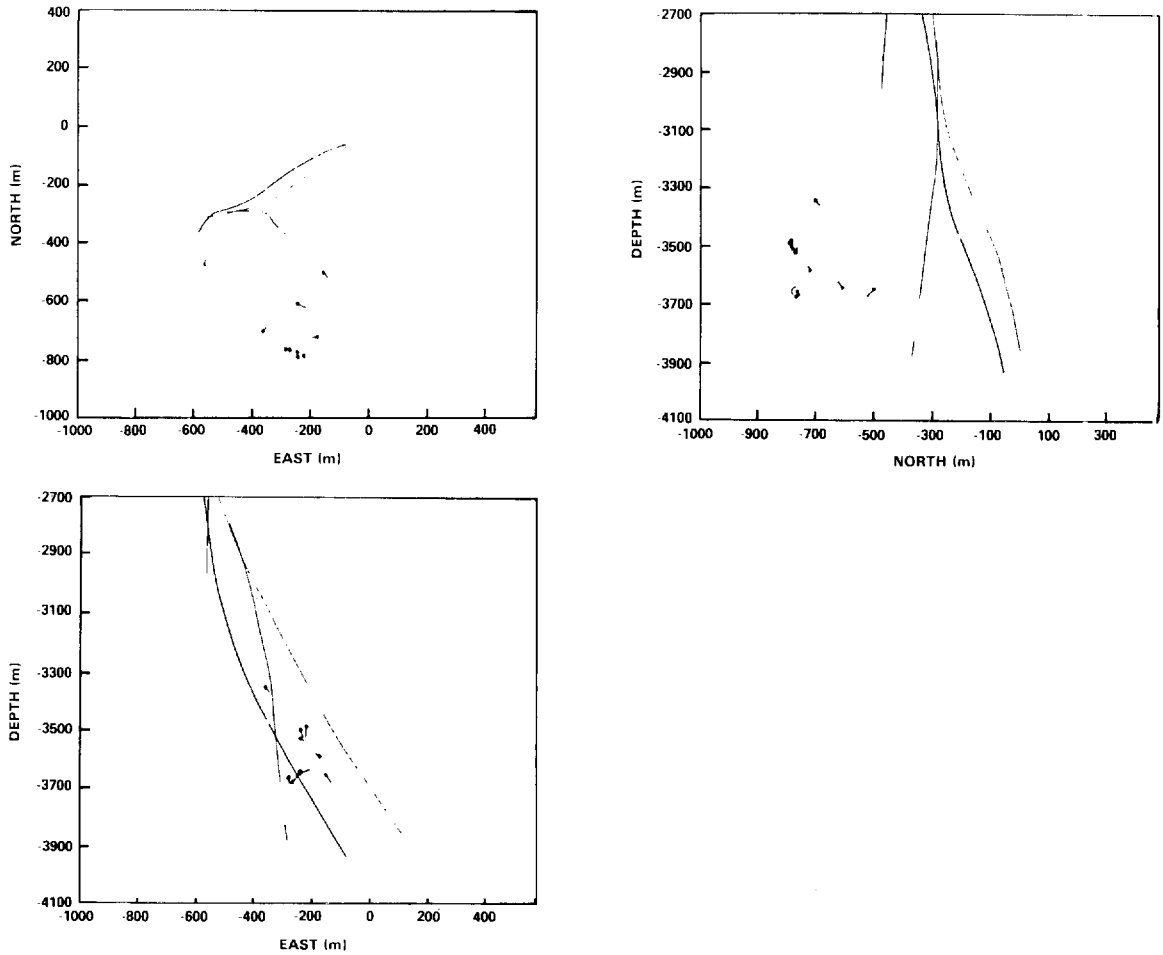

Figure VI-2. Event location changes with addition of EE-1 data. Filled circles represent locations based on P- and S-wave data from PC-1 and GT-1 and P-wave data from PC-2. Line segments represent the location change when P- and S-wave data from EE-1 are added and S-wave data from PC-1 are removed. A cluster of locations on the map view were not given line segment extensions since their horizontal changes were small.

B. ICFT Seismicity

The ICFT produced a considerable amount of seismicity; 684 events were located. Qualities of "A" or "B" were assigned to 611 events. Location quality can range from "A" to "D" depending on the number of arrivals, the data RMS, and the computed solution error (Table VI-VI). A time histogram of all locatable events is shown in Fig. VI-3. The first locatable event occurred the night of May 27, roughly corresponding to two intervals of high flow rates ($\geq$0.02 m^3/s). The

TABLE VI-VI

LOCATION QUALITIES

Quality	Arrivals	Solution Error	Data RMS
A	>5	≤25 m	<0.3 ms
B	>5	≤50 m	<0.3 ms
C	>4	≤75 m	
D	>4		

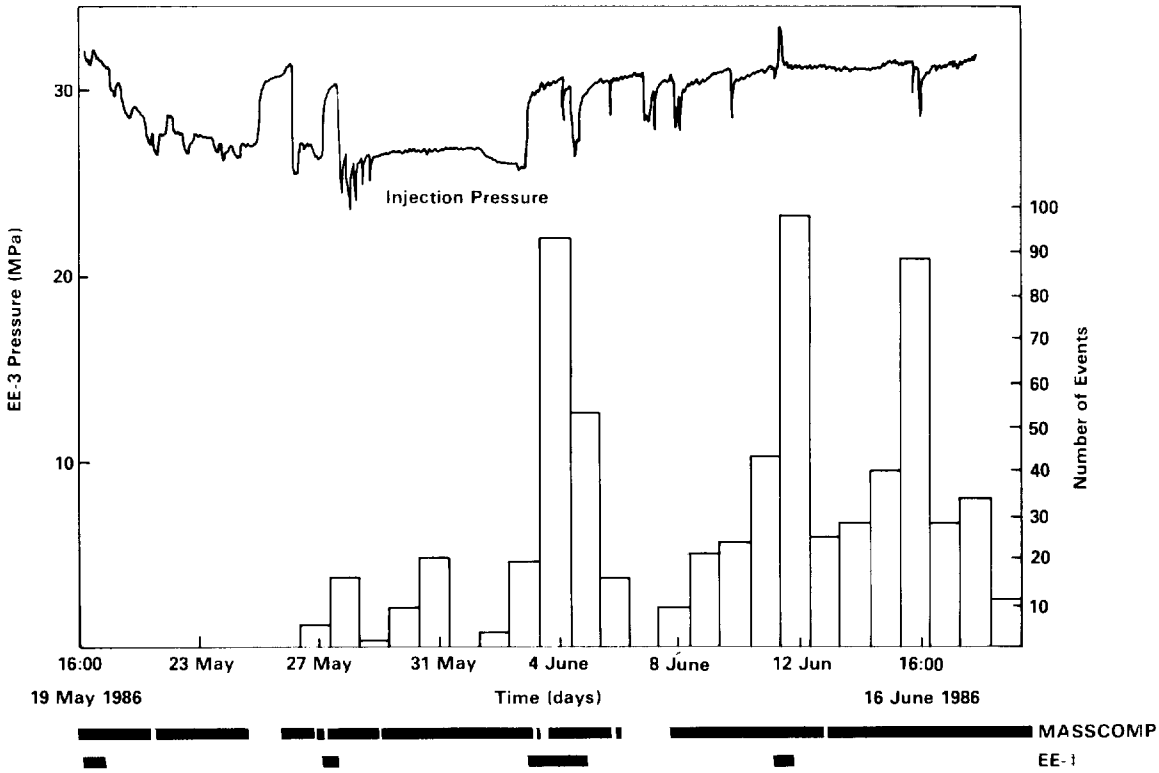

Figure VI-3. ICFT seismicity histogram. Time is measured in days from May 19 00:00 MDT. The top bar under the histogram indicates the times that the MASSCOMP was operating. The lower bar indicates the times that the EE-1 geophone was downhole. Injection pressure curve for the ICFT is also included for comparison.

majority of the seismicity followed the flow rate increase to 0.02 m^3/s on June 4. An average rate of 30-40 events per day was seen between this date and the final shut-in on June 18. Over 90 events were seen on June 12 alone, corresponding to a short, high flow rate injection (0.027 m^3/s) the previous night and early morning. A third peak in seismicity occurred on June 16. This may have been the most active day of the test as 90 events were located without the benefit of the EE-1 tool. No corresponding increases in flow or pressure were noted for this period. The majority of the activity was in seismic subvolume 4 (Fig. VI-4) and may represent a sudden breakthrough to shallow depths. A few events were seen after shut-in, including a number of anomalous

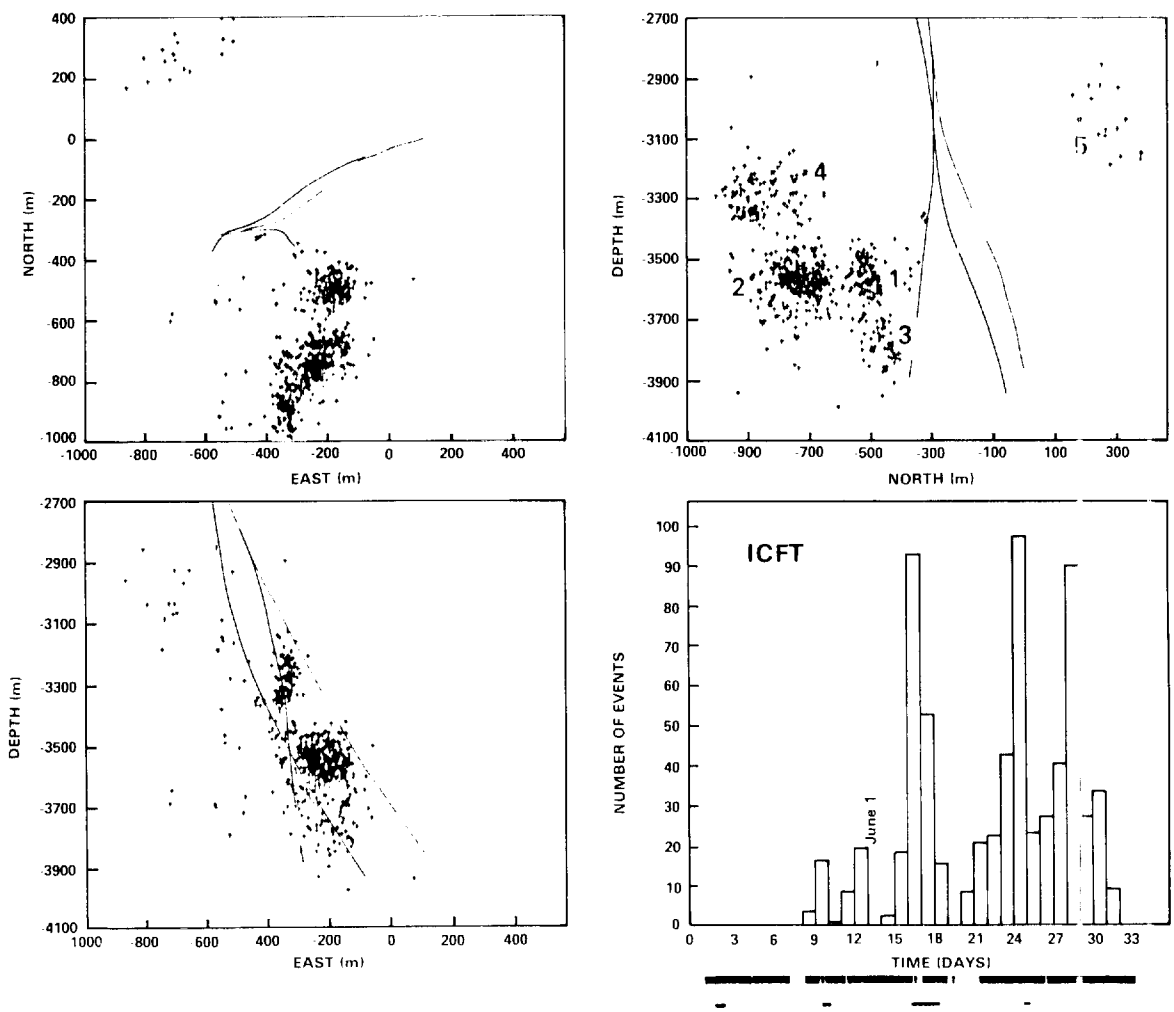

Figure VI-4. Event locations for the ICFT. Only results that have been assigned qualities "A" or "B" are shown.

shallow northerly ones. The event rate slowly decayed away from 20 events/day at shut-in to 1-2 events/day in mid-July as observed from the Precambrian network strip charts.

Events tended to group spatially during the ICFT. The temporal behavior of each of five event clusters is shown in histogram form in Fig. VI-5 (note that vertical scales are different on different plots). Activity in the first two (main) seismic regions occurred during similar times. Region 3, the deepest, was active at the same times as regions 1 and 2, but the event rate increased as the experiment progressed, including 14 events on June 18 after the initial shut-in. Region 4, the shallowest on the south side, was not active until June 5, following the midexperiment step to 0.02 m^3/s flow rates. Fourteen events occurred here June 12-13 after the short 0.027 m^3/s injection. Over 55 events were located in this region on June 16, just before initial shut-in. In region 5, located shallow and well to the north, activity was completely confined to initial and final shut-in periods (Fig. VI-6). This behavior may be due to increased pressures in the production side of the reservoir after shut-in, although shut-in pressures of 16 MPa should be too low for fracturing to occur in the Phase II reservoir. Alternatively, these events may represent fracturing in the low-pressure, Phase I region. However, a number were large enough to be seen by the surface stations. No event was seen on the surface during Phase I operation; however, coverage was relatively sparse at that time.

A plan and two elevation views of the ICFT seismicity are shown in Fig. VI-4. The events occur in a region similar to that observed during the massive hydraulic fracture experiment (MHF or 2032), Fig. VI-7. However, the ICFT seismicity only occupies the southern portion of the MHF seismic region except for the small number of events that occurred after shut-in. This could be due to the following reasons: 1) the injection and production intervals create a pressure dipole effect that results in pressures below the fracture threshold on the production (northern) side of the reservoir; or 2) if the fracture system emanating from the production interval (EE-2) is of dendritic or tree root form, then flow would naturally be channeled toward EE-2, effectively sealing off the northern portion of the fractured volume.

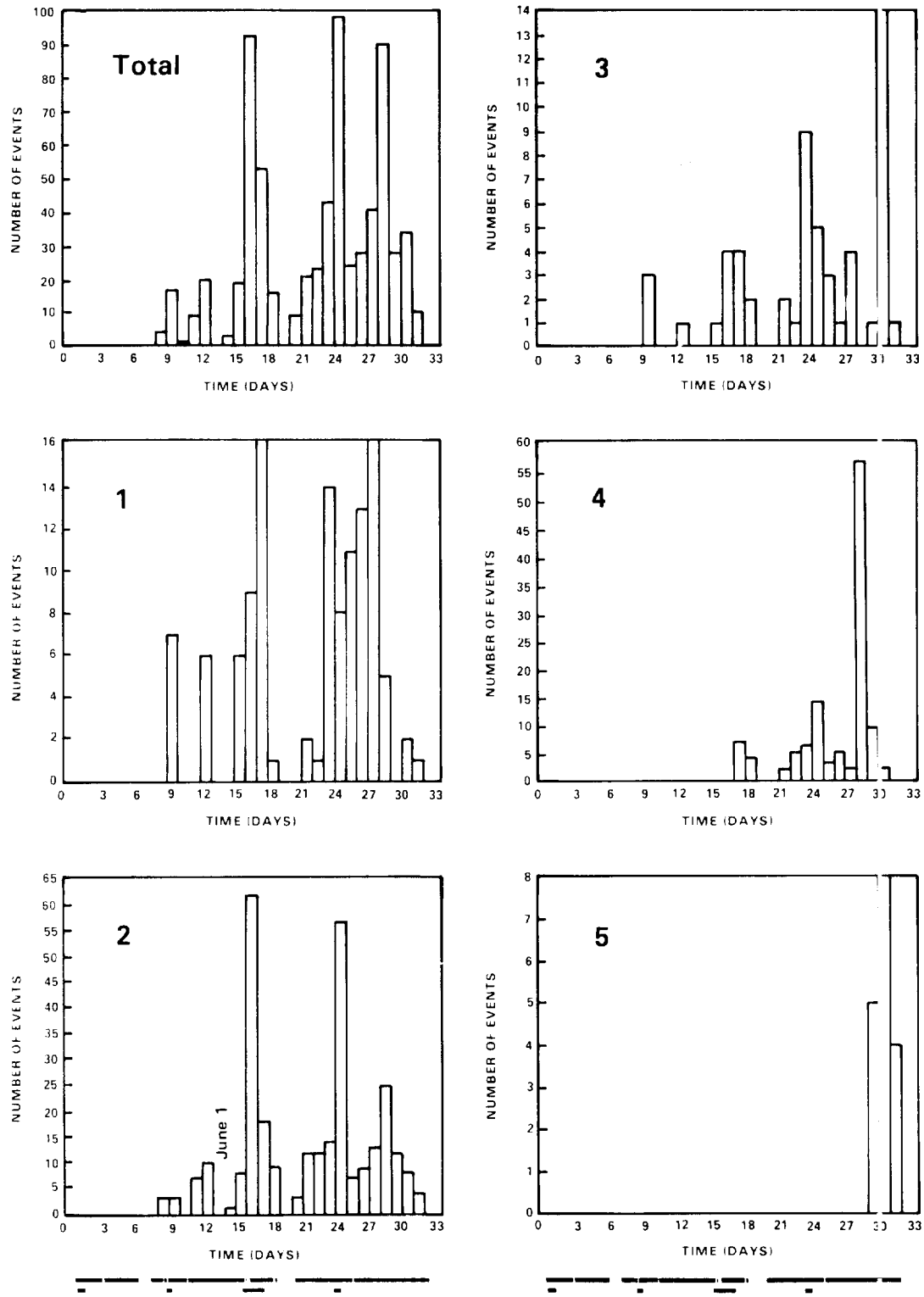

Figure VI-5. Histograms of various seismic clusters that appear in the ICFT results (see Fig. VI-4). MASSCOMP and EE-1 operation times are as in Fig. VI-3; note the different scales on the "number of events" axes.

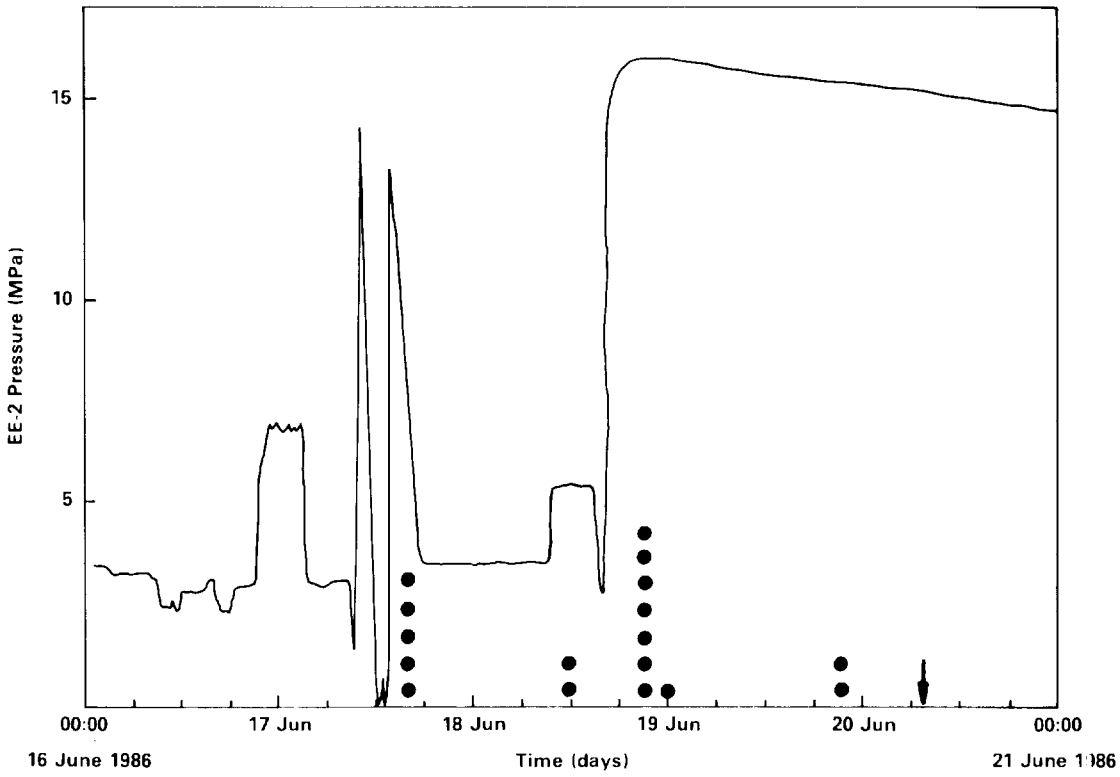

Figure VI-6. Times of anomalous northerly events (solid circles) and production well pressures indicating initial and final shut-ins. All events in group 5 (see Fig. VI-4) fall within the time interval depicted.

The ICFT seismicity also tends to lie on the eastern side of the planar fracture system defined by the MHF locations. This had been evident since the onset of seismicity and seems to indicate reservoir extension. In addition, toward the middle and end of the experiment, both shallow and deep activity intensified, the shallow region extending upward well beyond the MHF volume.

The bunching of events into distinct "patches" can be most easily seen in the westward-looking elevation view (Fig. VI-4). The reasons for such bunching are unknown but may be structurally caused, as similarly located seismic and aseismic regions can be seen in the MHF results. The aseismic regions are intriguing since water must be transmitted through them in order to reach outlying regions of high activity.

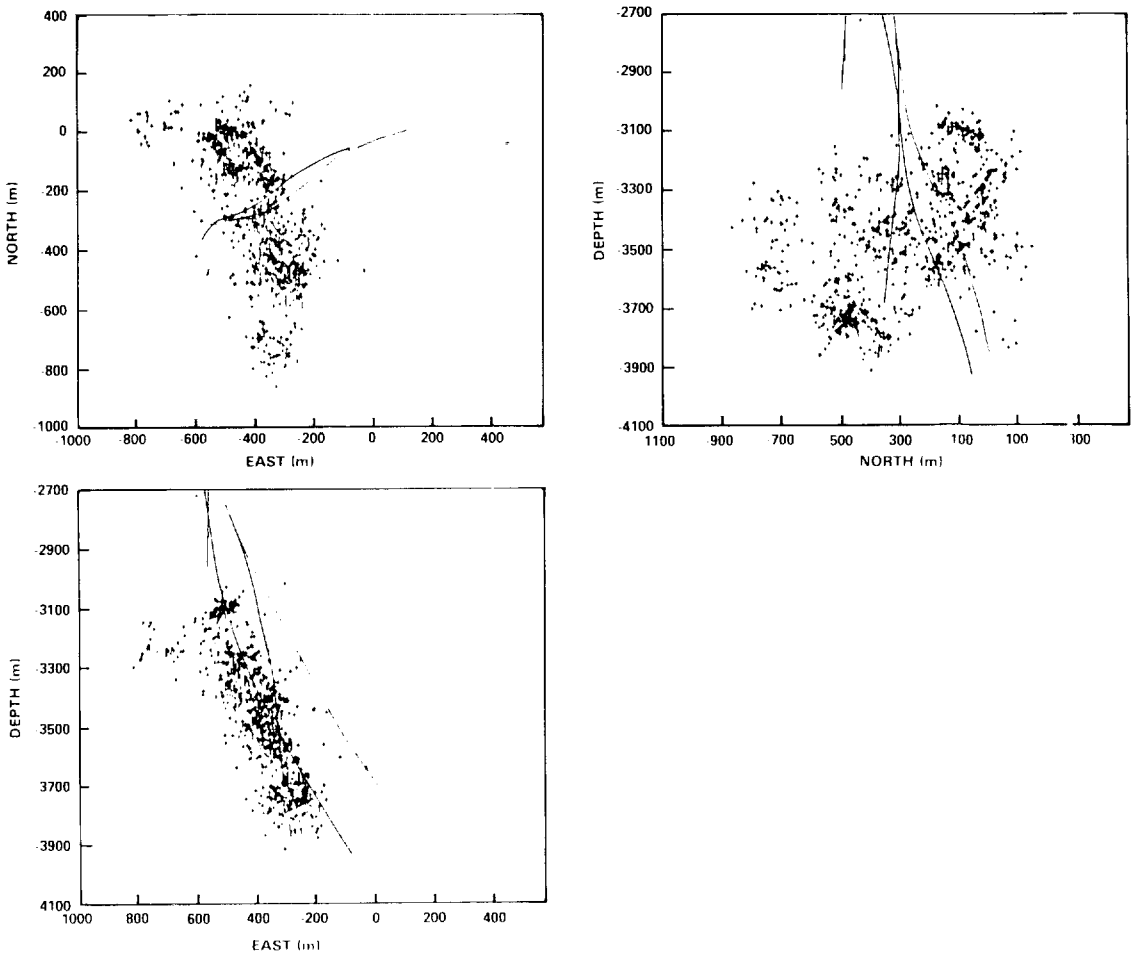

Figure VI-7. Event locations for the massive hydraulic fracture experiment; "A" and "B" qualities only.

Magnitude measurements have not been determined for the ICFT events; however, events can be grouped by size in a crude manner depending on whether or not waveforms were seen by the surface network. The network found 75 large microseismic events (10% of the total number); only 2 of these tripped the event detectors at stations FHA, FHB, FHC, and FHD (Fig. VI-8). All of these events occur after the June 4 flow rate increase. The first (time) histogram peak lags the ICFT total seismicity by 1 day, but the two match fairly well for the remainder of the experiment. Locations are spread fairly uniformly throughout the ICFT seismic volume, except for a concentration in the northern, post shut-in subvolume for which 50% of the events are observed on the surface.

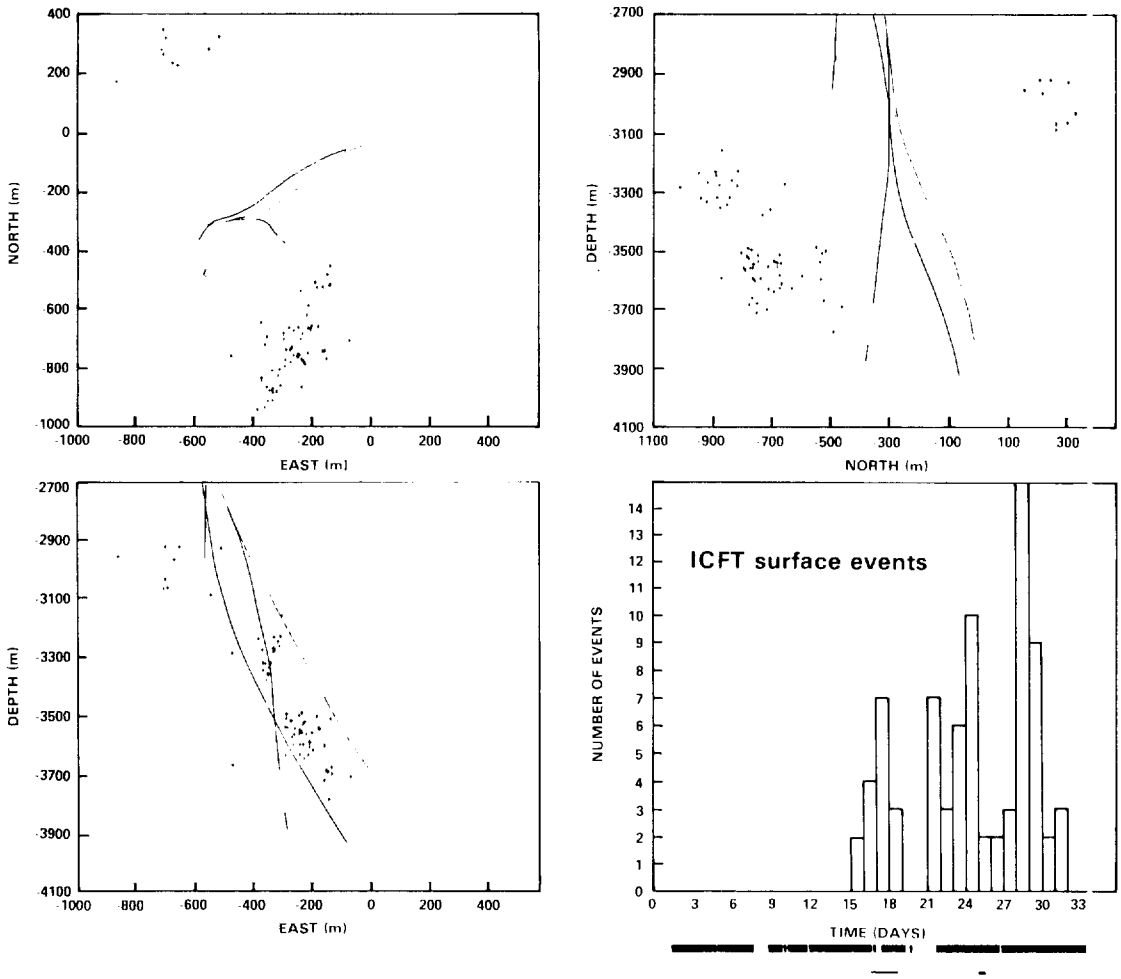

Figure VI-8. ICFT events that were strong enough to be recorded by surface network stations. A histogram is included, with MASSCOMP and 3E-1 operation indicated as in Fig. VI-3.

C. Seismic Attenuation

The quality factor (Q) of seismic waves was bounded using the single-scattering, coda-wave method (Aki and Chouet, 1975) with data from temporary stations FHA, FHB, FHC, and FHD. For frequencies (f) between 12 and 48 Hz, $Q = 24f^{0.7}$. This coda Q is thought to represent an upper bound on the average Q of the medium within a volume of radius less than 8 km about the Fenton Hill site. These measurements will be important to any spectral studies that must employ an attenuation correction in order to estimate source parameters of the micro-earthquakes.

D. Environmental Monitoring

An important aspect of the seismic surveillance at Fenton Hill was to monitor the incoming data for the possible occurrence of a large earthquake resulting from the perturbation of the environment during the experiment. A memo that was distributed before the ICFT concerning environmental monitoring is included in Appendix E. This memo addresses the following: 1) criteria for discriminating between near-site and distant earthquakes based on strip chart records, and 2) procedures to follow in the event of a large near-site earthquake. This memo is sufficient for use in future experiments with one modification. The 5-km radius cutoff is not practical; instead we should say "within the limits of the surface array." A program to discriminate between events occuring within and outside our array has been implemented on the MASSCOMP and can be run by entering

```
/usr/raven/RAVEN4.1/ICFT/progs/massloc -p  .
```

After determining arrival times, this routine simply fits a plane wave to the data in order to find the direction and apparent velocity of the incoming wavefront. For events located outside the array, the apparent velocities will be reasonable (<10 km/s). For events within the array, apparent velocities will be unreasonably large. Results of running this routine on data from various types of events are listed in Table VI-VII.

TABLE VI-VII

RESULTS OF PLANE-WAVE PROGRAM

Event	Apparent Velocity (km/s)
Redondo Creek "blast"	5.5
Local	6.8
Fenton Hill microearthquake	40.5

VII. CONCLUSIONS

A. Comparison of HDR Reservoirs

Only three deep HDR reservoirs have ever been field tested by circulating water down the injection well, through the reservoir, and up a production well for periods of several weeks. The first of these reservoirs, called Phase I, was also created at the Fenton Hill, New Mexico, site and was tested over the period 1978 to 1980 (Dash et al., 1983). This first reservoir, the results of which proved the scientific feasibility of the HDR concept, was created in two stages. In the first stage, a very small fracture system was hydraulically induced and then tested by circulating water through it in three run segments, which lasted 4, 75, and 28 days. In the second stage, the reservoir was enlarged by further hydraulic fracturing and then tested in two run segments lasting 23 and 280 days. For the purpose of making comparison with the present Phase II reservoir, we selected the enlarged Phase I reservoir, and we chose Phase I results at the end of 30 days of the final run segment lasting 280 days because the ICFT lasted 30 days.

The second comparison reservoir is the British one, located at Rosemanowes Quarry in Cornwall (Bachelor, 1984). Although not as deep nor as hot as either the Phase I or Phase II reservoirs at Fenton Hill, the British reservoir was also created in granite, and like the Phase II reservoir, it required redrilling and supplemental hydraulic stimulation before a satisfactory hydraulic connection was obtained. A circulating flow experiment has been ongoing at Rosemanowes since August 1985.

Table VII-I compares the three reservoirs at the end of 30 days of flow circulation. Because the ICFT was limited to this test duration, a 30-day basis is the obvious choice for comparison, but it can be misleading as a guide to reservoir behavior during longer-term testing. For example, after 280 days of operations the impedance of the Phase I Fenton Hill reservoir was reduced to 1.1 $GPa \cdot s/m^3$; and the water-loss rate was estimated, after correcting for flow out through a poorly cemented wellbore-to-casing annulus, at 7% of the injection rate. Likewise, after 14 months of flow, the impedance of the British reservoir was 0.6 $GPa \cdot s/m^3$, the production flow rate was 0.016 m^3/s, the water-loss rate was 11%, the modal volume was 495 m^3 (see Section V -

TABLE VII-I

COMPARISON OF THREE HDR RESERVOIRS AFTER 30 DAYS OF OPERATION

	Fenton Hill		
	Enlarged Phase I Reservoir	Current Phase II Reservoir	Rosemanowes Cornwall, UK
Depth of reservoir, m	2800	3550	2400
Temperature of reservoir, °C	195	240	85
Modal volume, m^3	160	350	270
Surface temperature, °C	135	192	76
Thermal power, MW_t	3	9	1
Production flow rate, m^3/s	0.007	0.013	0.004
Injection well pressure, MPa	10	30	4
Reservoir impedance, $Gpa \cdot s/m^3$	1.7	2.2	1.0
Water-loss rate, m^3/s	0.00011 (16%)	0.006 (33%)	0.0004 (10%)

Tracer Experiments - for a discussion of modal volume), and the produced power was 5 MW_t.

Although no assurance can be given that equally significant improvements will occur during long-term testing of the new Phase II reservoir, such improvements are quite likely. Even without improvement, the Phase II reservoir properties already exceed its predecessor's. The produced water temperature is considerably hotter (192°C), already high enough for electricity generation, and, based upon modal volume, the Phase II reservoir is already twice the size of the enlarged Phase I reservoir. The impedance is 30% higher, but improvement can be expected in the future, particularly when the EE-2 production well is repaired so that it can be subjected to high-pressure injections, which should reduce the localized reservoir impedance in the production well vicinity. Present water losses are expected to decline during longer future experiments because more and more of the country rock surrounding the fracture system will become water saturated. Based

on microseismic interpretation (see Section VI), future system operation should result in less fracture extension.

B. Conclusions from Thermal and Hydraulic Analysis

1) During the 30 days of operation, a total of 37 000 m^3 (9.76 million gal.) of water was injected, while a total of 23 300 m^3 (6.15 million gal.) of hot water was produced, cooled, and reinjected. Nearly 14 000 m^3 of fresh water was added to make up the difference. An additional 950 m^3 (0.25 million gal.) was vented directly to the EE-1 pond. A maximum injection rate of 0.0265 m^3/s (420 gpm) was obtained, although most of the pumping was done at 0.0106 m^3/s (168 gpm) and 0.0185 m^3/s (294 gpm) with surface pressures around 26.9 MPa (3900 psi) and 30.3 MPa (4400 psi), respectively. The injection well pressure was fairly constant with rate. Hence, LTFT planning should include high-pressure injection capabilities.

2) The production surface pressure was maintained between 1.4 MPa (200 psi) and 3.5 MPa (500 psi), resulting in surface production flow rates from 0.0063 m^3/s (100 gpm) to 0.0139 m^3/s (220 gpm). The production rate from EE-2 showed an overall increasing trend as a result of reservoir inflation and a decrease in overall impedance. Production flow measurements tended to be high when gas (i.e., CO_2 or N_2) content of the fluid was significant, confirming the need for gas separation in future operations.

3) The production well temperature increased throughout the test, reaching a maximum surface temperature of 192°C (232°C bottom hole). The production power showed a corresponding increase, reaching a maximum of about 10 MW_t after 28 days. The power increase resulted from the rise in production temperature combined with the rise in production rate. A projection of performance trends during the test, assuming no thermal drawdown in the reservoir, indicates that up to 12 MW_t could be produced after 1 year if the flow rate is maintained between 0.0126 m^3/s (200 gpm) to 0.0158 m^3/s (250 gpm) and production temperature is around 200 to 210°C.

4) The bottom-hole injection pressure did not change significantly with injection rate or time, indicating fracture inflation and stimulation were occurring near the injection wellbore. The overall reservoir impedance decreased throughout the test, mainly as a result of

the stimulation, especially near the injection well. The injection well impedance decreased from 0.72 $GPa \cdot s/m^3$ (6.6 psi/gpm) to 0.002 $GPa \cdot s/m^3$ (0.02 psi/gpm) during the early part of the test as a result of near-wellbore cooling and pressurization. However, the injection well impedance was only a minor portion of the overall impedance, and the decrease in the production well impedance was not as significant. Further plans for reduction in impedance should concentrate on improvement and repair strategies for the production well.

5) Although initially high, the rate of water loss decreased from around 70% after 4 days of pumping to 26% after 30 days of pumping. The high water-loss values during the early portion of the test were caused primarily by reservoir inflation. Almost 66% of the total injected water was recovered during this test with an additional 20% being recovered during a subsequent vent-down.

C. Conclusions from Geochemistry and Tracer Analysis

1) The geochemistry of individual dissolved chemicals in the production fluid over the first 5 days of the experiment fell into three categories: a) the decline of inert species from their initial concentrations to the injection fluid concentration; b) no change in concentration, indicating a supply of the dissolved species via dissolution reaction (SiO_2); and c) decline of concentration to below the injection concentration, caused by adsorption, precipitation, or ion exchange reactions.

2) The Na-K-Ca and SiO_2 geothermometers yielded temperatures that agree well with the known downhole background temperature. Also in agreement with these temperatures are the equilibrium reactions of calcite dissolution and bicarbonate-dissolved CO_2.

3) Corrosion coupon studies found generalized and uniform corrosion at rates of 0.25 - 0.38 mm/yr (10 - 15 mpy). One case of pitting was observed, which we attribute to increased dissolved O_2. An oxygen scavenger will be injected in future operations to minimize pitting corrosion. Scale deposition was minimal and did not affect operations.

4) Several periods of high dissolved CO_2 concentration, estimated at 1% by weight, created a temporary two-phase flow condition at a shallow depth in the production wellbore and in the surface loop.

Future operations will require gas separation to handle these transients.

5) Two radioactive tracer experiments indicated modal volumes about twice as large as previous reservoirs at Fenton Hill. Furthermore, tracer recoveries are lower, indicating flow through a large number of fractures. The total swept fracture volume increased during this flow test as injected fluid continued to fill the reservoir. The total swept rock volume, calculated from tracer-determined fracture volumes and reasonable estimates of fracture porosity, is equivalent to a sphere of diameter approximately equal to the wellbore separation distance. This agreement lends credence to a point-source, point-sink model of flow through a network of fractures.

D. Conclusions from Microseismic Analysis

1) Nearly all events that occurred during the operation of the MASSCOMP system were recorded. The success of our new data aquisition system was marred only by downtime that was due to power outages. Effort must be made to protect the MASSCOMP as well as to implement automatic recording of downtime for future experiments.

2) Because of the duration of the test, events were located both with and without data from the EE-1 triaxial tool. Tests indicated the "A" quality locations were reliable in the latter case.

3) The seismicity of the reservoir was sporadic during the experiment. Peaks in seismic activity generally followed abrupt increases in flow rate. A peak occuring on June 16 did not correspond to pumping changes and was part of an apparent breakthrough to shallow depths.

4) The asymmetry in event locations relative to those of Expt. 2032 may be due to a pressure dipole set up by the adjacent injection and production intervals.

5) Eastward extension from previous seismic zones was noted throughout, while downward and upward extension became apparent midway through the experiment.

6) Seismicity fell into well-defined clusters corresponding to patterns seen in previous experiments; perhaps an east-west-trending geologic structure controls these patterns.

7) The northern portion of the reservoir became seismically active only after shut-in. This may be the first time during the experiment that high pressures were felt in the production end of the reservoir; however, shut-in pressures should not have been high enough to fracture rock. These events may have been located in the lower-pressure Phase I reservoir, but the path between the two reservoirs is a matter of controversy.

8) The seismic quality factor (Q) was estimated using the coda-wave method: $Q = 24f^{0.7}$ for frequencies (f) between 12 and 48 Hz.

E. Conclusions About Loop Operations and Equipment

1) OPI Triplex pumps were used by B.J. Titan. These had 146.1-mm (5-3/4-in.) plungers with 203.2-mm (8-in.) strokes. At 0.0188 m^3/s (7.1 bpm), this equates to 110 rpm or a total of 330 pulses per minute, 19 895 pulses per hour, or about 0.5 million pulses per day.

2) The continuous noise from the diesel engines on the B.J. Titan pump trucks was heard inside homes in La Cueva even with windows closed. It was heard in Sierra Los Pinos, about 13 miles away, anytime one stepped outside and listened. The sound even reached an area that is several miles below La Cueva. This should be resolved before the LTFT.

F. Conclusions About Instrumentation and Control

1. Surface Instrumentation. Some problems with the surface instrumentation were unavoidable because of electrical power failures and/or fluctuations on the incoming power lines. On several occasions stormy weather caused damage from lightning. The use of transorbs as surge arrestors did minimize lightning damage to most of the data acquisition equipment.

Flow measurements in the turbine flow meters were erratic and questionable when there was a high concentration of gas in the circulating fluids.

A number of thermocouple failures were attributed to low-battery voltage in the electronic reference junctions. One pressure transducer located on the EE-3A wellhead was damaged during installation owing to excessive force used on a nearby hammer joint. One instrumentation cable was burned when inadvertently moved into contact with the EE-2 production wellhead.

The water level in the 150-m^3 (40 000-gal.) supply tanks to the Meyers pumps was initially measured using a pressure transducer near the bottom of the tank. The pressure port was eventually plugged with debris, which affected the output of this transducer. Level float switches were subsequently used to control the filling of the supply tank from the 18 930-m^3 (5 million-gal.) pond.

A dc power supply in the control valve and heat exchanger fan panel failed. There was no backup supply in this control panel. Before the problem could be determined, hot water was delivered to the B.J. Titan pumps that damaged the seals.

Some of the data acquisition equipment was affected by dust and insufficient cooling. The major concern was with the computer peripherals (primarily disk drives) and with the tape recorders. This equipment is very susceptible to dusty environments.

2. Seismic/Microseimic Networks. The major concern with monitoring all of the seismic data during this flow test was downtime on the MASSCOMP computer caused primarily by power fluctuations in the line power. The MASSCOMP was powered directly off the main line power and was not regulated through the Uninterruptable Power System (UPS). This computer was not located near the main data acquisition equipment and it was not always apparent to the operators when it was not operational. There was also a problem with adjacent air conditioning and dust accumulations in the DAT.

There were three occasions when one of the surface seismometer stations required maintenance. This was not a critical problem since the other eight stations were recording data with adjacent seismic coverage. The station with the malfunction was generally repaired within a 12-hour period.

VIII. RECOMMENDATIONS FOR THE LONG-TERM FLOW TEST

A. Loop Operations and Equipment

1. Pulsation Dampening. All B.J. Titan pumps were equipped with suction and discharge pulsation dampeners. When the dampeners were serviced and working, they were effective. Pulsation measured upstream, at the Meyers makeup pumps, was as low as a few psi when the equipment

was serviced and working. But it was as high as 0.6 to 0.7 MPa (90 to 100 psi) when the equipment was not performing well. The largest pulsations occurred when a suction valve or seat was washed out. One suction pulsation dampener and two discharge dampeners were replaced during the test.

Pulsation dampeners will be required for the LTFT. Dampeners without a rubber bladder should be specified to eliminate the blistering and failure that occurred as a result of the CO_2 in the water.

2. Plunger Pumps. Design for fatigue will be important for LTFT planning. Based on the performance of the OPI pumps, we can come to several conclusions.

First, two fluid ends were lost because of cracks in the highly stressed area of valve seats. Special order materials and analytical proof of a low-stress design will be necessary in the pump ends to prevent this during the LTFT. Second, several valve seats and insert snap rings indicate possible stress corrosion cracks because of the influx of sulfide and/or hydrogen. Special materials will be required for these. Third, three steel-reinforced suction hoses were lost from a combination of embrittlement, high pulsation loads, an occasional high suction pressure when pumps were off-line but still subjected to system pressures, and vibration abrasion of the hoses with the ground. Elimination of the hoses or replacement with hoses of a higher working pressure will be necessary as well as supporting them in an abrasion-free manner.

We conclude that for the LTFT to run with a minimum of downtime and materials-related failures, special fluid ends on the plunger pumps will be necessary, or water chemistry must be such that this is not a concern. Variable-speed, dc or ac drive pumps should be ordered to provide more flexibility in matching the performance curves of the various components that must work together as a system. The pump motors should be powered with electricity from Jemez Electric or with large, slow-running, stationary diesel generators. Finally, pulsation dampening is a necessity and will be an ongoing maintenance item.

3. Control Valves. CV-6 failed early in the test. Upon inspection after the test, it was found that the multiple small holes in the cage simply plugged, as did the strainers elsewhere in the system.

This valve needs to be replaced or have strainers upstream of it. A bypass line around the valve with a manually operated globe valve is suggested for the LTFT

CV-2 thru CV-5, the V-Ball type of control valves on the heat exchangers, were used during the ICFT to control flow and hold a back pressure on EE-2 because of the failure of CV-6. They were never intended for this and as a result they are in need of repair or replacement. In their study of a LTFT surface system, Kaiser Engineers suggested that the 38.1-mm (1-1/2-in.) pipes in the area of the heat exchangers be replaced because the velocity in these small pipes gets high enough to cause water hammer should the system flow rate be changed abruptly with these valves.

In general, all critical control valves should have a bypass line so that any necessary repairs can be made while maintaining loop operations.

For the LTFT we will need five 103.2-mm, 69-MPa (4-1/16-in., 10 000-psi) valves for both EE-2 and EE-3 (double master, a swab valve, and two wing valves). It would be best if these were geothermal grade so that any backflow could be handled safely. Five additional 101.6-mm, 34.5-MPa (4-in., 5000-psi) API-rated geothermal valves are needed for a double-strainer complex downstream of EE-2. A sixth 101.6-mm, 34.5-MPa (4-in., 5000-psi) valve is needed to replace valve V-3. V-3 is a Grove valve that is about 30 years old and is no longer manufactured.

Four 73.5-mm (3-in.) geothermal-grade valves are needed on the entrance to the heat exchangers. Three new valves are needed for a strainer/bypass upstream of CV-6 and a totalizer flow meter. There are many 50.8-mm (2-in.) valves that also need to be replaced.

4. Strainers. EE-2 is an open-hole completion, thus rocks and sand came to the surface. This required cleaning the strainer just downstream of the EE-2 wellhead several times during the ICFT. Each time this happened, it was necessary to shut in the well and vent to the EE-1 pond to allow the strainer to cool. A five-valve, double-strainer complex is needed to eliminate the perturbations which occurred to the experiments that were interrupted by the unplanned shut-ins. The strainer downstream of CV-6 should have a higher pressure rating and should be moved upstream of CV-6.

5. Expansion Joints. That part of the line between EE-1 and the heat exchangers which is located in the underground tunnel had thermally expanded. It caused no problems during the ICFT but left the pipe permanently deformed. This will be corrected by changing the anchor points or flexibility of the piping run. Additionally, all bolted flanges will be removed and the pipe will be welded.

The cold leg of the loop between the heat exchangers and EE-3 experienced one temperature excursion during the ICFT when the power went out during a storm and B.J. Titan continued to pump. The resulting temperature rise in this pipe moved concrete blocks, bent pipe, etc. This needs to be corrected for the LTFT, using either a simple interlock or an expansion joint. A single 0.3-m (12-in.) stroke expansion joint is currently available, as is one bellows type of expansion joint.

6. Makeup Water System. It is essential that the 18 930-m^3 (5 million-gal.) pond stay clean. There is only one transfer pump from the pond to the holding tank at the heat exchangers. Kaiser Engineers' report suggested that a backup pump be installed.

The 150-m^3 (40 000-gal.) tank used as the holding tank needs to be replaced. It is suggested that two 64-m^3 (400-bbl) frac tanks be purchased to replace it.

A system for control of O_2 and H_2S needs to be designed and installed. A filter has also been suggested in the event that the 5 million-gal. pond remains dirty or river water is used for the LTFT.

7. Makeup Pumps. The Meyers pumps are inflexible, old, and in need of rebuilding. New pumps with a capacity of about 0.013 m^3 (5 bpm) at 1.1- to 1.2-MPa (160- to 170-psi) operating pressure should be purchased.

8. Gas Separators. Gas-purge mode was used several times during the ICFT. It has been suggested that a high-pressure separator be installed downstream of EE-2 to eliminate the open system resulting from the gas-purge mode of operation. It has also been suggested that the separator be configured to allow settling of the sand and the rocks that are brought up with the production fluid. It is possible that this could replace the strainer complex mentioned above.

9. Pressure Relief Valves. The 4.1-MPa (600-psi) pressure relief valve worked well; however, it would have choked because of two-phase

flow if we had unloaded the well through it. To provide full production flow capability through the pressure relief valve, it is suggested that this valve and its line be upgraded.

10. Chicksans and Hammer Unions. All chicksans and hammer unions on the hot leg of the system should be replaced with special 1.2-m (4-ft) radius bend pipe and flanges or welds. We had numerous leaks in these components and had to shut the system down several times to replace them.

11. Geochemistry. The only serious problem during the ICFT was trying to obtain total gas samples. One possible solution is a gas separator. Other items that need to be considered are the domestic water and sewer system, a location where all three streams (i.e., production, makeup, and injection) of system loop water can be monitored, and an UPS for the computer in the chemistry trailer.

12. Corrosion. A corrosion sampling/coupon system for the LTFT needs to be integrated into the piping design. A means of injecting corrosion inhibitors down the backsides of EE-2 and EE-3 is also needed.

13. Safety. Hot exposed sections of pipe should be insulated, or a controlled access fence should be installed. Loop operations should be simplified and experiment managers should be better trained in the operation of the loop.

B. Instrumentation and Control

1. Surface Instrumentation. Little can be done to avoid the electrical storms that frequent Fenton Hill. The Uninterruptable Power Supply (UPS) system, however, can protect much of the data acquisition system from electrical power failures and/or fluctuations on the incoming power lines. Installation of additional air conditioners will provide needed cooling and may also result in a positive air pressure in the DAT that could reduce dust accumulations.

Although the flow meters cannot measure two-phase flow or read fluids with high gas concentrations, it would be beneficial if a bypass line was included in the main flow piping to allow removal of a damaged flow meter, especially in the heat exchanger area.

It is presently planned to replace all thermocouple temperature transducers with resistance thermometers (RTD) for more reliable operation.

It is also recommended that an automatic temperature shut-off valve be installed upstream of the main injection pumps to avoid the occurrence of hot water being cycled through these pumps. A backup power supply should also be installed in the remote control system.

The on-line analog strip chart recorders used to determine periods of high seismicity were operated continuously throughout the experiment. This equipment is more than 10 years old and is difficult to maintain since spare parts are no longer available. New strip chart recorders are needed for the LTFT.

The HP9835 is obsolete and cannot be repaired. It is recommended that it be replaced with an HP9845, which will also increase the capabilities of the data acquisition and control functions. Some reprogramming will be required.

The pressure transducer is a very reliable measurement of fluid level in the supply tank and can be alarmed in the DAT when predetermined fluid levels are exceeded. It will be necessary, however, to build a suitable screen around the pressure port in the tank to prevent clogging with sediments. The float switches should be installed as backup devices.

The current instrumentation and control setup worked for the LTFT; however, for a longer operating time a totally automatic system with manual override for nonstandard operations is needed. Transfer to emergency power should also be automatic, or simplified.

The resolution of the visual display screen was poor, and too much data were displayed for emergency operations. A remote monitor has been suggested both for the MASSCOMP and the system data display screen. A viewing screen at TA-33 would eliminate many questions, phone calls, and trips to Fenton Hill.

2. Seismic Network. Expanded accommodations for the MASSCOMP computer are under consideration. An existing office trailer could be moved to Fenton Hill that would only require electricity for lights and heat and a phone. The office equipment now housed in the DAT would be moved into this temporary office trailer. The MASSCOMP computer would then be installed in an area more accessible to adequate air conditioning and personnel attendance.

A separate UPS system should be procured to eliminate line-power fluctuations. A knowledgeable seismologist and/or on-site personnel trained in the operation of this equipment should be in attendance during the flow tests. Perhaps an alarm could be programmed into this system to alert operators when the computer malfunctions.

The surface seismic stations usually worked well. A new solar charging circuit is being designed to improve continuous battery operation. This charger will be installed in all nine surface stations and the three Precambrian stations. It is also recommended that the three Precambrian downhole packages be retrieved for redressing and maintenance and be redeployed before any long-term flow tests.

3. Borehole Surveys. Equipment could be purchased to allow logging of both the EE-3A and EE-2 boreholes under high-pressure conditions. The equipment essential to the logging operations would include a small-diameter, 4.8-mm (3/16-in.), seven-conductor, TFE-Teflon, insulated cable and a suitable lubricator/packoff system. New sheaves with proper cable grooves would also be required. The high-pressure borehole logging equipment would allow consistent and accurate surveys throughout the entire LTFT. There are a number of slimline tools that could be run in either the injection well (EE-3A) or the production well (EE-2) that would greatly enhance the evaluation of the HDR reservoir.

ACKNOWLEDGMENTS

The authors would like to thank J. Paskiewicz, R. Bigio, and F. Robichaud for drafting the many figures in this report. This work was carried out as part of a program under the auspices of the U.S. Department of Energy with financial and technical participation by the New Energy Development Organization of Japan through an International Energy Agency agreement.

REFERENCES

Aki, K., and B. Chouet, "Origin of Coda Waves: Source, Attenuation, and Scattering Effects," J. Geophys. Res. **80**, 3322-3342 (1975).

Bachelor, A. S., "Hot Dry Rock Geothermal Exploration in the United Kingdom," Modern Geology **9**, 1-41 (1984).

Dash, Z. V., and G. Zyvoloski, "Problems Associated with Application of a Wellbore Heat Transmission Computer Code," in Proceedings of the Eighth Workshop on Geothermal Reservoir Engineering, Stanford University, Stanford, California (1982).

Dash, Z. V., H. D. Murphy, R. L. Aamodt, R. G. Aguilar, D. W. Brown, D. A. Counce, H. N. Fisher, C. O. Grigsby, H. Keppler, A. W. Laughlin, R. M. Potter, J. W. Tester, P. E. Trujillo, and G. A. Zyvoloski, "Hot Dry Rock Geothermal Reservoir Testing: 1978 to 1980," J. Volcan. Geotherm. Res. **15**, 59-99 (1983).

Dash, Z. V., D. S. Dreesen, F. Walter, and L. House, "The Massive Hydraulic Fracture of Fenton Hill HDR Well EE-3," in Geothermal Resources Council Transactions, Vol. 9, part II, pp. 83-88 (1985).

Dreesen, D. S., and R. W. Nicholson, "Well Completion and Operations for MHF of Fenton Hill HDR Well EE-2," in Geothermal Resources Council Transactions, Vol. 9, part II, pp. 89-94 (1985).

Dreesen, D. S., J. R. Miller, F. A. Halbardier, and R. W. Nicholson, "Openhole Packer for High-Pressure Service in a 500°F Precambrian Wellbore," in Proceedings of the IADC/SPE Drilling Conference, Dallas, Texas, February 10-12, 1986, IADC/SPE 14745.

Fisher, H. F., "The Pressure Transient Testing of a Manmade Fractured Geothermal Reservoir: An Examination of Fracture Versus Matrix Dominated Flow Effects," Los Alamos Scientific Laboratory report LA-8535-MS (1980).

Grigsby, C. O., "Rock-Water Interactions in Hot Dry Rock Geothermal Systems: Reservoir Simulation and Modeling," MS Thesis, Massachusetts Institute of Technology, Department of Chemical Engineering (1983).

Grigsby, C. O., J. W. Tester, P. E. Trujillo, D. A. Counce, J. Abbott, C. E. Holley, and L. A. Blatz, "Rock-Water Interactions in Hot Dry Rock Geothermal Systems: Field Investigations of In Situ Geochemical Behavior," J. Volcan. Geotherm. Res. **15**, 101-136 (1983).

Hendron, R. H., "Fenton Hill Hot Dry Rock Overview," in Proceedings of the Twelfth Workshop on Geothermal Reservoir Engineering, Stanford University, Stanford, California (1987).

Henley, R. W., A. H. Truesdell, and P. B. Barton, "Fluid-Mineral Equilibria in Hydrothermal Systems," Rev. Econ. Geol. **1**, 4-5 (1984).

Hickman, S. H., and M. D. Zoback, "The Interpretation of Hydraulic Fracturing Pressure - Time Data for In-Situ Stress Determination," in Hydraulic Fracturing Stress Measurements, Proceedings of a Workshop, December 2-5, 1981 (National Academy Press, Washington, D.C., 1983), pp. 44-54.

House, L., H. Keppler, and H. Kaieda, "Seismic Studies of a Massive Hydraulic Fracturing Experiment," in Geothermal Resources Council Transactions, Vol. 9, part II, pp. 105-110 (1985).

Malzahn, M., "Spherical Model Update," Los Alamos National Laboratory internal memorandum ESS-4-86-156 (July 10, 1986).

Murphy, H. D., R. G. Lawton, J. W. Tester, R. M. Potter, D. W. Brown, and R. L. Aamodt, "Preliminary Assessment of a Geothermal Energy Reservoir Formed by Hydraulic Fracturing," Soc. Petr. Engr. J. **17**, 317-326 (1977).

Robinson, B. A., "Quartz Dissolution and Silica Deposition in Hot Dry Rock Geothermal Systems," MS Thesis, Massachusetts Institute of Technology, Department of Chemical Engineering (1982).

Robinson, B. A., and J. W. Tester, "Dispersed Fluid Flow in Fractured Reservoirs: An Analysis of Tracer-Determined Residence Time Distributions," J. Geophys. Res. **89**, B12, 10374-10384 (1984).

Trujillo, P. E., D. Counce, C. O. Grigsby, F. Goff, and L. Shevenell, "Chemical Analysis and Sampling Techniques for Geothermal Fluids and Gases at the Fenton Hill Laboratory," Los Alamos National Laboratory report LA-11006-MS (1987).

APPENDIX A
SURFACE SYSTEM

I. SURFACE SYSTEM FABRICATION

The system consisted of valves, control valves, pipe, flanges, flow meters, expansion joints, etc., purchased for an "interim surface system" and stored since 1982. The system also contained pipe and structures left over from the Phase I loop operations (i.e., heat exchangers, Meyers pumps, 4-in. schedule 160 flanged pipe, tunnel, etc). The system included API-rated wellhead equipment purchased since 1982 and contract pumping supplied by the B.J. Titan service company.

The system was fabricated by many sources: Smith and Smith Construction (the 5 million-gal. pond); Zia Co. (the line from the pond to the holding tank and the heat exchanger piping); and Albuquerque Heating and Ventilating, Zia, and CJC (the Phase I system). Fenton Hill technicians and CJC personnel fabricated remaining parts of the system. All of the Zia welds were done in Zia welding shops; the remainder of the welds were done in the field.

All critical welds in the ICFT system were performed by Jim Moore of CJC. Welds were done with E-7018-1 Lincoln Arc Welding Co. low-hydrogen rod. Fittings and flanges were tacked to the pipe; then the joint was preheated, using a gas torch to drive off moisture. Welding consisted of a stringer pass, hot pass, fill pass, and cap pass. All passes were hand chipped and then finished with a power wire brush. Weld preparation consisted of gas cutting and hand grinding.

Pipe anchors were cast into excavated holes using concrete. To compensate for poor control on cement strength, anchor blocks were oversized and had ample, even excess, reinforcing. Underground bends in pipes were supported with reinforced thrust blocks cast in place between the pipe bend and undisturbed earth, usually tuff.

II. CALCULATIONS

The thrusts applied to the line between EE-2 and the EE-1 tunnel by the expansion joint were calculated. This force is due to the piston effect of the expansion joint. The calculation was done according to Bulletin SCS 6651 published by the manufacturer of the expansion joint.

Pipe anchors were designed keeping in mind the manufacturer's recommendations.

Stresses in the pipe anchors at each end of the expansion joint run were calculated, sketches were made, and the anchors were field fabricated accordingly. Piston force on the line was calculated at 3000 psi since this is in a 4-in. schedule 160 line, which is rated at that pressure. Some components of this segment are rated at only 1450 psi.

Thermal expansion stresses in the segment of pipe between the pipe anchor at the heat exchanger end of the EE-1 tunnel and the heat exchanger were not calculated this time. However, the interim design was calculated in 1982 and accepted at that time. The ICFT piping is nearly identical, or more limber when not identical.

All other thermal expansions occur downstream of the heat exchangers and are of a small value because of the lower temperature extremes. Common practice, which eliminates trapped stresses, was employed.

Flows from the Kunkle safety relief valves were calculated. The size of the production line relief valve, set at 600 psi, is too small to flow 100% of the anticipated production flow from EE-2 (this was an experimental loop and this number was not known before the test). However, it would handle a large percentage of the anticipated flow, and if the pressure should continue to rise, the valve at the production wellhead (with high and low pressure controls) would close at 700 psi. The well would be put on a controlled manual vent through the choke manifold as quickly as possible should this occur.

III. SAFETY AND EXPERIENCE FACTORS

The system was constructed with the best material available from Los Alamos stock. The system was designed along the guidelines laid out in the ANSI B16.5 specifications and the ASME Unfired Pressure Vessel Code.

Supporting the pipe with safety blocks, as mentioned above, far exceeds any real need for them. This was done mainly out of a desire for safety.

The system was remotely controlled from two locations: the DAT trailer, which controls all the loop up to the contract pumps, and the

APPENDIX B

DATA CHANNELS AND TAPE SETUPS

TABLE B-I

ICFT DATA CHANNELS

Channel No.	Location	Range	Type
P1	EE-2 Wellhead Pressure	0-2500 psi	CEC
P2	EE-2 Wellhead Pressure-Strainer	0-2500 psi	CEC
P3	Heat Exchanger Inlet	0-2500 psi	B&H
P4	Heat Exchanger Discharge	0-2500 psi	B&H
P5	Heat Exchanger Strainer Inlet	0-500 psi	CEC
P6	Heat Exchanger Strainer Output	0-500 psi	CEC
P7	Meyers Pump Discharge	0-250 psi	CEC
P8	High-Pressure Pump Inlet	0-500 psi	Statham
P9	EE-3A Wellhead	0-10 000 psi	CEC
P10	EE-3A Annulus	0-1000 psi	CEC
P11	EE-3A Backside	0-2500 psi	B&H
P12	Kobe Pump Discharge	0-3000 psi	Dynisco
P13	EE-2 Annulus	0-250 psi	CEC
P14	EE-2 Backside	0-2500 psi	B&H
P15	Separator Inlet Pressure	0-1000 psi	Precise
P16	Separator Inlet Gas Pressure	0-200 psi	Gould
P17	Separator Discharge Gas Pressure	0-200 psi	Gould
P18	Air Compressor	0-500 psi	Celesco
T1	EE-2 Wellhead	0-300°C	Thermocouple
T2	Heat Exchanger Inlet	0-300°C	Thermocouple
T3	Heat Exchanger Discharge	0-100°C	Thermocouple
T4	Meyers Pump Outlet	0-100°C	Thermocouple
T5	High-Pressure Pump Inlet	0-100°C	Thermocouple
T6	Separator Inlet	0-300°C	Thermocouple
T7	Separator Discharge	0-300°C	Thermocouple
F1	EE-2 Wellhead Flow	0-420 gpm	3-in. Halliburton
F2	Heat Exchanger Bundle 1	0-150 gpm	1-1/2-in. Halliburton
F3	Heat Exchanger Bundle 2	0-150 gpm	1-1/2-in. Halliburton
F4	Heat Exchanger Bundle 3	0-150 gpm	1-1/2-in. Halliburton
F5	Heat Exchanger Bundle 4	0-150 gpm	1-1/2-in. Halliburton
F6	Meyers Pump Discharge	0-1000 gpm	Clampitron
F7	High-Pressure Pump Inlet	0-420 gpm	4-in. Halliburton
F8	Separator Liquid Flow Discharge	0-200 gpm	2-in. Halliburton
F9	Separator Liquid Flow Discharge	0-600 gpm	4-in. Halliburton

TABLE B-II

EXPERIMENT 2067 (ICFT) TAPE SETUP

Tape No. 1 (3020)/1-7/8 IPS

Track	Range	Channel
1	q 1.4 FM	EE-1 "VERT"
2	q14 FM	EE-1 "VERT"
3	q 1.4 FM	EE-1 "UPPER"
4	q14 FM	EE-1 "UPPER"
5	q 1.4 FM	EE-1 "LOWER"
6	q14 FM	EE-1 "LOWER"
7	q 1.4 DIR	Time Code "B" (1 kHz)
8	q14 FM	PC-1
9	q 1.4 FM	PC-1
10	q14 FM	PC-2
11	q 1.4 FM	PC-2
12	q14 FM	GT-1
13	q 1.4 FM	GT-1
14	q 1.4 DIR	Time Code "A" (10 kHz)

TABLE B-III

EXPERIMENT 2067 (ICFT) TAPE SETUP

Tape No. 3 (2230)/1-7/8 IPS

Track	Range	Channel
1	q14 FM	FNHR
2	q14 FM	BRLY
3	q 1.4 FM	PC-1
4	q14 FM	CEBM
5	q14 FM	CEBT
6	q14 FM	BANC
7	q 1.4 FM	GT-1
8	q14 FM	LAFK
9	q14 FM	THDM
10	q14 FM	TENT
11	q 1.4 FM	PC-2
12	q14 FM	LKFK
13	q 1.4 FM	EE-1 "VERT"
14	q 1.4 DIR	Time Code (100 Hz)

APPENDIX C

CHRONOLOGICAL SUMMARY OF ICFT PUMPING AND OPERATIONS

May 19:

Lines were pressure tested from the heat exchangers up to the EE-3 wellhead. By 1600 pressure testing was finished. BJ's strip chart showed a test pressure of 7550 psi, which dropped to 7200 psi in 30 min. The EE-3 frontside pressure transducer, P-9 SN-18771, was not working. It was replaced later with SN-15370.

A safety meeting was conducted. At 1608 EE-3 wellbore filling was started. At 1612 step-rate flow testing was started.

STEP-RATE FLOW TESTING EE-3

Start Time	Flow Rate (gpm)	Pressure at End (psi)
1612	72.0	4056.0
1736	140.0	4380.0
1849	172.0	4519.0
2000	310.0	4990.0

The pressure in EE-2 backside started rising above background at 1952. The frontside showed pressure at 2018. After this time the pressures followed each other and were reading 102 psi at 2115 when continuous rate pumping was started at 190 gpm or a nominal 4.5 bpm.

May 20:

At 0021 EE-2 pressure was up to 277 psi. It was decided to put EE-2 on production through the heat exchangers and then vent to the pond. Initial flow was at about 60 gpm and 170 psi. Control valve CV-6, the main system control valve, showed no ability to control the flow. Control of the system was switched to the backup for this valve (i.e., the individual control valves on each of the four heat exchanger bundles). When this valve was inspected at the end of the test, it was plugged with mud and scale. CV-6 is a slide-in cage type of control

valve with small-diameter holes (about 3/32 in.). We had thought the holes to be much larger based on manufacturer's pictures. The strainers downstream of this control valve should be moved upstream for the LTFT and/or this control valve should be replaced.

At 0127 a gas bubble was suspected, and vent through the heat exchangers was changed to vent through the choke. At this time flow measurements were lost, which brings up the second limitation of the ICFT surface system. All vents of any nature that were directed straight to the pond had no flow measurements. Meyers pump #2 heated up and had to be repaired later in the experiment.

At 0310 an attempt to put EE-2 back on production through the heat exchangers was made. Still too much gas. EE-2 backside was opened to the tank. At 0700 the loop was successfully placed in the gas-purge mode with flow directed through the heat exchangers and then dumped into the makeup water tank. The flow settled down at about 50 gpm at 265 psi. At 1708 EE-2 was placed in vent mode through the chokes to work on CV-6 and to balance pressure transducers. This mode of operation continued until the next day.

May 21:

At 0915 a check on the EE-2 flow was made by directing the flow through the separator. Flow was 53.5 gpm at 267 psi. At 0942 BJ was shut down to obtain a shut-in pressure. Pressure dropped from 4064 to 3870 psi and then slowly decayed to 2497 psi at 1102.

At 1314 the first of four shut-ins and vents to surge the system were conducted. At 2230 the flow rate was 64 gpm. Surging EE-2 continued till around midnight. During the first shut-in, EE-2 frontside pressure built up to 1118 psi at 1419 while the backside reached 1098 psi. During the vent, the frontside dropped to 127 psi at 1426 when it was shut in again. The corresponding backside pressure was 1043 psi and continued to drop down to 943 psi at 1433, when it increased. EE-2 reached 1110 psi at 1451 during the second shut-in; then the second vent started. The backside showed a momentary drop in pressure and then continued to rise in pressure till 1510 when it peaked at 1134 psi. At 1847 the third shut-in was started. EE-2 frontside pressure was 200 psi, while the backside was 184 psi. During the third

shut-in, the backside pressure lagged the frontside pressure by about 200 psi or 17 min. The third vent was started at 1943; the backside pressure continued to rise for another 12 min before following the vent. At the end of the fourth shut-in, at 2026, the frontside was vented down to 105 psi before it was leveled out at about 180 psi. This time the backside continued to climb, and by midnight it reached 1830 psi. Pumping by BJ was shut down and the backside watched. The pressure continued to climb.

May 22:

At 0203 the EE-2 frontside was shut in and the backside vented through the choke. Note that during this time the frontside and the backside shared the same choke and vent line. This was changed later in the experiment. At 0229 pumping was resumed. The backside was shut in and started to climb again by 0240. At 0442 the frontside was shut in and reopened at 0500. A bucket measurement at 0530 gave 68 gpm at 164 psi. At 0600 the vent rate was 62 gpm at 165 psi, and by 0715 the flow rate was 61 gpm at 160 psi.

The production was changed from vent mode to gas-purge mode between 0910 and 0930. At 1152 a leak was found in the tunnel under the road. Went back to vent mode to find and fix leak. Leak turned out to be the back pressure valve on the Meyers pump venting through a pipe and then leaking underground into the tunnel.

The MASSCOMP went off during the night. The system was returned to gas-purge mode with four heat exchanger bundles at 1510. An increased flow rate experiment was started at 1625. BJ increased their pump rate to 7.5 bpm, 315 gpm. Injection pressure rose to 4400 psi and then climbed slowly to 4600 psi during the next 80 min. During this time CV-6 was bypassed using two 1-in., high-pressure hoses. At 1820 Meyers pump #6 went off-line. It was later reset with the thermal relay and put back in service. Injection flow rate was cut back to 6 bpm (250 gpm) at 1851 and then to 4.3 bpm (180 gpm) at 1947. At 1920 the loop was taken out of gas-purge mode and placed in closed-loop operation. A few minutes later it was returned to gas-purge mode as BJ's pumps ran rough with the high gas content. The EE-2 backside was vented from 884 to 504 psi between 2257 and 2305.

May 23:

A flow meter on bundle 1 stopped working early in the morning. The meter started later in the day when flow was switched back to this bundle. There was some indication of a damaged vane on the impeller. The first dye tracer experiment was started at 1000. The rest of the day was simply pumping in the gas-purge mode with gas readings still about 0.23%.

May 24:

Since the last vent the EE-3 backside pressure steadily increased to 930 psi. At 0230 the pressure was vented down to 500 psi and then shut in again. A midday gas reading was given at 0.21%. At 1203 pumping was stopped to obtain a shut-in pressure reading. Pressure dropped from 3955 to 3667 psi and then decayed to 3231 psi at 1254. Pumping at 4.2 bpm (176 gpm) was resumed at 1334.

Tracer data were very scattered. The tracer injection line was changed to allow a more concentrated slug of dye to be injected for the next tracer experiment.

At 1433 EE-2 production was shut in to obtain buildup data. The well was shut in until 1531 and a pressure of 1473 psi and then vented. The system was left in the vent mode, to obtain bottoms up, until 1948 when it was put back into gas-purge mode. The first set of corrosion coupons was removed/replaced at 1700.

May 25:

A morning summary reported boiling water in the cellar of EE-2. BJ was reported to have all four trucks ready to pump except that two discharge pulsation dampeners were out of commission. The MASSCOMP was down again. A safety meeting was conducted to go over placing the system in closed-loop mode. The CO_2 at this time was 0.169%. At 1245 the loop was placed on closed-loop flow. BJ's pumps were able to handle this amount of CO_2. At 1620 the injection rate was increased from 180 to 280 gpm. The first report of a yellow stain was reported on filter paper in the chemistry trailer. This was later identified as arsenic sulfide. The first signs of strainer plugging were noticed during the evening of this day.

May 26:

The MASSCOMP was repaired and put back on-line by noon. EE-2 strainer still indicated signs of plugging. At 1403 the injection rate was increased from 6.7 to 7.5 bpm. Injection pressure before the increase was 4463 psi. Because of the venting to the EE-1 pond during the first days of the test, it was necessary to pump water from the EE-1 pond to the 5 million-gal. pond.

During the evening, the EE-2 annulus pressure started to climb and the backside pressure started to drop. The backside was vented and the annulus pressure leveled out.

The pressure difference across the strainer continued to rise during the day. At 1945 the injection rate was decreased to 4.5 bpm. Shortly thereafter, injection was stopped and EE-2 was shut in. By 2034 EE-2 had built up to 1500 psi and a vent to the pond was started. By 2316 the backside pressure had climbed to 1169 psi, and it was put on a vent till 500 psi was reached. The leak from the conductor pipe into the EE-2 cellar was reported to have increased.

May 27:

The strainer and flow meter at EE-2 were checked and ready to go back on-line shortly after midnight. There were no problems found with either except for some metal in the strainer. An attempt to place the system back into production was short lived as the pressure drop across the strainer required the system to be shut in again. At 0134 EE-2 was shut in; BJ continued to pump at 4.5 bpm. The strainer was removed from the system and the system put back on-line at 0310. The injection pressure into EE-3 during this period remained constant at 3930 psi. At 0830 a CO_2 reading of 0.164% was given. At 0910 the loop was switched from gas-purge mode to closed-loop operation. The loop ran smoothly except for Meyers pump #5, which had a leak and a defective pressure gauge. The MASSCOMP went down in the evening. At 2008 the injection flow rate was increased to 7.1 bpm. MASSCOMP was back on at 2205.

May 28:

The loop ran smoothly during the night and morning. At 0815 the injection flow was decreased to 4 bpm to allow for a temperature log in

EE-3 by Oil Well Perforators (OWP). At the same time Tefteller of Farmington was getting ready for a Kuster temperature log in EE-2. BJ was shut down from 0901 till 1219 while OWP was lubricating their tool into the well. A flowing temperature log was run with BJ pumping at 4.2 bpm and 3800 psi. The log was completed and BJ shut down to remove the temperature tool at 1514. Pumping resumed at 1729 at 4.2 bpm.

At 1750 the system was placed in closed-loop flow, and all went well until 2120 when the power supply to the DAT control panel failed. Remote control of the system was lost at this time. Meyers makeup pumps went off, the heat exchanger fans stopped, etc. Before BJ was shut down they received 140°C water, which caused considerable problems. One suction hose was lost, both flow meters had to be rebuilt, the rubber seals on the suction manifold valves failed, and BJ later dismantled the fluid end of the pump for inspection. It is probable that the pulsation dampeners were also damaged. The line running from the heat exchangers to the BJ pump trucks was bent because of the thermal growth. Concrete safety blocks were moved. The damage to equipment turned out to be small, and there were no injuries. A thermal switch was installed to shut down the system if this should occur again. It never did.

May 29:

At 0410 the 250-psi safety relief valve was leaking and had to be replaced. BJ shut down at 0936 to replace their flow meters. During the change out of the meters, it was assumed that some air was trapped in the heat exchangers, the highest elevation in the system. BJ was placed on-line with all water coming from the makeup water system. EE-2 was vented to the pond through the choke manifolds. All four of the heat exchangers were purged of gas, and the loop was put back into normal operation by 1130.

At 1620 MASSCOMP down again; at 1841 MASSCOMP back on-line. All ran smoothly for the rest of the day.

May 30:

The system ran quietly all night. This was the day of the first radioactive tracer experiment. The tracer experiment was to inject approximately 70 to 75 mCi of ^{82}Br. At 1015 RA material arrived at

Fenton Hill. A safety meeting was held at 1150. The pressure locks on each well were valved off and filled with water so that any leaks could be detected by the sight of water. The high/low valve on EE-2 was set to trip at 250 and 500 psi. The 500-psi set pressure was selected to shut in the well before the pressure relief valve, which was set at 600 psi, could open in the event of a high-pressure excursion in the wellbore. This would keep any RA material confined within the surface system. The backside of EE-3 was shut in to seal up that potential leak path. Then the planned step-by-step procedure was followed, and the RA tracer was injected by 1430.

The RA material was injected into EE-3 by first injecting the RA tracer into one of the two injection lines between BJ's pumps and the wellhead. Second, that line was valved off from the RA tracer pig and brought up to the injection pressure of 3875 psi by one of the pumps on that line. Next, the wing valve was opened and, while continuing to pump on the second line, a pump was started on the first line and the RA tracer injected into the well. As soon as the tracer was well below the surface, the pump on the second line was shut down and pumping continued on the RA tracer line. First arrival of the tracer from the production well occurred at 1924 and was reported at 2998 cpm with a background reading of 2815 cpm. The second set of corrosion coupons was removed/replaced at 1530.

May 31:

The RA tracer peaked in the sample analyzed at 0206 in the morning. Maximum counts were 32 554 cpm. An unknown problem with the remote start-up of Meyers pump #6 was encountered. Switching to local control and then later back to remote control corrected the problem. A power glitch knocked out the MASSCOMP. This happened several times during the experiment both to the MASSCOMP and the chemistry trailer computer. Neither were protected by an uninterrupted power supply system.

June 1:

All ran smoothly until near midnight when the chemistry trailer sampling line flowed only gas and no water. After a safety check the line was removed and cleaned. This did not cure the problem.

June 2:

The back pressure on EE-2 was increased for a short period around 0300 in an attempt to drive the gas back into solution. This had no effect on the gas. At 0313 the back pressure was lowered back down to 350 psi and we went on gas-purge mode. Meyers makeup pump #7 stopped working and was removed for inspection. A piece of rubber was found to be wedged between the impellers and the housing. It was removed and after reassembly the pump was put back into service. Meyers pump #5 was then taken down to repair the seals. From about 1340 to 2100 the back pressure on EE-2 was increased to 500 psi to drive the gas back into solution. This time the higher pressure seemed to work; however, it was decided to stay in gas-purge mode. A shut-in of EE-2 was scheduled for 0400.

June 3:

At 0512 EE-2 was shut in; it climbed to 1500 psi by 0534. The backside pressure in EE-2 during this time slowly decreased from 540 to 252 psi and continued to go down to as low as 145 psi. The 1500-psi pressure was vented through the choke manifold down to 350 to 400 psi. At 0808 a second shut-in occurred while the site crew changed out the strainer. At 1132 we changed from vent mode to gas-purge mode. For a short time, from 1343 to 1417, the system was placed on closed-loop. All went well, so at this time the injection rate was increased to 7.5 bpm. The rest of the experiment was basically run at 6.9 to 7.5 bpm.

A loss of electrical power caused the MASSCOMP to go down for several hours.

June 4:

Barley seismic station stopped sending signals at 0245. It was determined the problem was low batteries. It was repaired and back on-line at 1011. A Kuster temperature log was run in EE-2 between 0900 and 1600. The third set of corrosion coupons was removed/replaced at 1745. A sequence of EE-2 shut-ins and vents started at 1953. Pressure built up to 1799 psi, then was vented to 350 psi before being shut in again.

June 5:

Shut-in/vent of EE-2 continued for 12 total cycles. A leak on EE-2 frontside had to be repaired before restarting closed-loop operations. Closed-loop operation commenced at 0910 at 7 bpm and ran smoothly. The EE-1 geophone tool was off-line and removed from the well at 1300. The EE-2 flow meter was briefly off-line at 2107. The problem was corrected, and the meter was working by 2120.

June 6:

A brief shut-in occured at 0823 to replace check valves on Meyers pumps #5 and #6. They were back on-line and everything was running smoothly by 0842. The MASSCOMP was down for servicing between 0915 to 1430. It went down again at 1610; seismicity was being recorded on analog tapes. It was determined that the tape drive was bad and needed to be replaced with the one from the TA-33 system.

June 7:

The system had to be shut down at 1245 to clean the EE-2 strainer. Closed-loop operations were restored by 1800. The system was run in gas-purge mode due to high CO_2 content of the production fluid.

June 8:

A 1500-kg (155 000-SCF) slug of nitrogen was injected into EE-3A from 1121 to 1200. The main purpose of the gas injection was to attempt to clean out the EE-2 production interval where it was assumed debris was filling and possibly covering near-wellbore fractures. Because of a storm one phase of power was lost at 1255; the site and DAT switched to emergency backup power. Jemez power was back on-line at 1436, so normal loop operations were reinitiated. The loop was back to normal by 1500. The DAT switched back to normal power at 1630 and all was running normally by 1636, including the MASSCOMP which was back on-line.

First sign of N_2 at EE-2 was seen at 1212 and was back to background by 1240. This was probably not a result of N_2 injection. The major pulse arrived at EE-2 at 1715 with an increase to 45% nitrogen fraction in the gas stream. Too much gas was present in the production stream to make reliable measurements of total gas. The system was

switched to gas-purge mode operation. The vent line on EE-2 was opened at 1737 to prevent fouling the heat exchangers with sand or other debris if the nitrogen was successful in cleaning EE-2. It was determined by 1800 that the debris being produced was minimal, and a side stream was run through the surface system and heat exchangers to allow good gas measurements. At 2136 production pressure was reduced to 250 psi to surge fractures as much as possible during projected peak nitrogen production. BANC and CEBT seismic stations were not working at 2305.

June 9:

At 0630 the EE-2 production pressure was increased to 550 psi, and at 0715 the vent was shut in and all production was through the loop. The N_2 content of the gas stream peaked at 1044 with 79%. Surface loop was still being operated in gas-purge mode. High/low valves on EE-2 were reset so the back pressure on EE-2 could be raised to 800 psi and N_2 could be kept in solution. The EE-2 flow meter was reading 40 gpm higher than the sum of the flow through the heat exchanger flow meters, probably as a result of gas in the system. BANC seismic station was checked out and back on line at 0937. The MASSCOMP was down from 1930 to 2332.

June 10:

Rough calculations indicated more N_2 was being produced than was injected. Not getting good gas measurements from the way system was set up. Saw second peak in N_2 content of gas stream (79%) at 1315. A water sample taken of fluid being sent to injection pumps indicated not much N_2 was recycling through the system. Seismic station CEBT was still down; water in the electronics enclosure caused the problem and the electronics had to be brought to the site for repairs.

June 11:

The N_2 content was going down in the gas stream. EE-2 back pressure was dropped from 456 to 350 psi in preparation of going to closed-loop operation. Gas concentration went up, so EE-2 pressure was raised to the previous level. The system was operating in closed-loop mode with 500 psi on EE-2 at 2225. EE-3A injection rate was increased

to 10 bpm at 2323. The CEBT electronics were repaired and the station put back on-line.

June 12:

Operations running smoothly. Significant seismicity occurred as a result of high-rate pumping but with a considerable time lag. Changed operation to gas-purge mode, flowing nominal 7 bpm. Seismic activity from high-rate pumping down; therefore pulling EE-1 geophone at 1000. It was noticed that water, about 1 gpm, was flowing from GT-2 at 1240. Wellhead will be shut in, and pressures from GT-2 and EE-1 will be recorded.

June 13:

MASSCOMP was down and put back on-line by 0613. EE-2 strainer was cleaned out from 0830 to 0930. Preparations were made for the second radioactive tracer test. System is being run in vent mode. The RA tracer was injected at 1207 to 1224. At 1228 "fresh" water flush mode was initiated. RA tracer was first seen at EE-2 at 1656; peak of 23 580 counts/min was seen at 2151. MASSCOMP was down from 1205 to 1408.

June 14:

System was running smoothly. At 2354 system was switched to gas-purge mode and water was being recycled.

June 15:

System was switched to closed-loop mode at 0745. The RA count was down to 3340 at 0630. Tefteller started Kuster survey of EE-2 at 2115.

June 16:

Kuster tool was out of EE-2 at 0305. At 1100 OWP was starting temperature log of EE-3A while injecting 6.5 bpm. Log was completed at 1606. At 2045 back pressure on EE-2 was increased to 1000 psi and was maintained between 950 and 1068 psi.

June 17:

EE-2 back pressure was reduced to 435 psi at 0320. EE-2 was shut in from 0933 to 1032; then system was put in vent mode. EE-2 wellhead was shut in at 1138 for repairs. Vent mode was reinitiated at 1336. EE-2 strainer was cleaned out starting at 2352.

June 18:

EE-2 strainer cleaned out and back on-line at 0036. System back in closed-loop operation by 0051, pumping at 7 bpm. BJ is down to one pump that will operate. Fourth set of corrosion coupons were changed out. The pumping was terminated at 1600, and EE-3A and EE-2 were shut in. BJ trucks and missile were moved out by 1730. The DAT will be kept on-line to monitor the shut-in.

June 19:

EE-2 backside had to be vented intermittently to maintain pressure below 1000 to 1500 psi.

June 20:

EE-2 backside was plumbed so it will vent to pond automatically. MASSCOMP was shut down at 1130. At 1406 DAT was set up for unmanned operations.

June 23:

OWP ran temperature and tracer logs in EE-3A.

June 25:

Tefteller ran a Kuster survey of EE-2.

APPENDIX D

GEOCHEMISTRY NOMENCLATURE

a^*	quartz surface area to fluid volume ratio (m^2/m^3)
b	fracture aperture (m)
C	concentration (kg/m^3)
C^*	dimensionless concentration in Eq. (V-1)
C_{in}	injection fluid concentration (kg/m^3)
C_o	initial production fluid concentration (kg/m^3)
C^∞	silica saturation concentration (kg/m^3)
f_q	fraction of quartz present in granite
$f(V)$	residence time distribution curve (m^{-3})
k	quartz dissolution rate constant (m/s)
K_{eq}	equilibrium constant
K_H	Henry's law constant (bar/mole fr.)
m_p	mass of tracer injected (kg)
P	pressure (bar)
P_{CO_2}	partial pressure of CO_2 (bar)
P_w	vapor pressure of water (bar)
t	time (s)
V	cumulative produced fluid volume (m^3)
x_{CO_2}	mole fraction of CO_2
γ_i	activity coefficient for component i
Φ	dimensionless concentration in Eq. (V-2)

APPENDIX E

ENVIRONMENTAL MONITORING: DISCRIMINATION CRITERIA

Strip charts containing surface and Precambrian station recordings will be run during the ICFT for the purpose of environmental monitoring. In the event that a large earthquake is suspected to have occurred, the following simple criteria should be applied before contacting the on-call seismologist if he is not on-site. A calendar containing names and phone numbers will be posted on the MASSCOMP.

If a large earthquake has occurred under Fenton Hill, the following must have been observed at all working stations:

1. The strip chart recordings must show coherent arrivals at all stations (within a few seconds).
2. The <u>initial</u> portions of the recordings will be saturated (truncated).
3. The <u>initial</u> portions will contain high frequencies; if individual "wiggles" are seen, then the event is fairly distant.
4. The signal (coda) duration will be large: 100 sec = magnitude 2.5; 160 sec = 3.0; 360 sec = 4.0 (be sure to check strip chart speed before measuring duration). See following procedures for appropriate action based on the coda duration.

The following may also be observed:

1. The event should be felt.
2. Rapid changes in pumping parameters may occur.

If a large-magnitude, nearby earthquake is suspected, the on-call seismologist should be contacted in order that on-site personnel may be "talked through" the location procedure on the MASSCOMP. See following section (Procedures) for subsequent action.

Environmental Monitoring: Procedures

ALERT - $M_L > 2$ (Duration > 100 sec)

Event must be located. Contact on-call seismologist for a "talk through" location on the MASSCOMP if he is not on-site. If location is within 5 km of injecton point, proceed to:

1. Notify needed personnel in case further seismic activity requires shut-in or immediate vent under the criteria below.
2. Notify project management.
3. Pay close attention to pressure/flow data.

SHUT-IN - $M_L > 2.5$ (Duration > 150 sec)

Event must be located as above. If within 5 km of injection, proceed to:

1. Inform experiment manager of need to shut in. Pumping should resume only after consultation with project management.
2. Inform project management.
3. Pay close attention to pressure/flow data.

IMMEDIATE VENT - $M_L > 3.5$ (Duration > 360 sec)

Event will be located as above. If within 5 km of injection, inform experiment manager of need to begin venting reservoir fluids. Further action will be determined by project management.

Printed in the United States of America
Available from
National Technical Information Service
US Department of Commerce
5285 Port Royal Road
Springfield, VA 22161

Microfiche (A01)

Page Range	NTIS Price Code	Page Range	NTIS Price Code	Page Range	NTIS Price Code	Page Range	NTIS Price Code
001-025	A02	151-175	A08	301-325	A14	451-475	A20
026-050	A03	176-200	A09	326-350	A15	476-500	A21
051-075	A04	201-225	A10	351-375	A16	501-525	A22
076-100	A05	226-250	A11	376-400	A17	526-550	A23
101-125	A06	251-275	A12	401-425	A18	551-575	A24
126-150	A07	276-300	A13	426-450	A19	576-600	A25
						601-up*	A99

*Contact NTIS for a price quote.

Los Alamos National Laboratory
Los Alamos, New Mexico 87545

Plate I. Event Chronology with ICFT Performance Data.

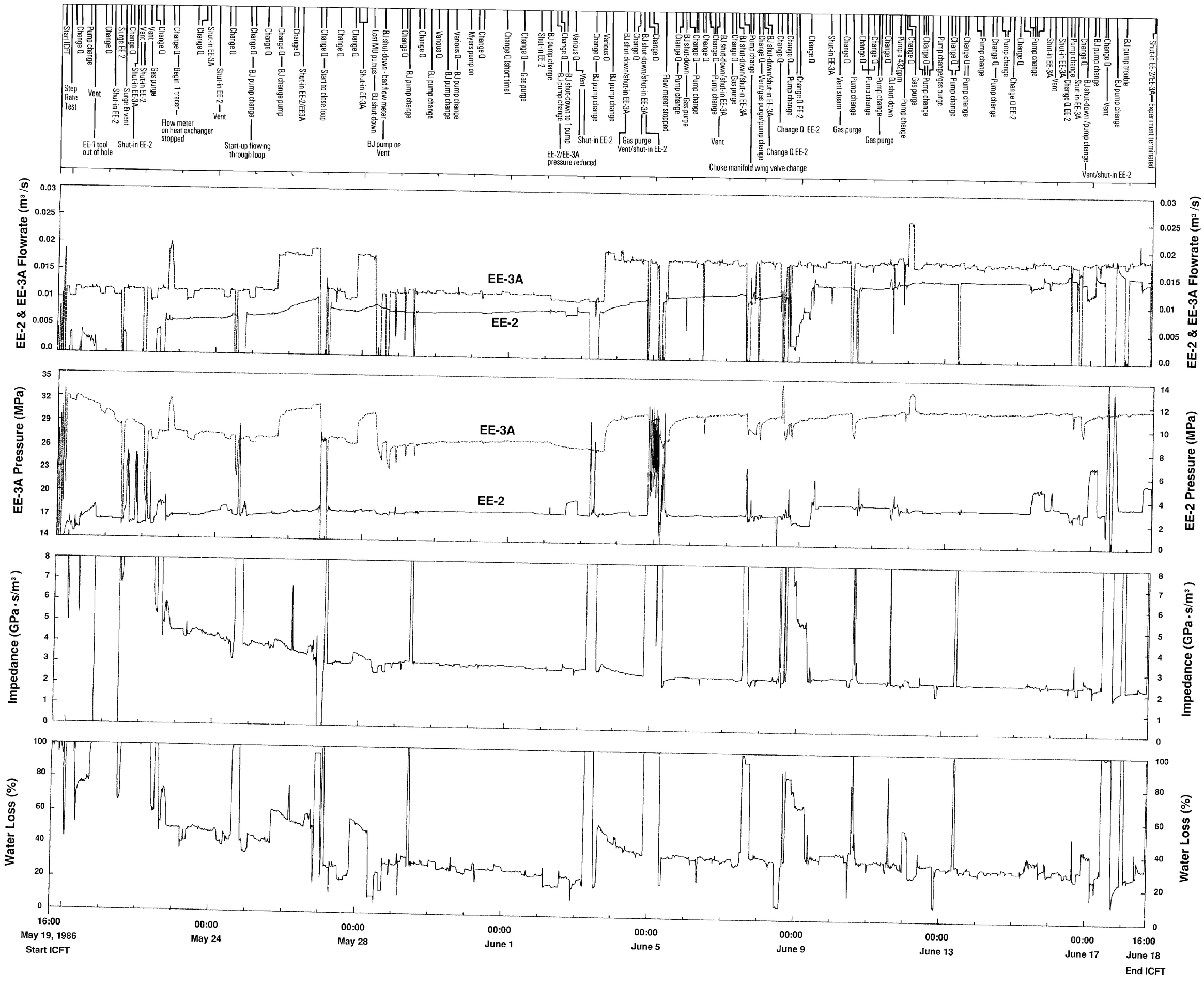
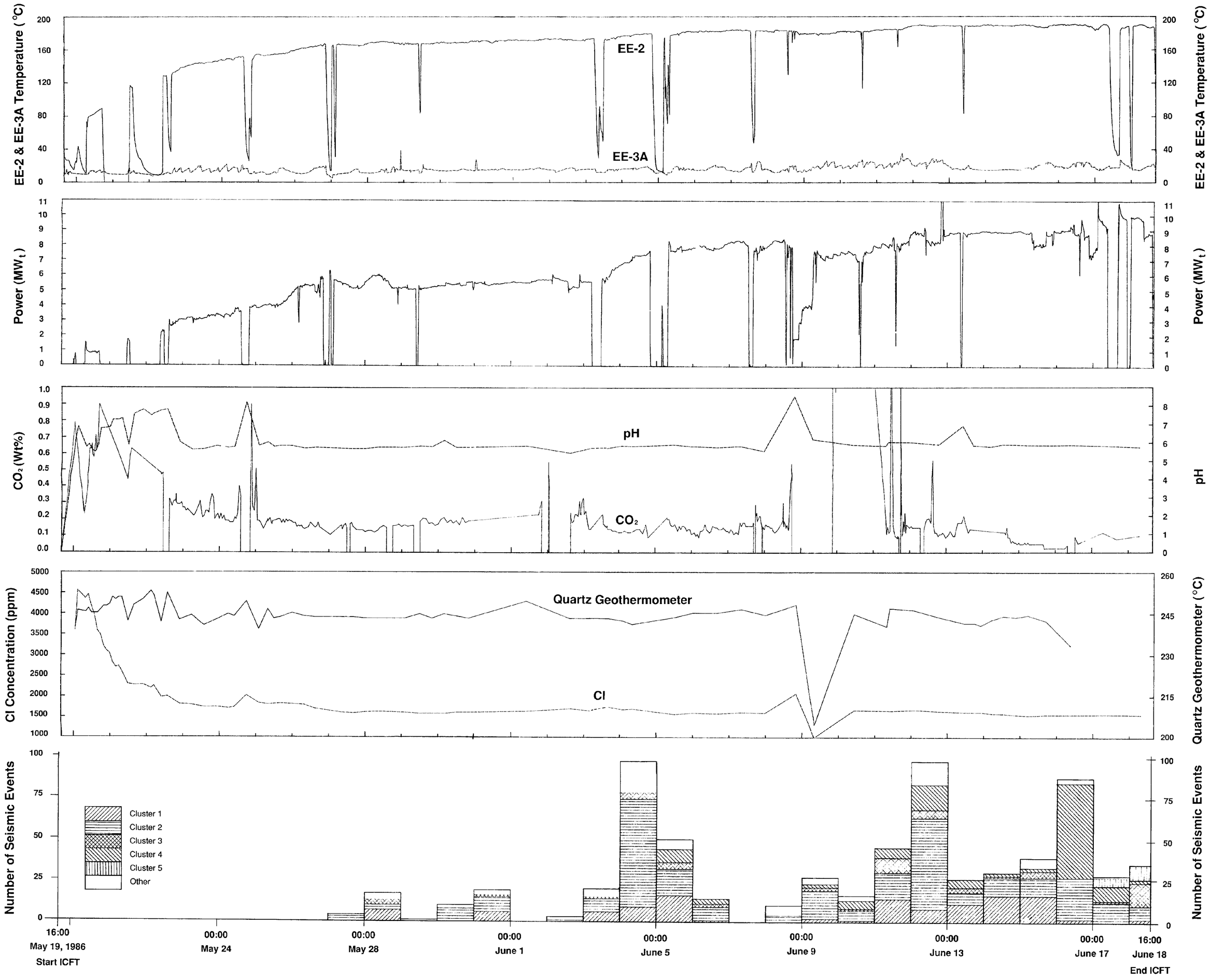
Plate II. ICFT Performance Data.